Universität Stuttgart

Institut für Wasser- und Umweltsystemmodellierung

Mitteilungen

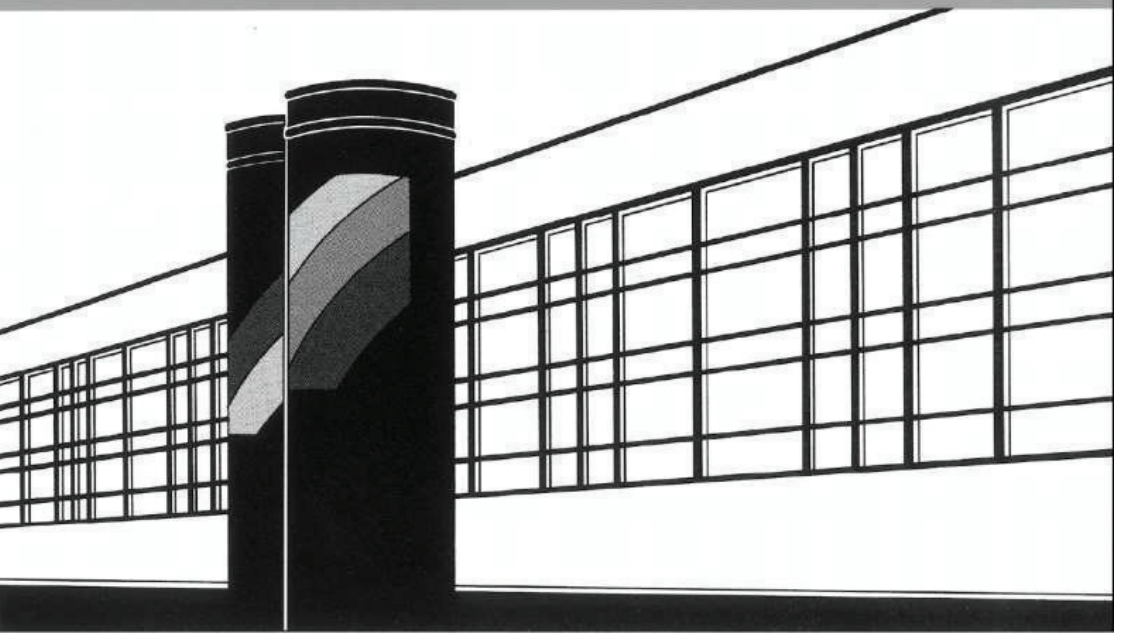

Heft 268 Sebastian Christopher Most

Analysis and Simulation of Anomalous Transport in Porous Media

Analysis and Simulation of Anomalous Transport in Porous Media

Vom Stuttgarter Zentrum für Simulationswissenschaft unter der Beteiligung der Fakultät Bau- und Umweltingenieurwissenschaften der Universität Stuttgart
zur Erlangung der Würde eines Doktors der Ingenieurwissenschaften (Dr.-Ing.) genehmigte Abhandlung

vorgelegt von

Sebastian Christopher Most

aus Oberhausen-Rheinhausen

Hauptberichter:	Prof. Dr.-Ing. Wolfgang Nowak
Mitberichter:	Prof. Diogo Bolster
Mitberichter:	Dr. Branko Bijeljic

Tag der mündlichen Prüfung: 12. April 2019

Institut für Wasser- und Umweltsystemmodellierung
der Universität Stuttgart

2019

Heft 268

Analysis and Simulation of Anomalous Transport in Porous Media

von
Dr.-Ing.
Sebastian Christopher Most

Eigenverlag des Instituts für Wasser- und Umweltsystemmodellierung der
Universität Stuttgart

D93 Analysis and Simulation of Anomalous Transport in Porous Media

Bibliografische Information der Deutschen Nationalbibliothek
Die Deutsche Nationalbibliothek verzeichnet diese Publikation in der Deutschen Nationalbibliografie; detaillierte bibliografische Daten sind im Internet über http://www.d-nb.de abrufbar

Most, Sebastian:

Analysis and Simulation of Anomalous Transport in Porous Media, Universität Stuttgart. - Stuttgart: Institut für Wasser- und Umweltsystemmodellierung, Universität Stuttgart. - Stuttgart: Institut für Wasser- und Umweltsystemmodellierung, 2019

(Mitteilungen Institut für Wasser- und Umweltsystemmodellierung, Universität Stuttgart: H. 268)
Zugl.: Stuttgart, Univ., Diss., 2019
ISBN 978-3-942036-72-6
NE: Institut für Wasser- und Umweltsystemmodellierung <Stuttgart>: Mitteilungen

Gegen Vervielfältigung und Übersetzung bestehen keine Einwände, es wird lediglich um Quellenangabe gebeten.

Herausgegeben 2019 vom Eigenverlag des Instituts für Wasser- und Umweltsystemmodellierung, Universität Stuttgart
Druck: DCC Kästl e.K., Ostfildern

Acknowledgments

Ein herzliches Dankeschön geht an Wolfgang Nowak, für die großartige Förderung und Unterstützung. Ich bin jeden einzelnen Tag gerne an die Uni gekommen. Das ist nicht selbstverständlich und dafür bin ich sehr dankbar. Genauso herzlich möchte ich mich bei Diogo Bolster für die Zusammenarbeit und für die drei Monate in South Bend bedanken. Die Zusammenarbeit war und ist mir eine Freude. Danke auch an Branko Bijeljic ohne dessen Unterstützung und Equipment diese Arbeit nicht möglich gewesen.

Großen Dank geht auch an meine Kollegen vom LS3, die jederzeit für fachliche Diskussionen aber auch für persönliche Gespräche offen waren. Besonderen Dank geht hierbei an Aline, Anneli, Jonas, Micha, Sergey und an meinen langjährigen Bürokollegen Felix, mit denen ich über die Jahre auch abseits der Arbeit viele lustige Momente teilen durfte.

Abseits der Uni möchte ich mich noch bei meiner Familie und bei meinen Freunden bedanken. Ohne die riesige Unterstützung meiner Eltern, wäre mir das Studieren nicht möglich gewesen. Vielen Dank auch an meine Großeltern, meine Schwester und an Ian. Die Zeit mit euch ist einfach immer sehr schön und ein hervorragender Ausgleich zum Unialltag. Ein ganz besonderer Dank geht an Dani für die Geduld, das Verständnis, die unendliche Unterstützung und für die Freiheiten die ich habe. Besonders aber dafür, dass du für mich da bist.

Contents

Notations

The following table summarizes the symbols that are repeatedly used throughout this work. Occasionally used notations are explained in the text.

Symbol	Definition	Dimension
Latin Letters:		
D_{e}	Effective Dispersion Coefficient	$\left[L^2T^{-1}\right]$
D_{m}	Diffusion Coefficient	$\left[L^2T^{-1}\right]$
$\overline{D}$	Dispersion Matrix	$\left[L^2T^{-1}\right]$
J	Flux	$\left[L^3T^{-1}\right]$
K	Pearson Correlation Coefficient	$[-]$
V	Volume	$\left[L^3\right]$
c	Concentration	$\left[ML^{-3}\right]$
n_{e}	Effective Porosity	$[-]$
q	Specific Flux	$\left[LT^{-1}\right]$
t	Temporal Coordinate	$[T]$
v	Velocity	$\left[LT^{-1}\right]$
Greek Letters:		
η	Rate	$\left[T^{-1}\right]$ or $\left[L^{-1}\right]$
θ	Displacement	$[L]$
x	Spatial Coordinate	$[L]$
λ	Correlation Length	$[L]$
τ	Waiting Time	$[T]$

Operators and Functions

δ	Dirac Delta Function
Δ	Differential Operator
∂	Partial Derivative
∇	Nabla Operator
$() \cdot ()$	Scalar Product

Abbreviations

ADE	Advection-Diffusion Equation
A$\overline{\text{D}}$E	Advection-Dispersion Equation
AR (n)	Auto-Regressive Process of Order n
BTC	Breakthrough Curve
CLT	Central Limit Theorem
CT	Computer Tomography
CTRW	Continuous Time Random Walk
CV	Control Volume
DNS	Direct Numerical Simulation
DRP	Digital Rock Physics
FPE	Fokker-Plank Equation
MRMT	Multi Rate Mass Transfer
Pe	Péclet
PTRW	Particle Tracking Random Walk
RO	Research Objective
RV	Random Variable
SMM	Spatial Markov Model
TDRW	Time Domain Random Walk
TTA	Training Trajectory Approach
fADE	Fractional Advection Dispersion Equation
gCLT	Generalized Central Limit Theorem
gME	Generalized Master Equation

i.i.d.	Independent and Identically Distributed

Subscripts:

i	Running Index
d	Number of Dimensions
e	Effective (e.g., Porosity or Diffusion)
m	Molecular Diffusion
n	Number (e.g., of particles or simulation steps)

List of Figures

Abstract

Transport through porous media affects our daily life as it is relevant for biological processes, technical applications, and our drinking water supply. The focus of this thesis lies on transport through porous geologic media. Porous geologic media are highly relevant for our drinking water supply since porous sub-surface aquifers are the most important resource of drinking water. To optimally protect or operate this resource, we need to better understand and simulate transport in porous media.

Traditionally, advective-diffusive transport through porous media is described by Fickian transport laws, which consider transport as an independent stochastic process. The assumption of independence is very strong but frequently not true because process dependence affects the motion of solute particles over many scales. Process dependence (e.g., the typical residence time of particles in slow or fast velocity zones) is the reason why Fickian transport schemes underestimate the concentration of dissolved transported substances especially at the front and at the tail of a measured spatial solute distribution. Hence, Fickian models systematically underpredict the residence times of solute in the catchment, and thus contradicts a secure operation of our drinking water supply.

Many studies show that process dependence causes the non-Fickian evolution of the dissolved plumes. Therefore, the main hypothesis of this work is:

Main Hypothesis: Extracting and reflecting process dependence is the key to understand and simulate transport in porous media.

Recent advances in X-ray tomography made it possible to describe advective-diffusive transport in the pore space of micro-CT images with a high degree of accuracy. Digital rock physics (DRP) allow us to simulate particle transport through the pore space very close to reality. From these simulations, we obtain particle trajectories in very high resolution (10^{-6}m), which we can use, for instance, to extract process dependence.

The access to such detailed information about particle motion and the relevance of process dependence triggers my overall research question:

Research Question: How can we use the latest advances of DRP best to better understand and simulate transport in porous media?

In this thesis, I provide a framework to answer this question by addressing the following three **research objectives**: (RO1) Gain detailed process understanding, (RO2) improve predictions with data-driven techniques, and (RO3) obtain a generalized model formulation. As approach to address these objectives, I propose a novel technique to analyze particle motion (RO1), and two approaches that overcome some significant shortcomings of current simulation tools (RO2) and transport models (RO3).

These **approaches** follow below:

Copula-based analysis framework (RO1): One of the most interesting questions is to ascertain the time scales at which it is possible to describe transport as a statistically independent process. Therefore, I study the mechanisms for evolution and then the decrease of non-Fickianity as a function of increasing time. Adopting the Lagrangian perspective, I provide a nonlinear copula analysis of advective-diffusive processes by analyzing particle trajectories in a real porous medium. First, I analyze the memory effects between time-consecutive particle position increments and cross dependence between longitudinal and transversal particle position increments. Second, I investigate the influence of the Péclet regime on the temporal evolution of dependence.

Training Trajectory Approach (RO2): I propose a spatial Markov model to simulate transport in three-dimensional complex porous media flows. The methodology is inspired by the concept of training images (obtain from DRP-data) from geostatistics which reflect higher-order dependence in space. Instead of using a training image, I use highly-resolved training trajectories from which I sample increments in my random walk model. To reflect higher-order processes, subsequent increments are correlated.

Adaptive Time Domain Random Walk (RO3): I propose a time domain random walk (TDRW) method with velocity correlation that is pa-

rameterized only by properties of the velocity field. I demonstrate implementation of correlation by sampling the velocity distribution in a micro-CT image of a given DRP data set where subsequentially sampled velocities are dependent. In each simulation step, I draw corresponding waiting times from an appropriately chosen probability distribution that reflect the effect of advection and diffusion on particle motion. The proposed TDRW simulates the evolution and decay of non-Fickian transport by simulating correlation itself not just its effects.

The **contributions**, **novelties** and **conclusions** in each approach are as follows:

Copula-based analysis framework: It is not always straightforward to draw meaningful conclusions from a classical copula analysis. Therefore, I extended the traditional copula framework to facilitate the interpretation of the results. The extended copula-based analysis framework suggests (1) that the analysis of particle motion through porous media in spherical coordinates is more beneficial than using Cartesian coordinates as it is physically more sound and intuitive. (2) Cross-dependence between longitudinal and transversal particle position increments is persistent over the investigated range of time increments, even though this aspect has been neglected up to date. (3) Lower Péclet numbers lead to a weaker dependence that is, however, more persistent over time than in higher-Péclet transport regimes. Altogether, the outcomes clearly demand that process dependence has to be incorporated into the simulation tools.

Training Trajectories Approach: Process dependence is incorporated into the training trajectory approach directly via re-sampling the original trajectory that contains all information about dependence (see main hypothesis). This training trajectory approach overcomes three common shortcomings of spatial Markov models: (1) I simulate finite-Péclet transport in three dimensions without commonly made simplifications (e.g., dimensionality reduction, neglecting diffusion). (2) I do not parameterize dependence via a high-dimensional transition matrix. (3) I simulate transport at the spatial resolution of the (highly-resolved) training trajectories, which can be important for processes such as mixing and reaction. In summary, the novel implementation of process dependence directly

into the re-sampling mechanism is successful and enables the simulation of particle motion in full complexity.

Adaptive Time Domain Random Walk: For the adaptive TDRW, we no longer need a transport simulation for parameterization. We only need the properties of the velocity field. This brings us one step closer towards using only the properties of the pore geometry to parameterize a transport model. In essence, the adaptive TDRW not only extends current TDRW frameworks, but it also enables us to scale transport across Péclet regimes. This is a significant generalization of the current simulation frameworks.

In sum, these three approaches provide the answer to my research question of how can we use DRP best to better understand and simulate transport. All proposed methods employ DRP-data in a novel way and this results in a powerful analysis tools, a fully predictive simulation technique, and a generalized model formulation that all overcome significant shortcomings.

The main overall conclusion is that the key to understand and simulate transport in porous media is indeed to extract and reflect process dependence. With improved process understanding, modeling tools, and predictive models for advective-diffusive transport in porous media, it will be possible to better safeguard our subsurface water quality, and hence to protect our key source of safe drinking water.

Kurzfassung

Transport in porösen Medien spielt in unserem Alltag eine wichtige Rolle. Biologische Prozesse, technische Anwendungen aber auch unsere Trinkwasserversorgung hängen direkt von Transportprozessen in porösen Medien ab. Der Fokus dieser Arbeit liegt auf Transportprozessen in geologischen porösen Medien. Geologische poröse Medien sind besonders für unsere Trinkwasserversorgung relevant, da poröse Grundwasseraquifere unsere wichtigste Trinkwasserresource darstellen. Um diese besser zu schützen und zu bewirtschaften müssen wir Transportprozesse in porösen Medien zum einen besser verstehen und zum anderen genauer modellieren.

Traditionell beschreiben wir advektiv-diffusiven Transport im porösen Medium mit Fickschen Transportgesetzen, welche den eigentlichen Transportprozess als einen unabhängigen stochastischen Prozess verstehen. Dabei handelt es sich um eine sehr starke Annahme, die in vielen Fällen nicht zutrifft, da Prozessabhängigkeit (die typische Aufenthaltszeit von gelösten Stoffen in schnellen oder langsamen Bereichen des Grundwassergeschwindigkeitsfeldes) die Ausbreitung der Partikel über viele Skalen beeinflusst. Deshalb unterschätzen Ficksche Modelle auch die Verweilzeit der gelösten Stoffe (z.B. eine Kontamination) im Einzugsgebiet des Brunnen systematisch, was einer sicheren Trinkwasserversorgung gänzlich im Weg steht.

Viele Untersuchungen haben ergeben, dass Abhängigkeiten im Transportprozess die nicht-Ficksche Ausbreitung der Kontamination verursachen. Das legt folgende Hypothese nahe:

Hypothese: Der Schlüssel zu besserem Verständnis von Transportprozessen und zu besseren Transportmodellen ist die Extraktion und die Reflektion der Prozessabhängigkeit.

Seit relativ kurzer Zeit können wir mit Hilfe der Mikro-Computertomographie Transportprozesse im Porenraum sehr genau beschreiben. Digital Rock Physics (DPR) (=digitale Gesteinsphysik)

ermöglicht uns, die Bewegung von gelösten Partikeln durch den Porenraum sehr exakt zu simulieren. Aus diesen Simulationen können wir sehr detaillierte Partikeltrajektorien generieren, die wir dann wiederum nutzen können um die Prozessabhängigkeit zu extrahieren. Der Zugang zu solch detaillierte Informationen über die Partikelbewegung und die Relevanz der Prozessabhängigkeit drängen folgende Frage auf:

Forschungsfrage: Wie können wir die neuesten Errungenschaften der DRP optimal nutzen, um den Transport in porösen Medien besser zu verstehen und zu modellieren?

Diese Frage möchte ich mit dieser Arbeit beantworten und zwar indem ich die folgenden **Forschungsziele** erfülle: (1) Zugewinn an Prozessverständniss, (2) Verbesserung der Vorhersagen mit datengetrieben Methoden und (3) Generalisierung existierender Transportmodelle. In Summe liefert die Erfüllung dieser Forschungsziele die Antwort auf meine Forschungsfrage.

Als Methoden zur Erreichung meiner Ziele, stelle ich hier einen neuartigen Ansatz vor, um die Partikelbewegung statistisch zu erfassen und außerdem zwei Simulationsansätze, welche einige Defizite gegenwärtig angewandter Simulationsmethoden überwinden:

Copula-basierte Analysemethode: Eine der interessantesten Fragen ist es, die Zeitskalen zu untersuchen über die wir den Transport im porösen Medium tatsächlich als stochastisch unabhängigen Prozess beschreiben können. Deshalb untersuche ich die Mechanismen, welche zur Entwicklung und im Anschluss wieder zum Abbau nicht-Fickscher Charakteristiken führen. Dazu stelle ich eine Analysemethode vor, welche die nicht-lineare Abhängigkeit eines advektiv-diffusiven Transportprozesses in einem realen porösen Medium (Doddington Sandstein) extrahiert. Zum einen analysiere ich die Prozessabhängigkeit anhand zeitlich aufeinanderfolgenden Partikelverschiebungen (räumliche Inkremente). Zum anderen untersuche ich den Einfluss des Péclet Regimes auf die zeitliche Entwicklung der Abhängigkeit.

Training Trajectory Approach: Hier stelle ich ein räumliches Markov Modell (spatial Markov Model) vor, um Transport in komplexen dreidimensionalen porösen Medien zu simulieren. Die Methode ist eng

mit dem Training Images (Trainingsbilder) Konzept aus der Geostatistik verwandt. Anstatt Training Images nutze ich hoch-aufgelöste Trainingstrajektorien (aus DRP-Daten), von welchen ich zufällig gewählte Segmente für mein Random Walk Modell verwende. Die hochdimensionale Prozessabhängigkeit bilde ich dadurch ab, dass aufeinanderfolgende Segmente korreliert sind.

Adaptiver TDRW: Außerdem stelle ich eine Time Domain Random Walk Methode vor, welche Prozessabhängigkeit abbildet und welche nur mit den Eigenschaften des DRP-Geschwindigkeitsfeldes parametrisiert werden kann. Prozessabhängigkeit wird durch systematisches Ziehen aus der Geschwindigkeitsverteilung implementiert, wobei aufeinanderfolgende Geschwindigkeiten korreliert sind. In jedem Simulationsschritt ziehe ich die jeweiligen Wartezeit (inverse Geschwindigkeit) aus einer geeigenten Wahrscheinlichkeitsverteilung, um den Effekt von Advektion und Diffusion auf die Partikelbewegung abzubilden. Der adaptive TDRW simuliert die Entwicklung und den Zerfall der nicht-Fickschen Charakteristiken in dem Korrelation selbst modeliert wird, nicht nur deren Effekt.

Die wissenschaftlichen Beiträge, Neuerungen und Schlussfolgerungen der jeweiligen Methode sind im Folgenden zusammengefasst:

Copula-basierte Analysemethode: Es ist nicht immer trivial stimmige Rückschlüsse aus einer Copula-Analyse zu ziehen. Deshalb habe ich die klassische Copula-Theorie dahin gehend weiterentwickelt, dass die Interpretation der Analyse sehr viel intuitiver ist. Die Copula-basierte Analyse zeigt deutlich, (1) dass eine Beschreibung der Partikelbewegung durch das poröse Medium in sphärischen Koordinaten (anstatt in kartesischen) intuitiver und physikalisch stimmig ist, (2) dass Kreuzabhängigkeit zwischen longitudinaler und transversaler Partikelverschiebung über die gesamte untersuchte Zeitskala bestehen bleibt und (3) dass niedrigere Péclet Zahlen zu einer schwächeren Abhängigkeit führen, die jedoch über eine längere Zeit bestehen bleibt als für höhere Péclet-Zahlen. Insgesamt, weisen die Ergebnisse klar darauf hin, dass Prozessabhängigkeit ein elementarer Bestandteil der Modelle sein muss.

Training Trajectory Approach: Prozessabhänigkeit ist beim Training

Trajectory Approach direkt in einen konditionellen Selektionsprozess des anschließenden Segments integriert, welches die gesamte Information über die Prozessabhängigkeit beinhalten. Mit dem Training Trajectory Approach überwinde ich folgende Defizite: (1) Ich simuliere Transport im drei-dimensionalen Medium ohne die üblichen Vereinfachung (z.B. Dimensionsreduktion oder das Vernachlässigen der Diffusion). (2) Ich parametrisiere Prozessabhängigkeit nicht mittels Transitionmatrix. (3) Ich simuliere Transport in der selben (räumlichen) Auflösung, in der die Trainingstrajektorien aufgelöst sind. Eine solch hohe Auflösung spielt eine wichtige Rolle für Prozesse wie Verdünnung, Mischung oder Reaktionen, welche auf dieser Skala stattfinden. Die neuartige Implementierung der Prozessabhängigkeit ist erfolgreich und ermöglicht uns den Transport in seiner ganzen Komplexität zu simulieren.

Adaptiver TDRW: Anstatt eines Transportmodels brauchen wir zur Parametrisierung des adaptiven TDRWs lediglich die Eigenschaften des Geschwindigkeitsfelds. Das wiederum ist ein Schritt näher an einer Parametrisierung nur über die Eigenschaften der Porengeometrie. Der hier vorgestellte adaptive TDRW erweitert gegenwärtige TDRWs nicht nur, vielmehr ermöglich er uns den Transportprozess durch verschiedene Péclet-Regime zu skalieren. Das ist eine signifikante Generalisierung bestehender Modelle.

Ziel dieser Arbeit ist es meine Forschungsfrage zu beantworten und meine Haupthypothese zu testen. Die drei beschriebenen Ansätze bilden in Summe die Antwort auf meine Forschungsfrage, wie wir DRP am besten nutzen, um Transport im porösen Medium besser zu verstehen und zu simulieren. Alle präsentierten Methoden verwenden die DRP-Daten in annähernd optimaler Art und Weise. Das wiederum resultiert in sehr leistungsfähigen Analyse- und Simulationsmethoden mit denen wir unsere Modelle signifikant verbessern können.

Die hauptsächliche Schlussfolgerung dieser Arbeit ist, dass der Schlüssel zum Verständnis und zur Simulation von Transportprozessen im porösen Medium tatsächlich das Extrahieren und die Reflektion von Prozessverständnis ist. Mit einem besseren Prozessverständnis, Vorhersagen und Modelen für advectiv-diffusiven Transport in porösen Medien, können wir die Grundwasserqualität besser bewahren und gle-

ichzeitig können wir das Grundwasser, als wichtigeste Trinkwasserressource, besser schützen.

Part I

Prologue

Chapter 1

Introduction

Part I may contain similar and/or identical formulations from my publications *Most et al.* (2016) [86]. I omit a clear identification for readability and use parts of the article by kind permission of the publisher WRR.

1.1 Motivation & Goal

Transport through porous media affects our daily life; for instance in biological applications (e.g., root water uptake [61, 100], uptake of pharmaceuticals [1, 52, 88, 135]). We exploit the properties of porous media in technical applications (e.g., fuel cells [7, 31, 96], filter [48, 101]), and it is of crucial relevance for us in (hydro-)geological applications. This thesis focuses on hydro-geological applications for which a detailed understanding of the underlying transport process is essential to achieve secure drinking water supply from groundwater aquifers [25, 56, 58], for subsurface contaminant remediation [32, 136], for reservoir engineering [68, 91, 94], for carbon dioxide storage [59, 92, 130], or for nuclear waste storages [2, 95, 137].

Transport processes in porous media are highly relevant in our everyday life but also for the economy and society. Computer-based transport simulations become more and more indispensable to better understand the driving forces of transport and to optimally operate the respective application of transport through porous media. With this thesis I want to *deepen the understanding of transport in porous media* by proposing analysis and simulation techniques that improve state-of-the-art methods to

model and predict transport in porous media at small yet fundamental scales.

Even though solute transport is driven only by two relatively simple processes - advection and diffusion - we observe a surprisingly complex spatial distribution of transported solutes due to the interplay of advection and diffusion through the complex pore structure [21]. Via digital rock physics (section 2.4), we obtain the pore geometry in a very high resolution through which we can then simulate transport very accurately. Due to computational limitations, however, we cannot run large-scale transport simulations at a resolution scale that resolves all relevant detail of the pore space, and hence of the transport process [18, 87]. Unfortunately, fine-scale properties (e.g., stagnant zones or high-velocity channels) significantly affect the spatial solute distribution at the macro-scale [20, 27, 74]. Nonetheless, we are interested predominately in macro-scale transport simulations (e.g., the (centi-) meter or kilometer scale). At that scale, we are forced to describe the effects of the unresolved, sub-pore scale at a larger scale without explicitly simulating the small-scale process. Such a derivation of large-scale behavior from small scale principles is called upscaling. The accurate representation of the sub-scale effects without explicitly modeling them is the primary challenge for upscaling transport in porous media.

Upscaled transport in porous media is traditionally described with Fickian transport laws that understand transport as a normal (or Gaussian) process with drift. The normal process represents approximately the effect of the unresolved sub-scale onto transport. The Eulerian advection-dispersion equation (ADE) represents transport as the temporal evolution of a spatially discretized concentration field. Alternatively, Lagrangian methods discretize the solute mass into a number of mass-containing particles and describe transport as the temporal and spatial evolution of particle positions. The ADE is a deterministic equation that can be viewed as describing the probability density equation for the positions of Lagrangian particles in a continuum [112]. Essentially, the ADE, and its Lagrangian counterpart, the Fokker-Plank equation (FPE), describe the same process and converge to the same solution for an infinitesimal spatial discretization and an infinite number of particles.

For my purpose of improving dispersion models, the Lagrangian perspective (section 1.3.1) is beneficial because Eulerian methods describe transport only as the evolution of a concentration field. The concept of concentration automatically implies a volumetric average that causes numerical and conceptual dispersion. Numerical dispersion is a systematical over-prediction of solute dilution. The same holds for conceptual dispersion, which automatically arises from volume averages. Both is very problematic when we consider mixing and reaction process. Lagrangian approaches, in contrast, do not suffer from numerical or conceptual dispersion. When we apply Lagrangian methods, we have the opportunity to represent the effect of the unresolved sub-scale in the advective term where spreading and its effects have its origin.

Independent from using an Lagrangian or Eulerian approach, many (or most) models that apply Fickian transport laws (e.g., the ADE or FPE) to simulate transport through porous media (laboratory [6, 75, 85, 118, 119, 122] or field experiments [35, 55, 117, 124, 139]) significantly underestimate the concentration at the tails of the concentration distribution. Fickian transport models cannot capture the characteristic asymmetry of such concentration distributions. Transport processes that go beyond Fickian transport laws are known as anomalous, pre-asymptotic, non-Gaussian or as non-Fickian. But from where does this anomalous behavior come from?

Transport is driven only by diffusion and advection. Therefore a normal process with drift is the correct process description. This is true for simulations at a simulation scale below the size of the governing heterogeneities [15], which means that the typical particle displacement per simulation step does not exceed the size of the heterogeneity. At this simulation scale, the advective velocity of each particle stays constant throughout each simulation step, and that is why we can consider the medium (i.e., the velocity field) as a continuum without sub-scale heterogeneities in which transport follows indeed a normal process with drift [9, 39, 112].

When we simulate transport at a simulation scale beyond the size of the heterogeneity, a particle (per simulation step) experiences a large variety of velocities along its trajectory segment. At that scale, we cannot

consider the medium as a continuum anymore. If we apply Fickian transport laws at that larger scale, the normal process does not only have to represent diffusion; it also has to compensate for all the unresolved, sub-scale features of the velocity field that affect transport. This goes beyond the capabilities of a normal process that cannot describe sub-scale effects such as trapping in dead-end pores or particles within a fast flow channel. These effects result in a highly skewed displacement distribution (per simulation step) which cannot be represented by a normal distribution.

Interestingly, at much larger scales, a normal process with drift becomes the valid process description again. At some scale, a particle's velocity distribution sampled along its trajectory does not depend anymore on its initial condition [112]. This is the scale at which transport can be seen as the sum of an independent and identical (not normally) distributed (i.i.d.) random variable (RV) that converges, according to the central limit theorem (CLT), to its asymptotic normal limit distribution. At that scale (in main flow direction) at which the displacement distribution has converged to the normal distribution, the porous media effectively again acts as a continuum where we can describe transport with Fickian transport laws.

Following this argumentation, we can conclude that Fickian modeling approaches are either valid at simulation scales below the size of heterogeneity or at a scale large enough for the CLT to converge. This property is unfortunate for two reasons. Firstly, computational limits prohibit macro-scale simulations at very high resolution. Secondly, many studies indicate (or found) that the heterogeneity of porous media, especially of porous geologic media, prohibits the convergence to the asymptotic normal limit distribution [35, 112, 138]. Usually, we are interested in simulation domains that are far beyond the scale of heterogeneity, e.g., (centi-) meter-to-kilometer scale for transport in groundwater aquifers where the scale of heterogeneity is at the sub-pore scale. Thus, the scale in which we are most interested in either (a) cannot be simulated by Fickian transport models because of computational limitations or (b) transport described as a normal process with drift at the larger scale would distinctively oversimplify the process.

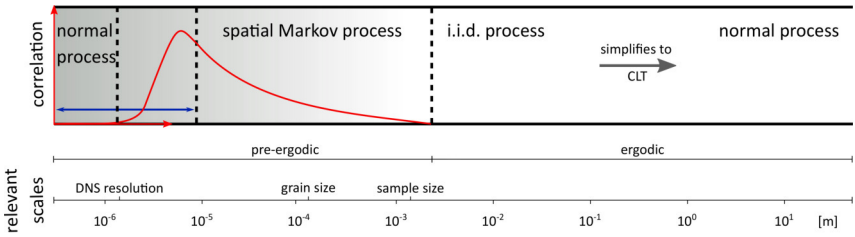

Figure 1.1: Sketch of the herein relevant scales together with the underlying correlation structure (marked in red). At the small scale without correlation, transport follows a normal process with drift. At the larger scale where correlation has just vanished, transport follows an ergodic (or i.i.d.) process that converges according to the CLT to a normal process with drift. At the scale where correlation decays exponentially, transport can be described as a spatial Markov process. Yet, this is the lower resolution limit for surrogate models. Below that scale (marked by the blue arrow), surrogates linearly interpolate the particle path between simulation steps.

While we have to accept computational limits, we can generalize Fickian transport methods. Therefore, a large variety of pre-asymptotic or non-Fickian transport models exist. Exemplary Eulerian methods are multi-rate mass transfer (MRMT) [57, 77] or the fractional advective dispersion equation (fADE) [12, 112]. Both methods generalize the ADE so that we can simulate strongly-tailed spatial concentration distributions that are caused by the medium-specific heterogeneity. Lagrangian approaches to model pre-asymptotic transport are continuous-time random walks (CTRW) or spatial Markov models (SMM).

Even if all approaches generalize Fickian simulation techniques, there is one fundamental difference between the mentioned pre-asymptotic simulation approaches. MRMT, fADE, and CTRW consider transport as an stochastic process with independent increments which is only valid at scales at which dependence (e.g., the memory of speed) has vanished. In contrast, spatial Markov models can be applied below that scale because process dependence is taken into account.

A process with independent increments demands a minimum scale to ensure total loss of memory; below that scale transport does not follow an independent stochastic process. This in very inconvenient, especially if we are interested in processes (e.g., mixing and reaction processes) that occur at very fine scales below that scale of independence.

SMMs account for the process dependence that is the reason for emerging non-Fickian effects. Thus they are valid at much smaller scales than CTRWs. Therefore, spatial Markov processes are most promising if we want to (a) simulate the mechanisms (e.g., memory of speed and direction) that cause non-Fickian transport and (b) if we want to do that efficiently enough to enable macro-scale simulations.

However, to the best of my knowledge, current SMMs are not yet applied to advective-diffusive transport problems within real three-dimensional porous media. One possible reason for that is that current SMMs require a high-dimensional transition matrix, which is difficult to parameterize. In general, the parameterization of the transition matrix requires a highly resolved simulation of particle motion (e.g., a direct numerical simulation; section 2.4), which is computationally expensive and has to be re-done when parameterizing the transition matrix for another transport (Péclet) regime (e.g., with less advection).

Nonetheless, spatial Markov models inherently reflect process dependence that causes the non-Fickian characteristics. This is why SMMs are in an excellent position to simulate the mechanisms (i.e., the memory of speed and direction at the sub-pore scale) that lead to non-Fickian transport. However, yet SMMs rely on transition matrices that are hard to parameterize and that cannot be scaled across Péclet regimes for any porous medium. Furthermore, SMMs derive the particle paths between the states as a linear interpolation. Small-scale processes (i.e., dilution, mixing, and reaction) requires more than just the average location of a particle as they are nonlinear processes. These three shortcomings are central to my thesis and are directly linked with my research objectives.

1.2 Main Hypothesis, Research Question & Objectives

Digital Rock Physics (DRP) is a relatively new scientific technique that uses highly-resolved images of the pore-scale geometry provided by X-ray tomography to numerically simulate transport distinctively below the size of the governing heterogeneities [3]. From this pore-scale image, we can derive (via the Navier-Stokes equation) the pore-scale velocity field in which we can run a particle tracking random walk (PTRW) simulation. The PTRW generates fine-scale particle trajectories by a sequence of advective and diffusive displacements. Simulations that follow that procedure are known as direct numerical simulations (DNS) of pore-scale transport (see section 2.4).

Studying particle trajectories during advective-diffusive transport through natural rocks is greatly facilitated by having such detailed information on pore-scale geometry. These particle trajectories contain all information about the dependence structure that controls particle motion through porous media. The term *dependence structure* can be understood as the characteristic residence time a particle stays within a specific velocity quantile, for instance in a slow zone. The access to such highly-resolved particle trajectories suggests to analyze the information contained in the trajectories thoroughly. Therefore, the main hypothesis of this work is:

Main Hypothesis: Extracting and reflecting process dependence is the key to understand and simulate transport in porous media.

Many studies use the information provided by DRP (e.g., [23, 42, 63, 81]), but this information can be exploited beyond what has been done so far. This raises the question:

Research Question: "How can we use the latest advances of DRP best to better understand and simulate transport in porous media?"

This thesis provides a framework to answer this question by addressing the following three research objectives:

RO1 Gain detailed process understanding:
Process dependence is the key to understand non-Fickian transport. Hence, objective one is to *extract the governing dependence structure* from the DNS-trajectories, which incorporates all relevant information about transport to design spatial Markov models.

RO2 Improve predictions with a data driven technique:
So far, spatial Markov models are currently not applied to advective-diffusive transport through real three-dimensional porous media. Research objective two is therefore to design a SMM *without* using classical techniques to parameterize a Markov process (i.e., a transition matrix), which can act as an obstacle to generalize SMMs to three dimensions. Current SMMs represent the particle path between states simply as a linear interpolation. This is not sufficient when considering small scale processes like dilution or reaction. Therefore I aim to provide a more realistic description of particle trajectories.

RO3 Obtain a generalized model formulation:
Classically, SMMs require transport simulations (e.g., DNS) to parameterize the Markov process. As a consequence, the resulting SMM is only valid for this particular transport (Péclet) regime. Research objective three is, therefore, a transport simulation that can *scale the transport process across Péclet regimes* without requiring another DNS transport simulation at the Péclet number of interest.

1.3 Approaches & Advances

In this section, I introduce the overall perspective onto transport that is adapted in this work (i.e., the Lagrangian approach). Then, I introduce the approaches that address the research objectives. This is followed by the advances made in this this work, before I finish this section with the general structure of this thesis.

1.3.1 The Approaches

The Lagrangian Perspective on Transport

As indicated before, we can describe transport from the Eulerian or the Lagrangian perspective. Both approaches describe the same processes, but Eulerian methods are disadvantageous because they rely on a spatial discretization of the simulation domain which subdivides the domain into control volumes (CV). Transport is then simulated as advective-diffusive mass flux across these control volumes. The concept of control volumes is inherent to Eulerian methods as well as the assumption of complete mixing within the CVs. This is problematic because the solute plume is considered to occupy the whole CV instantly, even if the solute has just arrived at the inlet face of the CV.

I call this effect conceptual dispersion, which is amplified by numerical artifacts that result in additional numerical dispersion and it systematically overestimates the spatial distribution of solutes. In specific, this artificial dispersion is highly inappropriate when we have to consider small-scale processes (e.g., dilution, mixing or reaction), where an overprediction of dispersion can easily result in a significant overprediction of mixing and reaction rates [66]. In general, numerical and conceptual dispersion, as systematic error components, are obstructive, when we want to develop better dispersion models (see RO2 and RO3).

Lagrangian methods, instead, discretized the solute mass into a large number of particles, which does not involve control volumes at all. Therefore, these methods do not suffer from artificial dispersion. This is an important feature and the reason why Lagrangian methods are the better approach to fulfill research objectives two and three.

A1: Understanding transport via copulas and hybrid copulas

My first research objective (RO1) is to gain process understanding, which is assumed to be the key to improve the accuracy of our transport mod-

els. In most cases, process dependence affects particle motion through porous media. Additionally, the magnitude of dependence between consecutive velocities (i.e., now and later) depends on the particle velocity, for instance, the velocity of slow particles are correlated over a larger temporal scales than as those of fast particles.

This kind of dependence goes beyond correlation, which merely expresses linear dependence. Copulas, that extend correlation to higher-order dependence, are designed to express this quantile-specific dependence. Copulas are very powerful, when the marginals are heavily tailed and when the random variables can be ranked. Both conditions apply to the distribution of the absolute particle velocities, especially when heterogeneity is strong. For that reason, I choose copulas to better understand memory of speed (absolute velocity now vs. later).

The description of particle motion in three dimensions, however, is more intuitive in a spherical than in a Cartesian coordinate system, where the angles naturally constrain the tailing and where a unique ranking of angles does not make sense ($-180^\circ = 180^\circ$). In this case, the straight copula theory is not entirely helpful. Therefore, I propose a second approach, the hybrid copulas (introduced in chapter 3), to exploit the advantages of copulas, even if angles are involved in the description of particle motion.

A2: A data-driven approach to simulate transport

My second research objective (RO2) is to develop a model that simulates advective-diffusive transport through a real three-dimensional porous media. For that objective, I use a fully data-driven approach that is inspired by the concept of training images, known from geostatistics. Instead of using a training images, I use the highly-resolved DNS trajectories that act as training trajectories.

The overall assumption herein is that all information about the dependence (memory of speed and direction) is an inherent property of the particles' trajectories. Hence, the main concept of the training trajectory approach (TTA) is to (a) cut DNS-trajectories (=training trajectories) into

segments that are then (b) re-arranged in an appropriate manner in order to (c) built segments with the same process dependence pattern as the training trajectories.

The key to obtaining realistic trajectories - and the transition rule for the involved Markov process - is to ensure smooth transitions in velocity and direction at the transition from one to the other trajectory segment. The whole training trajectory approach does not require a transition matrix at all and it provides a detailed description of particle trajectories beyond a linear interpolation. In combination, this fulfills research objective two (see section 4).

A3: A process-driven approach to simulate transport

My third research objective (RO3) is to develop a model that scales transport across different transport (Péclet) regimes. Usually, we need a fine-scale transport simulation (e.g., DNS) to parameterize an upscaled transport simulation (e.g., a SMM). However, this parameterization is only valid for the transport regime at which we performed the DNS.

In the workflow of DNS, it is the velocity field that is scaled when transport should be simulated at another Péclet number. I, essentially, do the same. Instead of using the full DNS to parameterize the SMM, I only use the DNS-velocity field that is scaled to simulate transport across different Péclet regimes.

The actual transport simulation is inspired by how particles move through the velocity field. The particles adapt many different advective velocities over time, what I interpret as a sampling process. Therefore, I simulate transport by sampling systematically from the velocity distribution function. The velocity distribution function, from which I draw the particle velocities, is parameterized by the DNS-velocity field.

Then, the velocity of each particle determines the distribution from which I draw the advective-diffusive transit time per simulation step. I draw transit times from an exponential if diffusion dominates and from an inverse Gaussian distribution if advection controls particles motion.

This reflects the underlying physics much closer than other model that merely approximate the transit time distribution. This process-driven approach is again designed as a spatial Markov model, which is parameterized only by properties of the velocity field 5).

The Advances

The purpose of this work is to better understand and simulate transport in porous media. In this context, I make three significant advances:

1) Higher-order Dependence Analysis: According to RO1, I provide a framework for a detailed *analysis of the higher-order process dependence* of an advective-diffusive transport process in real porous media. Furthermore, I extend the copula framework to analyze particle motion also in spherical coordinates as this perspective is closer to the underlying physics (chapter 3). This analysis framework provides detailed process understanding that acts as the basis for the upcoming modeling exercises.

2) Fully-complex Transport Simulation: According to RO2, I develop a simulation approach that *simulates transport in full complexity* by resampling segments of the DNS-trajectories (=training trajectories). Instead of using transition matrices to parameterize the Markov process, I use a physically motivated transition rule to produce trajectories that are smooth in velocity and direction (i.e., no infinite acceleration and edges). By doing so, we obtain trajectories that reveal very similar statistics than the original trajectories.

While the resolution of other SMMs is limited from below (chapter 4), the TTA reflects particle motion at the resolution of the DNS input data. Such a high resolution is relevant for small-scale processes such as dilution, mixing, or reaction. To better assess the veracity of the TTA, also with regards to the small-scale processes, I propose a novel analysis technique that focuses on the interaction of particles instead of analyzing the ensemble of single particles (e.g., particle arrival time statistics or spatial particle distribution).

3) Generalized Model: According to RO3, I propose a *generalized simulation framework* that scales transport across Péclet regimes. Classically, we need a transport simulation to parameterize a surrogate model. The model I propose goes one step back - it requires solely the velocity field, which can easily be scaled across Péclet regimes (section 2.4). The re-scaled velocity field is then used to simulate transport at transport regimes of arbitrary Péclet number (chapter 5).

1.4 Structure of the Work

The thesis is divided in three parts:

Prologue Part I consist of two chapters. In chapter 1.1, I already gave the introduction to the topic and its relevance. In specific I introduce the main hypothesis, the main research question and the three research objectives. This is followed by an overview of the applied approaches and by an overview of the advances of this work.

In the upcoming chapter 2, I thoroughly describe the state-of-the-art to simulate transport in porous media.

Contributions Part II is subdivided in three chapters. In each chapter, I address one research objective by proposing an analysis tool (chapter 3) and a simulation tool (chapter 4) and a modeling framework (chapter 5), respectively.

Each chapter not only describes the respective analysis or simulation approach. Each chapter also presents at least one contribution to overcome some of the current shortcomings of existing analysis or simulation tools.

Summary and Conclusions In part III, I thoroughly summarize the main contributions, then I provide an outlook before I finally draw my conclusions.

Chapter 2

State of the Art & Existing Methods

In chapter 2, I introduce state-of-the-art modeling and analysis tools to simulate and describe transport in porous media, respectively.

Models and simulation tools for transport in porous media are often subdivided into Fickian and non-Fickian methods. In section 2.1, I outline Fick's first law of diffusion and I introduce some simulation schemes that apply Fick's law to model transport through porous media. Next, I discuss the limitations of Fickian transport descriptions (section 2.1.5 - 2.2) and introduce some simulation schemes that can be applied to non-Fickian transport.

Whether we have to use Fickian or non-Fickian modeling schemes depends on the statistics of (solute) particle motion or, more specifically, on its dependence structure (i.e., the typical residence time of solute particles in fast or slow velocity zones). It is not trivial to describe process dependence thoroughly, and therefore I introduce some useful analysis frameworks for complex dependence in section 2.3.

To perform such an advanced transport analysis, I need access to very accurate information about particle motion. I obtain this information via direct numerical simulation (DNS) of particle motion within a highly-resolved, three-dimensional micro-CT image of the pore space of a Doddington sandstone sample conducted at Imperial College, London [21]. In section 2.4, I briefly describe the general workflow to obtain this data.

2.1 Fickian Transport

In this section, I first introduce Fick's first law which is the basis to describe transport in porous media. Next, I introduce the advection-diffusion equation (section 2.1.2) and advection-dispersion equation (section 2.1.3), which can be seen as the classical way of describing transport processes through porous media. Both adopt the Eulerian perspective. In section 2.1.4 I outline how to describe the ADE from the Lagrangian perspective as a particle tracking random walk.

2.1.1 Fick's First Law

Fickian transport describes the evolution of the solute concentration in the system by applying Fick's first law of diffusion. Fick's first law relates the isotropic diffusive flux to the concentration under the assumption of steady boundary conditions. It postulates that the diffusive flux $\mathbf{J}_\mathrm{D}$ $\left[MT^{-1}L^{-2}\right]$ goes from regions of high concentration to regions of low concentration, with a magnitude that is proportional to the concentration gradient

$$\mathbf{J}_\mathrm{D} = -D_\mathrm{m}\nabla c \tag{2.1}$$

with D_m $\left[L^2T^{-1}\right]$ $\in$ $\mathbb{R}_+^{1\times 1}$ as the proportionality coefficient and ∇c $\left[ML^{-d-1}\right]$ as the concentration gradient in d-dimensions.

Solute particles exhibit random motion on the molecular level and this random motion levels out concentration gradients over time [34]. The efficiency of leveling out concentration gradients (and hence the strength of diffusion) is quantified by the molecular diffusion coefficient D_m. Thus can be examined by a simple finite-difference model:

Imagine we have two rectangular control volumes (CVs) $z \in \{a, b\}$ and we have a number of particles M_z in each of the CVs, e.g., $M_a = 2$ particles in CV a (Figure 2.1). The concentration in each CV is given by $c_z = \frac{M_z}{\Delta V}$ with $\Delta V = A\Delta x$ being the volume of the CV and A as the face of

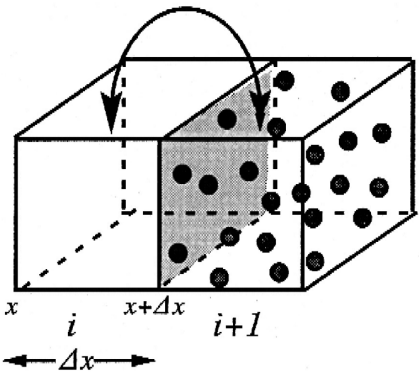

Figure 2.1: Particles diffusing between two control volumes of length Δx. Grey shaded area is the face A of the CV. Source: [112]

the CV with the edge length Δx. Diffusion is defined as a process without directional bias and therefore the rate η (jumps per time step) of jumping forward or backward is the same [34]. The average number of particles that jump in one time step Δt is then $M_z \eta \Delta t$. The diffusive flux $\mathbf{J}_\mathrm{D}$ is the net number of particles per unit area that jump between the CVs in the interval Δt:

$$\mathbf{J}_\mathrm{D} = \frac{\left(\frac{1}{2}M_a - \frac{1}{2}M_b\right)\eta}{A} = \frac{\frac{1}{2}\left(c_a - c_b\right)\Delta V \eta}{A} = \frac{1}{2}\left(c_a - c_b\right)\eta \Delta x \qquad (2.2)$$

As $c_a - c_b$ is equivalent to $c\left(x + \Delta x, t\right) - c\left(x, t\right)$, the Taylor expansion in space x as a function of time t is:

$$c\left(x + \Delta x, t\right) = \sum_{n=0}^{\infty} \frac{\partial^n c\left(x, t\right)}{\partial x^n} \frac{\Delta x^n}{n!} = c\left(x, t\right) + \frac{\partial c\left(x, t\right)}{\partial x}\Delta x + I(\Delta x) \qquad (2.3)$$

where:

$$I\left(\Delta x\right) = \frac{\partial^2 c\left(x,t\right)}{\partial x^2}\frac{\Delta x^2}{2!} + \frac{\partial^3 c\left(x,t\right)}{\partial x^3}\frac{\Delta x^3}{3!} + \ldots \quad . \tag{2.4}$$

Inserting equation (2.3) into equation (2.2) leads to:

$$\mathbf{J}_{\mathrm{D}} = \frac{1}{2}\left(\frac{\partial c\left(x,t\right)}{\partial x}\Delta x + I(\Delta x)\right)\eta\Delta x. \tag{2.5}$$

For an infinitesimal Δx, the transition from equation (2.3) to Fick's law (equation (2.1)), we require:

1. $\frac{1}{2}\Delta x^2\eta \rightarrow D_{\mathrm{m}}$
2. $\frac{1}{2}I\left(\Delta x^2\right)\eta \rightarrow 0.$

The molecular diffusion coefficient D_{m} is constant and therefore $\eta \rightarrow \infty$ when $\Delta x \rightarrow 0$. To keep D_{m} constant (as in equation 2.1), η has to increase with the same rate as Δx^2 decreases, hence Δx has to increase with $\Delta t^{1/2}$. This spatial growth with the square root of time is characteristic of (normal or Fickian) diffusion. According to Fick's first law, diffusive mass flux is a mass balance between adjacent CVs and hence the particles displacements, per simulation step must not exceed the dimension of the CV. As a consequence, the size of the CV and therefore the spatial resolution of the model has to be large enough to ensure that particles do not jump beyond the adjacent CV. Especially when the velocity contrast in the velocity field is strong, this restricts spatial resolution and might prohibit a meaningful resolution when considering smaller scale processes. This limitation will become relevant in the following.

2.1.2 The Advection-Diffusion Equation

As transport in porous media is driven by advection and diffusion, the total mass flux $\mathbf{J}\ \left[MT^{-1}L^{-2}\right]$ is the sum of the advective mass flux $\mathbf{J}_{\mathrm{A}} \in \mathbb{R}^{d\times 1}$and diffusive mass flux $\mathbf{J}_{\mathrm{D}} \in \mathbb{R}_{+}^{d\times 1}$:

$$\mathbf{J} = \mathbf{J}_\mathrm{A} + \mathbf{J}_\mathrm{D} = \mathbf{q}c - D_\mathrm{m}\nabla c, \tag{2.6}$$

where $\mathbf{J}_\mathrm{A}$ is the product of $\mathbf{q} \in \mathbb{R}^{d\times 1}$, which is the specific flux (flux per unit area) $\left[LT^{-1}\right]$ in d-dimensions, and the concentration c within the fluid.

Traditionally, we describe transport in porous media by the advection-diffusion equation (ADE) [9, 112], as the spatial distribution of the solute in a homogeneous continuum [9, 112]. We can derive the ADE by applying the principles of mass balance to the total mass flux between adjoining control volumes. Under the assumptions of complete mixing (in the CVs), incompressibility of the fluid, and a divergence-free flow field, we receive the ADE:

$$\frac{\partial c^*}{\partial t} + \nabla\mathbf{J} = \ldots = \frac{\partial c}{\partial t} + \mathbf{v}\nabla c - \nabla\cdot(D_m\nabla c) = 0, \tag{2.7}$$

where $c^* = c \cdot n_\mathrm{e}$ with n_e $[-]$ the effective porosity, and $\mathbf{v}$ $\left[LT^{-1}\right]$ the d-dimensional velocity vector. For further detail about the derivation of equation 2.7, I recommend *Bear* (1972) [9].

The ADE is a mass balance equation that describes the mass exchange between consecutive control volumes due to advective-diffusive mass fluxes. The concept of control volumes incorporates volumetric averaging, which destroys detail (e.g., heterogeneity such as fast flow channels or stagnant zones) below the scale of the control volume. However, the resulting error becomes negligible if the size of the CV is below the size of the heterogeneities [17]. At that resolution, the CV can be considered as an internally homogeneous continuum for which the advection-diffusion equation is the correct transport description [15] (Figure 1.1).

A pore-scale velocity field at that resolution enables us to represent advective mass flux accurately enough to neglect error arising from the averaging procedure. Diffusion is then the only remaining process, and particle positions under diffusion are given by a normal process [47], which is parameterized by the molecular diffusion coefficient D_m. Hence, if we simulate transport at a scale where we resolve all heterogeneities (i.e., below the size of the heterogeneities of the velocity field),

transport is thoroughly described by a normal process with a drift, which is controlled by the local velocity and the molecular diffusion coefficient D_{m}.

As Gaussian distributions are fundamental solutions of the ADE [112], Fickian transport (in a homogeneous continuum) is given by the sum of independent and normally distributed random numbers.

2.1.3 The Advection-Dispersion Equation

Computational limits usually prohibit a resolution of the velocity field below the scale of the heterogeneity for large-scale models, e.g., at the aquifer scale [133]. For transport simulations at these scales, we need to upscale the relevant transport properties of the porous medium [108]. Usually, upscaling involves block-wise averaging over a representative elementary volume (REV) of the porous medium [9, 133]. The upscaling procedure results in a grid-based hydraulic conductivity field in which we assign a representative permeability κ $\left[L^2\right]$ to each of the REVs that act as CVs. Darcy's law [9] establishes a proportionally relationship between permeability κ, the specific flux $\mathbf{q}$ $\left[LT^{-1}\right]$ through a porous medium, the viscosity of the liquid phase μ_{L} $\left[ML^{-1}T^{-1}\right]$, and a pressure gradient ∇p_{L} $\left[PaL^{-1}\right]$:

$$\mathbf{q} = \frac{\kappa}{\mu_{\mathrm{L}}} \nabla p_{\mathrm{L}} \tag{2.8}$$

The relation between flow rate and the actual fluid velocity fluid is $\mathbf{v}$ $\left[LT^{-1}\right]$ is $\mathbf{v} = \mathbf{q}/\mathrm{n_e}$. The process of upscaling results in the need to account for the lost details leading to the advection-dispersion equation (A$\overline{\mathrm{D}}$E).

Classically, the advection-dispersion equation (A$\overline{\mathrm{D}}$E) describes transport in porous media through:

$$\frac{\partial c}{\partial t} + \mathbf{v}\nabla c - \nabla \cdot (\overline{\mathbf{D}} \nabla c) = 0. \tag{2.9}$$

It describes the spatial distribution of the solute in an upscaled medium. Similarly to the ADE, it is also a mass balance equation that describes advective-dispersive mass fluxes across consecutive control volumes. The difference between ADE and A$\overline{\text{D}}$E is that the molecular diffusion coefficient D_m is exchanged by an d-dimensional dispersion tensor $\overline{\mathbf{D}} \in \mathbb{R}_+^{d\times d}$ $\left[L^2T^{-1}\right]$typically parameterized as:

$$\overline{\mathbf{D}} = \frac{\mathbf{v}\mathbf{v}^T}{|\mathbf{v}|}\left(\Lambda_\text{l} - \Lambda_\text{t}\right) + \mathbf{I}\left(D_\text{e} + \Lambda_\text{t}|\mathbf{v}|\right) \tag{2.10}$$

where Λ_l and Λ_t are scaling factors in longitudinal and transversal direction, respectively, and $D_\text{e} = D_\text{m} \cdot n_\text{e}$ is the effective dispersion coefficient [9]. The dispersion tensor scales molecular diffusion (along the axes) to compensate for the effect of the unresolved sub-scale on the upscaled transport process. In the following, I refer to this as an *effective* description of transport.

The A$\overline{\text{D}}$E - as well as the ADE - describes a normal process with drift. Thus, it is valid only if the heterogeneous medium affects particle motion in a similar way as a homogeneous continuum does. The problem is that advective-diffusive transport in a heterogeneous medium does not behave like a normal process at all scales. The heterogeneities at the pore scale (e.g., from small-scale features like stagnant zones or fast flow channel) lead to a non-Gaussian spatial distribution of the solute, which cannot be captured with Fickian transport laws and hence cannot be represented by a normal process with drift [72].

Nonetheless, beyond some spatial scale (e.g., the size of the CV or typical size of a particle jump), the spatial distribution of the solute might return to a normal distribution, and again, transport obeys Fickian transport laws at the scales above. However, the only way back to Fickianity is the **central limit theorem** (CLT) [51]. The central limit theorem postulates that the sum of any i.i.d. random variables (with finite mean and variance) converge to a normal distribution and thus to Fickianity. The conditions under which the CLT holds and an explanation of i.i.d. will be discussed thoroughly in section 2.2.

So far, transport in upscaled porous media returns to Fickianity if all

solute particles have sampled all relevant heterogeneities sufficiently often. This demands for a minimum scale over which the integration of the solute particles' velocities (along the trajectories) result in a normal distribution of velocities. This is the scale at which we can apply Fickian transport laws again. Hence, Fickian transport laws apply either at the highly resolved scale or after the return to Fickianity via the CLT - in between those scales, transport processes go beyond the description of Fickian models and have to be simulated differently (section 2.2).

2.1.4 Lagrangian Modeling Approaches

From the Lagrangian perspective, we describe advective-diffusive or advective-dispersive transport mathematically as a stochastic Markov process [27], whenever the future system state (e.g., particle positions X at time step $t+1$) depends solely on the current system state X_t:

$$X_{t+dt} = X_t + \Delta X_t. \tag{2.11}$$

The transition between the system states ΔX_t under the influence of advection and diffusion can be described by the Itô-Taylor expansion [54]:

$$\Delta X_t = \mathbf{v}(X_t)\Delta t + \mathbf{B}(X_t)\Delta W_t. \tag{2.12}$$

In equation (2.12), $\mathbf{v}(X_t, t) \in \mathbb{R}^{d\times 1}$ represents a d-dimensional drift vector $[LT^{-1}]$ acting as advection and $\mathbf{B} \in \mathbb{R}^{d\times d}$ is the displacement matrix $[LT^{-1/2}]$, which is related to the diffusion coefficient or dispersion tensor via

$$\text{ADE}: \; 2D_\text{m} = \mathbf{B}\mathbf{B}^T \qquad \text{or} \qquad \overline{\text{ADE}}: \; 2\overline{\mathbf{D}} = \mathbf{B}\mathbf{B}^T. \tag{2.13}$$

The term $\Delta W_t \in \mathbb{R}^{d\times 1}$ is a Wiener process [54] described by $\Delta W_t = \sqrt{\Delta t} \cdot \xi$ with ξ_t as independent and normally distributed random variables with zero mean and unit variance, and with Δt, as the temporal interval in which the process occurs [71].

In the limit of infinite number of particles and an infinitesimal Δt, the Itô-Taylor expansion (equation 2.12) approximates the Fokker-Planck equation (equation 2.14), which describes the temporal evolution of the probability density function $P(\mathbf{x}, t)$ of particle position under the influence of a deterministic drag force $\bar{A}$ (= advection) and a random force D (= diffusion):

$$\frac{\partial}{\partial t} P(x,t) = -\frac{\partial}{\partial x}\left[\bar{\mathbf{A}}_i(x,t) P(x,t)\right] + \frac{1}{2}\frac{\partial^2}{\partial x^2}\left[D_{ij}(x,t) P(x,t)\right]. \tag{2.14}$$

As long as ΔX in equation 2.12 is an i.i.d. random variable, the particle positions should remain normally distributed at all times because they are a summation of i.i.d. random variables ΔX_t (results from the CLT) [51]. The A$\overline{\text{D}}$E (as well as the ADE) and the Itô-Taylor expansion are formally equivalent for:

$$\mathbf{v}(X_t) = \bar{\mathbf{A}} + \nabla \cdot D. \tag{2.15}$$

The model formulated in equation 2.12 is widely known as a particle tracking random walk (PTRW) simulation [110]. The PTRW scheme is a numerical approximation of the Itô-Stratonovich stochastic differential equation (it computes approximate trajectories that solve it). It can be used to compute solutions to the ADE through the equivalence I mentioned above. As a consequence of Fickian transport laws, PTRWs have the same limitations concerning the scales of validity. These limitations are discussed in the upcoming section.

2.1.5 The Limitations of Fickian Transport Models

Most models for transport through porous media (laboratory [6, 75, 85, 118, 119, 122] or field experiments [35, 55, 117, 124, 139]) show that Fickian transport models (e.g., the ADE or PTRW) significantly underestimate the concentration at the tails of the concentration distribution.

Transport processes that go beyond Fickian descriptions are known as pre-asymptotic, anomalous or non-Fickian. The most prominent characteristics of non-Fickian transport are, for instance, anomalously early or late arrival times of solute particles, power-law tailing of the breakthrough curves (BTC), and a time-dependent dispersion coefficient. The latter is often observed as a non-linear scaling of the mean square displacement of the particles. A Gaussian process, which inherently reflects Fickian transport laws, cannot capture these effects.

All Fickian simulation methods rely on convergence according to the central limit theorem. This theorem claims that the sum of independent and identically distributed random variables with finite mean and variance converge to a normal distribution [50]. Hence, by applying Fickian models, we aim to describe transport as a collection of i.i.d. random variables that form a stochastic process. For convergence of this stochastic process according to the CLT, the following conditions have to be fulfilled:

Stationarity The stochastic process has to be statistically stationary in time, which means that it follows the same probability rules at all times. Under stationary conditions, we obtain the (ensemble of) trajectories by summing up spatial increments that follow a distribution, which does not change its properties (i.e., moments) over time.

Ergodicity In general, ergodicity means the equivalence of two (or more) types of average. For particle motion through porous media ergodicity means that the system has the same behavior averaged over time (i.e., along the trajectory) than averaged over space (i.e., the ensemble of particles). In the particular case, our stochastic process is ergodic if the distribution of the sum of random variables (i.e., spatial increments sampled along a trajectory) reaches some limit that does not depend on its initial conditions [50]. At this temporal or spatial scale of ergodicity, the probability of a particle being at position x is given by the ergodic displacement distribution. Hence, under the assumption of temporal stationarity, the position of solute particles over time is given by the sum of *independent and identically* distributed spatial increments.

Finiteness Solely the sum of i.i.d. RVs with finite means and variances converge according to the CLT to the asymptotic normal distribution, which is the only way back to Fickianity. This, however, requires the heterogeneity of the porous medium to be sufficiently moderate as otherwise, we observe displacement distributions with diverging means and variances.

In general, stationary and ergodic conditions are those under which equations that are based on limit theorems approximate the stochastic processes (i.e., particle motion) [113]. However, *Zhan* (1999) [138], *Schumer et al.* (2003) [113] and *Cushman and O'Malley* (2015) [35] indicate, that not even ergodicity can be reached when heterogeneity is strong and, as a result, particle motion will never converge to the asymptotic normal distribution for which Fickian transport laws apply. Hence, the reason why Fickian models for transport in upscaled porous media fail is that the fundamental assumptions of Fickian transport are too strong. As an alternative, we could simulate transport at the size of the governing heterogeneity where Fickian assumptions are valid, i.e., at the pore scale. This resolution, however, is often infeasible because we are strongly constraint by computational limits that do not allow pore-scale simulation domains larger than a few millimeters [22].

Nonetheless, transport simulations in porous media beyond the millimeter-scale are of increasing interest for biological, technical and hydro-geological applications (see Figure 1.1 and section 1.1 for examples) but Fickian transport laws are not valid at the scale of our interest. This is why we need to generalize Fickian transport models towards non-Fickianity to make them applicable at a broader range of scale and also for strongly heterogeneous media.

2.2 Non-Fickian Transport

In this section, I introduce the most popular non-Fickian simulation tools. Firstly, I show how these tools reflect the effect of process memory without specifically modeling it (section 2.2.1). Then, I introduce spatial

Markov models that simulate correlation instead of describing its effect (section 2.2.2).

2.2.1 Effective models for non-Fickian transport

We can describe non-Fickian transport either from the Eulerian or from the Lagrangian perspective. Below, I give an overview of the most frequently used effective Eulerian and Lagrangian models to describe non-Fickian transport:

Eulerian methods: 1. The fractional advection-dispersion equation

The *fractional advection-dispersion equation* (fADE) is a generalization of the classical ADE in which the integer-order derivative of the dispersion equation is replaced by a fractional-order derivative. Two flavors of the fADE exist: By employing the *space*-fractional ADE, we assume that the effects of the heterogeneity are large particle displacements that follow distributions with a power-law tailing. Such distributions allow very long displacements in a short amount of time, which refers to features like preferential flow paths or fractures. Accordingly, by employing the *time*-fractional ADE, we assume that non-Fickianity results form trapping events (e.g., in dead-ends or due to adsorption) that cause a power-law tailing of arrival times.

With this fractional-order formulation of transport, we can capture highly skewed and heavily tailed solute arrival times and spatial particle distributions, which are characteristic of non-Fickian transport. The space-fractional formulation of transport allows particle motion from any point to points in large distance in the domain (not only between consecutive CVs) in just one simulation step. Therefore, the spatial resolution (the size of the CVs) is no longer restricted to the convergence scale of the CLT (Figure 2.2). This allows us to simulate transport at an upscaled but still meaningful spatial scale.

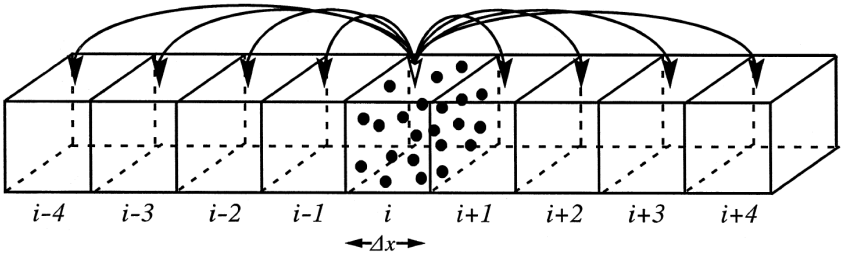

Figure 2.2: The non-local formulation allows mass exchange across all CVs with a probability that decreases with distance. Source: [112]

The derivation of the space-fractional ADE is very much the same as it was for the ADE (section 2.1.1), except employing the *generalized* Taylor expansion in time (see [112] for more detail) that results in:

$$\mathbf{J}_{\mathrm{F}} = \frac{1}{2}\left(F_{\beta}^{q}(c)\,\frac{\Delta x^{q}}{\Gamma(q+1)} + I\left(\Delta x^{q}\right)\right)\eta\Delta x \tag{2.16}$$

in which $\mathbf{J}_{\mathrm{F}}$ is the fractional diffusive mass flux, $F_{\beta}^{q}(c)$ is the qth fractional derivative of the concentration at a given point x in the domain, Γ indicates the gamma-function, $q \in \mathbb{R}^{+}$ is the order of the fractional derivative and $\beta \in [-1, 1]$ is the skewness parameter with $\beta \in \mathbb{R}$. The higher-order members of the generalized Taylor expansion are indicated by $I\left(\Delta x^{q}\right)$ (for comparison see equation (2.3)). The parameter η is the rate (jumps per time step) known from equation (2.5).

For $\Delta x \to 0$, we obtain the fractional Fick's law when:

1. $\frac{1}{2}\frac{\Delta x^{q}}{\Gamma(q+1)}\eta \to \mathbf{D}_{\mathrm{F}}$
2. $\frac{1}{2}I\left(\Delta x^{q}\right)\eta \to 0$

Fractional Fick's law is then:

$$\mathbf{J}_{\mathrm{F}} = \mathbf{D}_{\mathrm{F}}F_{\beta}^{q}(c)\,. \tag{2.17}$$

According to section 2.1.1, for $\mathbf{D}_\mathrm{F}\left[L^2T^{-1/\alpha}\right]$ to be constant, we need $\eta \to \infty$ at the same rate as $\Delta x^\alpha \to 0$ and hence, Δx grows with the same rate as $\Delta t^{1/\alpha}$ decreases, where $\alpha = q + 1$ and $\alpha \in [1, 2]$.

The derivation of the fADE follows a similar procedure than the derivation of the classical ADE (see equations (2.2) - (2.5)). The fADE is the mass balance due to advective and *fractional* dispersive mass fluxes across all (not necessarily adjacent) CVs, which we can formulate as:

$$\frac{\partial c}{\partial t} + \mathbf{v}\frac{\partial c}{\partial x} - \mathbf{D}_\mathrm{F} F_\beta^\alpha\left(C\right) = 0. \tag{2.18}$$

The parameters α and β control the power-law decay (forward and backward) of the displacement distributions and are typically obtained by fitting data. The parameter α approaches one for highly heterogeneous, and to two for homogeneous media, and this is when equation (2.18) simplifies to the ADE. The parameter β approaches to 1 when particles move preferably faster or to $\beta = -1$ when the particles move preferably slower thsn the mean solute velocity.

In contrast to fractional-order derivatives, integer-order derivatives only depend on local properties (e.g., slope) of the function (e.g., of the velocity field). For $\alpha = 2$, the fADE simplifies to the classical ADE, and we describe transport in a homogeneous medium where we can measure the hydraulic properties for the whole medium at an arbitrary point in space. For fractional-order derivatives, the properties at a given point x depend on the entire function f [16]. The more the order of the fractional derivative α converges to one, the more we weight the influence of function values $f\left(x\right)$ in the direct periphery of x onto the fractional derivative at x. This non-locality represents the effects of memory in space that allows large displacements in a limited amount of time (e.g., as effects of preferential flow paths or fractures).

Similarly, the time-fractional ADE reflects process memory in time that is caused by particle trapping events (e.g., in dead-ends of the pore geometry or due to adsorption) zones. Hence, the time-fractional ADE reflects the effects of binding events via a fractional derivative on the time

operator. If non-Fickian transport effects are caused by both - memory in time and space - we can adapt equation 2.18 and obtain:

$$\frac{\partial^{\alpha^*} c}{\partial t} + \mathbf{v}\frac{\partial c}{\partial x} - \mathbf{D}_{\mathrm{F}} F_{\beta}^{\alpha}(C) = 0 \tag{2.19}$$

where $\alpha^* \in [0,1]$ and $\alpha^* \in \mathbb{R}$. We obtain the classical ADE for $\alpha^* = 1$ and $\alpha = 2$ but for any other parameter set $\mathbf{v}$ and $\mathbf{D}_{\mathrm{F}}$ result in generalized notations of velocity and dispersion without their typical dimensions.

Therefore, the fADE belongs to the group of effective models. The formulation of a three-dimensional fADE is more demanding as the order of the fractional derivative and the skewness parameter do not have to be the same along all individual coordinates [78] (see *Schumer et al.*, *Benson et al.* (2001, 2002) [112, 12] and *Sokolov* (2012) [121] for more detail). In any case, fADE models reflect the effects of process memory instead of specifically modeling dependence.

Eulerian methods: 2. Multi-rate mass transfer models

From the physical perspective, particles that get trapped in the pore space cause the anomalously late arrival times of solute particles. We could simulate this simply by a first-order mass exchange rate between the mobile (high-velocity zones) phase where transport follows, for instance, the ADE and the immobile (low-velocity zones) phase. However, structural heterogeneities (e.g., different minerals with different adsorption behavior, dead-ends in the pore space, small clay lenses, ...) of the pore space affect the overall transport process in a way such that one single transfer rate (as applied in mobile/immobile models) cannot capture the complex interaction between these zones [57]. *Multi-rate mass transfer models* (MRMT) describe the mass transfer between immobile and mobile zones as a series of transfer rates in which each rate accounts for a specific feature of the rock matrix which, in the end, controls the solute arrival times.

The mobile/immobile mass transfer model (that will be generalized to MRMT models below) is formulated as:

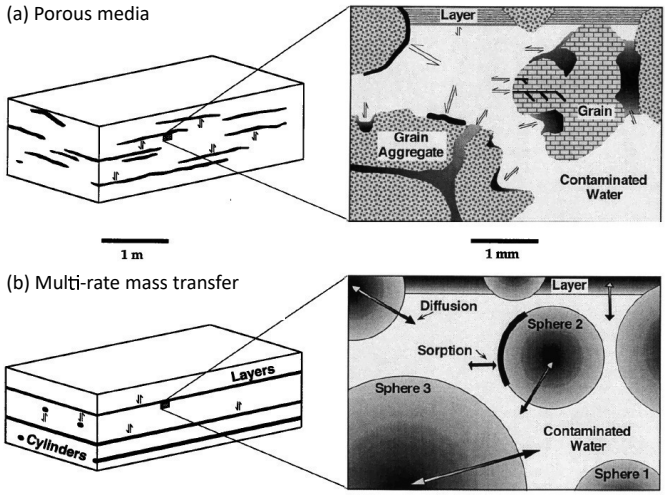

Figure 2.3: Conceptual illustration of the multi-rate mass transfer models: (a) Sketch of a porous medium where the mass exchange between high- and low-velocity zones is indicated by arrows. (b) Sketch of how a multi-rate mass transfer model describes this mass exchange. Source: [57]

$$\frac{\partial c_{\mathrm{m}}}{\partial t} + \gamma \frac{\partial c_{\mathrm{im}}}{\partial t} = L c_{\mathrm{m}} \tag{2.20}$$

where c_{m} and c_{im} are the concentration in the mobile and the immobile phase, respectively. The parameter γ $[-]$ is the capacity ratio. It is the ratio of the total solute mass in the immobile zone and the solute mass in the mobile zone at equilibrium. The right-hand side of equation (2.20) is denoted by $L(x) = -\mathbf{v}\frac{\partial}{\partial x} + \overline{\mathbf{D}}\frac{\partial^2}{\partial x^2}$, with $\mathbf{v}$ the average velocity and $\overline{\mathbf{D}}$ the dispersion tensor. The relationship between c_{m} and c_{im} is typically given by one or more coupled mass transfer equations [57]. *Haggerty and Gorelick* (1995) [57] have shown that many mobile/immobile (as well as MRMT) formulations relate to the linear non-equilibrium mass transfer equation:

$$\frac{\partial c_{\mathrm{im}}}{\partial t} = \omega \left(c_{\mathrm{m}} - c_{\mathrm{im}} \right) \tag{2.21}$$

where ω is a first-order rate coefficient.

As already mentioned above, this single-rate mass transfer formulation can hardly express the full complexity of the structural heterogeneity of the porous media. Therefore, *Haggerty and Gorelick* (1995) [57] suggest a series of single-rate mass transfer equations. We can reformulate the solute transport equation (2.20):

$$\frac{\partial c_{\mathrm{m}}}{\partial t} + \sum_{i=1}^{N} \gamma_i \frac{\partial \left(c_{\mathrm{im}} \right)_i}{\partial t} = L c_{\mathrm{m}}. \tag{2.22}$$

The mass transfer equation for the MRMT becomes:

$$\frac{\partial \left(c_{\mathrm{im}} \right)_i}{\partial t} = \omega_i \left(c_{\mathrm{m}} - \left(c_{\mathrm{im}} \right)_i \right) \tag{2.23}$$

where the ω_i are mass-transfer-rate coefficients describing the local mass transfer controlled by the respective structural heterogeneity (e.g., dead-ends or small clay lenses etc.).

Unfortunately, it is in practice not possible to measure all mass transfer rate coefficients ω_i and capacity ratios γ_i. This is why we consider these parameters rather as distributions than as sets of n independent sets of measurable parameters [57]. The series of mass transfer rates are expressed in many ways (e.g., [30, 57, 104]) and a variation of MRMT models have successfully been applied to many non-Fickian transport problems. *Carrera et al.* (1998) [30] presented an elegant way to express mass transfer rates that involves a convolution to express the unmeasurable parameter set effectively. According to this work, the solution of equation (2.21) is given by:

$$c_{\mathrm{im}} = \omega e^{-\omega t} * c_{\mathrm{m}} + c_{\mathrm{im}}\left(x,0\right) e^{-\omega t} \tag{2.24}$$

where $*$ denotes the convolution:

$$c_{\mathrm{m}}\left(x,t\right) * \omega e^{-\omega t} = \int_0^t c_{\mathrm{m}}\left(x,t-\iota\right) \omega e^{-\omega \iota} d\iota. \tag{2.25}$$

The convolution acts as an exponential filter that takes the function c_{m} to spread it according to a convolution with an exponential function $f\left(t\right) = \omega e^{-\omega t}$ which is known as the "memory function" [30].

By taking the time derivative of equation (2.24), we can express the mass transfer equation (2.23) under consideration of the memory function. This leads to the mobile solute transport equation with general initial conditions in the mobile and immobile phases (the full derivation is provided in [30] and [113]):

$$\frac{\partial c_{\mathrm{m}}}{\partial t} + \gamma \frac{\partial c_{\mathrm{m}}}{\partial t} * f\left(t\right) = L c_{\mathrm{m}} - \gamma \left(c_{\mathrm{m}}\left(x,0\right) - c_{\mathrm{im}}\left(x,0\right)\right) f\left(t\right). \tag{2.26}$$

In equation (2.26), it is the memory function $f\left(t\right)$ that controls the deviation from the classical $\overline{\mathrm{ADE}}$. With an appropriate choice of $f\left(t\right)$, which does not necessarily have to be an exponential function, we can capture a variety of non-Fickian behaviors including the effects of displacement distribution with a power-law tailing. MRMT models, just like the fADE, do not simulate correlation specifically but reflect its effects.

A Lagrangian method: Continuous-time random walks

Continuous-time random walks (CTRW) are one of the most popular mathematical models to simulate transport from the Lagrangian perspective. So far, CTRWs are the most general simulation framework and are equivalent to particular cases of the *generalized Master equation* (gME). The generalized Master equation results from the ensemble average over a set of local-in-time kinetic equations (e.g., the Master equation that represents mass balance) for a disordered system:

$$\begin{aligned}\frac{\partial P(x,t)}{\partial t} = &-\sum_{x'}\int_0^t \phi\left(x'-x, t-t'\right) P\left(x,t'\right) dt' \\ &+\sum_{x'}\int_0^t \phi\left(x-x', t'-t\right) P\left(x',t'\right) dt'\end{aligned} \tag{2.27}$$

where $P(x,t)$ is the normalized concentration at current phase state (x,t). In our particular case, the function ϕ describes the effect of the velocity field on particle motion, and therefore ϕ is related to the transition rates know from the MRMT framework.

The Master equation in equation (2.27) represents a mass balance of particles that have just arrived at position x at time t versus particles that have just left position x at time t. *Kenkre et al.* (1973) [67] and *Dentz et al.* (2016) [42] show, using Laplace transformation, that the generalized Master equation is completely equivalent to a CTRW, which is often written as,

$$R(x,t) = \sum_{x'}\int_0^t p\left(x-x', t-t'\right) R\left(x',t'\right) \tag{2.28}$$

where $R(x,t)$ is the probability per time step to just arrive at position x at time t, $p\left(x-x', t-t'\right)$ assigns the probability of making a displacement $x-x'$ within the time interval $t-t'$ (x' and t' denotes the previous state). The link between (2.28) and the gME is:

$$P(x,t) = \sum_{x'} \int_0^t \Omega\left(t - t'\right) R\left(x, t'\right) \tag{2.29}$$

where $\Omega(t) = 1 - \int_0^t p\left(t'\right)$ is the probability for a particle to stay on site x.

The recursion relations given in equation (2.30) produce trajectories that are characterized by a probability flux at (x,t) and obey equation (2.28):

$$x_{i+1} = x_i + \theta_i, \qquad t_{i+1} = t_i + \tau_i \tag{2.30}$$

where the transit times τ follow some probability distribution $\Psi(\tau)$ and the displacements θ follow some distribution $\Phi(\theta)$. In equation (2.30), consecutive transit times and displacements but also transit times and the respective displacements at the same simulation step are all independent.

CTRW models are the generalization of the classical random walk theory (e.g., the PTRW, see equation (2.12)) where a simulation step is a fixed increment in time. Within these temporal increments, a particle makes a random jump. In the CTRW theory, the concept of a simulation step is generalized as the temporal and the spatial increment are described by the distributions Ψ and Φ. Thus, the challenge in the design of a CTRW is to map all important aspects of particle motion within the porous medium onto Ψ and Φ. The identification of Ψ and Φ to represent particle motion and the interaction with the pore matrix (e.g., binding and unbinding events) lies at the heart of CTRWs [15].

CTRWs describe transport as a stochastic process with statistically independent increments. Therefore, all particle displacements must be large enough to ensure the total loss of dependence, which establishes a lower limit below which CTRWs are invalid. To maximize the spatial resolution of particle motion, CTRWs apply equidistant displacements ($\theta \sim const$) at this very scale of independence. These equidistant CTRWs are parametrized by a (de-)correlation length λ and a respective transit time distribution $\Psi(\tau)$.

The relation between the effective transport models

The phenomenological difference between CTRW and fADE models, on the one hand, and MRMT models, on the other hand, is that MRMT models distinguish between the concentration in the mobile and the immobile phase. CTRWs (but also fADE models) do not make this distinction, and by applying CTRWs, we assume that we can track the particles, no matter whether they are in the mobile or the immobile zone. In a real hydro(geo)logic setting, however, we measure the solute concentration in the mobile phase. From that perspective, the concept of MRMT models is closer to what we would expect from arrival times measured in real, large-scale groundwater systems.

Nonetheless, CTRW, fADE and MRMT models describe the effect of process memory on particle motion. Therefore these models are similar and, for particular cases, even equivalent. *Berkowitz et al.* (2002) [15] show that the space-fractional ADE is approximated by equidistant CTRWs with a power-law decay of the displacement distribution Φ, while equidistant CTRWs approximate the time-fractional ADE with a power-law decay in Ψ. The fADE formulation given by equation (2.19) allows both, a power-law decay of Φ and Ψ, and is thus approximated by the CTRW formulation given by equation (2.28). *Schumer et al.* (2003) [113] and *Dentz and Berkowitz* (2003) [38] show that MRMT models that formulate the memory function via fractional derivatives are equivalent to fractional ADE models and hence as well to specific CTRW models.

2.2.2 Spatial Markov Models

A transport model that describes solute particle positions as the sum of i.i.d. RVs is valid only at a scale λ at which consecutive velocities are independent. This scale, if it exists, might be too coarse for the application of interest, e.g., dilution [69], mixing [74] and mixing-limited reaction kinetics [126], that occur at the pore scale. Hence, if we refine the resolution of the transport simulation, we must account for process memory as the assumption of independence between simulations steps becomes invalid.

At this scale, consecutive particle velocities (and their directions) are no longer independent, and hence particle positions over time are no longer given by the sum of i.i.d. random variables. The correlation structure of the transport process is determined by the spatial coordination of the velocity field [72]. Consecutive Lagrangian particle velocities $\{v_i\}_{i=0}^{\infty}$ at equal longitudinal distances ($\theta \sim$ const and $\theta < \lambda$) along the trajectories form a Markov process in space. To incorporate a series of correlated velocities into a random walk with equidistant displacements θ, we can re-write equation (2.30):

$$x_{i+1} = x_i + \theta, \qquad t_{i+1} = t_i + \frac{\theta}{v_i}. \tag{2.31}$$

The transition probabilities $r\left(v = v_i, x = x_i | v' = v_{i-1}, x' = x_{i-1}\right)$ between consecutive particle velocities can be expressed as a conditional probability in which we describe the transition probability r from velocity v' at position x' to a velocity v at position $x = x' + \theta$ as:

$$r\left(v, x | v', x'\right) = \langle \delta\left[v - v_{i+1}\right] \rangle |_{v_i = v'} \tag{2.32}$$

where the angular brackets denote the average over all realizations (e.g., an ensemble of particle trajectories). The function $\delta\left[v - v_{i+1}\right]$ is 1 if $v = v_{i+1}$ and zero otherwise. For a stationary velocity field, transition probabilities are stationary in space, i.e., $r\left(v, x | v', x'\right) = r\left(v, x - x' | v'\right)$ for all x and x' in the domain.

The random walk described in equation (2.31) is a Markov process in phase space (x, t, v) and can be considered as a correlated CTRW. In contrast to a classical CTRW with independent increments, equations (2.31) and (2.32) form a CTRW in which consecutive velocities v are correlated. CTRWs with correlated consecutive velocities are better known as spatial Markov models (SMM). SMMs simulate correlation itself not just its effects and correlation is what controls particle motion including the evolving non-Fickianity and its potential asymptotic return to Fickianity [73].

We can describe the spatial particle distribution after i simulation steps of an SMM by:

$$p_i(x,t,v) = \langle \delta(x - x_i)\,\delta(t - t_i)\,\delta(v - v_i)\rangle . \tag{2.33}$$

We can further approximate the series of Lagrangian velocities along the particle trajectories as a Markov process with transition probabilities that satisfy the Chapman-Kolmogorov equation [54]:

$$p_{i+1}(x,t,v) = \int\int\int p\left(x,t,v|x',t',v'\right) p_i\left(x',t',v'\right) dx'dt'dv', \tag{2.34}$$

where the transition probability p is defined as [111]:

$$p\left(x,t,v|x',t',v'\right) = \left\langle \delta(x - x_{i+1})\,|_{x_i=x'}\,\delta(t - t_{i+1})\,|_{t_i=t'}\,\delta(v - v_{i+1})\,|_{v_i=v'}\right\rangle . \tag{2.35}$$

Using equations (2.31) and (2.32), we obtain

$$p\left(x,t,v|x',t',v'\right) = \delta\left(x - x' - \theta\right)\delta\left(t - t' - \frac{\theta}{v'}\right) r\left(v,\theta|v'\right). \tag{2.36}$$

Inserting equation (2.36) into the Chapman-Kolmogorov equation, which quantifies the transition probabilities of a Markov process [54], (2.34), we get

$$p_{i+1}(x,t,v) = \int_0^\infty dv' r\left(v,\theta|v'\right) p_i\left(x - \theta, t - \frac{\theta}{v'}, v'\right). \tag{2.37}$$

Now, we define $R(x,t,v)$ as the probability per unit time step to just arrive at position x with the velocity v by summing p_i (equation (2.33)) over all i [111],

$$R(x,t,v) = \sum_{i=1}^{\infty} p_i(x,t,v). \tag{2.38}$$

By summing equation (2.37) over i we obtain

$$R(x,t,v) = g_0(x,t,v) + \int_0^\infty dv' r\left(v,\theta|v'\right) R\left(x - \theta, t - \frac{\theta}{v'}, v'\right) \tag{2.39}$$

where g_0 is the initial distribution of the particles. In equation (2.39), we assume that a particle that just arrives at position x with a velocity v remains there for a certain waiting time $\tau = \theta/v$. The probability $P(x,t,v)$ for a particle to be at (x,v) at time t is defined by the probability per time to arrive at (x,v) at some time $t' < t$ and to remain there until time t [73]:

$$P(x,t,v) = \int_0^t \Omega\left(\frac{\Delta x}{v} - t'\right) R(x, t-t', v) \tag{2.40}$$

where Ω is the probability of a particle to stay on site x. We obtain the spatial particle distribution from $P(x,t,v)$ by integrating over all velocities v:

$$c(x,t) = \int_0^\infty dv P(x,t,v). \tag{2.41}$$

But how is this related to the classical continuous-time random walks from section 2.2.1? In equation (2.41) consecutive particle velocities are correlated according to the transition probability r given in (2.32). CTRWs assume consecutive particle velocities to be independent and therefore $r(v,x|v',x') = p(v)$ where $p(v)$ is the Lagrangian velocity distribution. If consecutive particle velocities are independent, we can decouple $R(x,t,v) = R(x,t)\,p(v)$ and $P(x,t,v) = P(x,t)\,p(v)$ and replace these expressions in equations (2.39) and (2.40) to recover the CTRW from *Berkowitz et al.*, *Scher and Lax* (2002, 1973) [15, 111] which is numerically approximated by the recursive relations given in equation (2.30).

To evaluate the velocity transition probabilities in SMMs (equation (2.31)) as a function of spatial increments θ, we can discretize the velocity distribution into N classes, $v \in \cup_{j=1}^{N} (v_j, v_{j+1})$, and we obtain a transition probability matrix T:

$$T_{ji}(\theta) = \frac{\int_{v_k}^{v_{k+1}} dv \int_{v_j}^{v_{j+1}} dv' r(v, \Delta x|v')\, p(v')}{\int_{v_j}^{v_{j+1}} dv' p(v')} \tag{2.42}$$

where $\int_{v_j}^{v_{j+1}} dv' p(v')$ is the probability of the velocity class j. The transition matrix T_{ji} is a $N \times N$ doubly stochastic matrix ,$\sum_{k=1}^{N} T_{ji} = \sum_{l=1}^{N} T_{ij} =$

1, that represents the transition probabilities between discrete velocity states. The convergence rate of the transition matrix towards the uniform matrix ,$[\lim_{n\to\infty} T^n]_{ji} = \frac{1}{N}$, can be related to the decay rate of the second largest eigenvalue χ_2 of T [64, 128, 132].

Markov processes are characterized by an exponentially decaying correlation that can be expressed by:

$$K(n) \propto \exp\left(-\frac{n}{\tau_{\exp}}\right) \tag{2.43}$$

where $\tau_{\exp}$ is the exponential autocorrelation time of a Markov process, which is related to the second largest eigenvalue χ_2 via $\tau_{\exp} = -\frac{1}{ln|\chi_2|}$ [63]. Hence, the description of transport as a Markov process is only valid within the range of an exponentially decaying velocity autocorrelation below which we cannot describe transport as a spatial Markov process of order one. Below that scale, another process description is required, e.g., a Markov process of order n, which means that the future state depends on past n states [54].

2.3 Describing Dependence

Spatial Markov models simulate transport at a scale at which consecutive particle velocities are correlated. Throughout this thesis, I subdivide process memory into *memory of speed* and *memory of direction*. In most cases, we describe dependence by the Pearson correlation coefficient, which is a linear measure of dependence. Particle motion, however, reveals dependence beyond linearity and copulas are powerful tools to describe such higher-order dependence. In the following, I introduce the Pearson correlation coefficient (section 2.3), and I also give a brief overview over the copula theory (section 2.3).

Pearson correlation coefficient

The Pearson correlation coefficient (denoted as correlation in the following), is a generalization of the variance. The linear relationship between two data sets B and Z is given by the covariance,

$$s_{bz} = \frac{1}{n-1} \sum_{i=1}^{n} \left(b_i - \bar{b}\right) \cdot \left(z_i - \bar{z}\right) \tag{2.44}$$

where n is size of the data sets and s_{bz} is the covariance. Covariance in equation 2.44 is a formal extension of the variance by another index z. The covariance is large when high values of b causes high values of z and becomes negative when a high value of b causes a small values of z. Such as the variance, the covariance is scale (or unit) dependent, e.g., it matters whether we calculate the covariance in meters or centimeters. Therefore we need to normalize the covariance. This normalization results in the Pearson correlation coefficient $K \in [-1, 1]$,

$$K = \frac{\sum_{i=1}^{n} \left(b_i - \bar{b}\right) \cdot \left(z_i - \bar{z}\right)}{\sqrt{\sum_{i=1}^{n} \left(b_i - \bar{b}\right)^2} \cdot \sqrt{\sum_{i=1}^{n} \left(z_i - \bar{z}\right)^2}}, \tag{2.45}$$

$K = 1$ and $K = -1$ indicate a perfect correlation between the data sets. It occurs only in case of an increasing or decreasing functional (deterministic) relationship between B and Z of order one, respectively. For all $-1 < K < 1$ and $K \neq 0$, there is a linear statistical relationship between B and Z that decreases for $K \to 0$. For $R = 0$, there is also a stochastic component that totally dominates (no correlation anymore).

It is important to highlight again, that the Pearson correlation coefficient is a measure of linear dependence only. Transport processes in porous media exhibit a dependence structure in which the degree of dependence depends on the current particle velocity, e.g., very slow particles exhibit memory in time while fast particles seem not to have any temporal memory. Correlation, applied as the measure for that, is unable to detect or describe such a velocity-dependent dependence. For transport processes in porous media, however, non-linear dependence is of

highest interest to deeply understand (and then simulate) the governing mechanisms of particle motion. Instead of correlation, copulas are very well positioned to express non-linear dependence.

Copula

Copulas can describe dependence without being constrained to a first-order second-moment description of dependence like correlation. Copulas, instead, quantify the strength of dependence within different quantile ranges. Thus, they could indicate whether high quantiles exhibit stronger dependence than low quantiles [76]. As an example, copulas in the time domain will be used to quantify the dependence between the velocity (quantile) now and some Δt later. Therefore, copulas are very similar to transition matrices (section 2.2.2) with an equiprobable binning. Here, a high transition probability between the velocity classes can be interpreted as a strong dependence between velocity quantiles.

Apart from reflecting dependence beyond linearity, copulas are very powerful to visualize and interpret dependence. In *Most et al.* (2016) [86] we have shown that the interpretation of bivariate dependence of two sets of random variables (i.e., the 3D velocity pdf now and later) is hard, when the marginal distributions are dominated by their extreme values (Figure 2.4 a)). Extreme values are characteristic for transport in porous media as a result of the strong pore-scale velocity gradients within the medium (e.g., velocity in fractures vs. velocity in the rock matrix). Bivariate distributions are inappropriate to visualize the dependence structure of this kind of data [8] and as a result, they are not very useful to gain a detailed process understanding (see RO1).

Copulas, as an alternative representation of dependence, avoid the difficulties introduced by such extreme values. Instead, they express the strength of dependence independently of the marginal distribution [8]. For that reason, they are often said to reveal the pure dependence. The marginals are removed by a probability integral transformation that transfers the marginals to uniform distributions. This transformation can

be understood as a transformation from the value space to the rank space [8].

Figure 2.4 shows (a) the bivariate density and (b) the copula density (equation (2.51)) of longitudinal displacements separated by a time lag τ_L. We cannot easily derive a meaningful conclusion about the underlying dependence just from the bivariate distribution. The copula, however, reveals that the magnitude of dependence between consecutive displacements depends strongly on the displacement quantile. In this case, there is a very high probability for a particle that just made a small displacement to make another small displacement in the upcoming step. For a large displacement, this probability is distinctively smaller.

Mathematically, a copula is a multivariate (cumulative) distribution function of two or more random variables on the unit hypercube [120],

$$C : [0,1]^n \rightarrow [0,1], \tag{2.46}$$

with marginals that are all distributed uniformly, that is, for any number $0 \geq u_i \geq 1$:

$$C\left(\mathbf{u}^{(i)}\right) = u_i \quad \text{if} \quad \mathbf{u}^{(i)} = (1,\ldots,1,u_i,1,\ldots,1)\,, \tag{2.47}$$

and has to be zero if any of the arguments is zero:

$$C\left(\mathbf{u}\right) = 0 \quad \text{if} \quad \mathbf{u} = (u_1,\ldots,0,\ldots,u_n)\,. \tag{2.48}$$

Furthermore, for any n-dimensional hypercube in the unit hypercube the corresponding probability has to be non-negative:

$$\sum_{j=0}^{2^n-1} (-1)^{n-\sum_{i=1}^{n} j_i}\, C\left(u_1 + j_1\Delta_1,\ldots,u_n + j_n\Delta_n\right) > 0 \tag{2.49}$$

if $0 \leq u_i \leq u_i + \Delta_i \leq 1$ and $i = \sum_{k=0}^{n-1} j_k 2^k$.

The copula is the link between any continuous multivariate distribution function $F(t_1, ..., t_n)$ and its univariate marginals $F_{t_1}, ..., F_{t_n}$. This fact is known as Sklar's theorem [120]:

$$F(t_1, ..., t_n) = C(F(t_1), ..., F(t_n)). \tag{2.50}$$

If the copula is continuous, the copula density is given by:

$$c\left(F(t_1), \ldots, F(t_i)\right) = \frac{\partial^n C\left(F(t_1), \ldots, F(t_i)\right))}{\partial F(t_1), \ldots, \partial F(t_i)}. \tag{2.51}$$

For more detailed descriptions and explanations of the basic concept of copulas, the interested reader is referred to *Nelsen* (2013) [89].

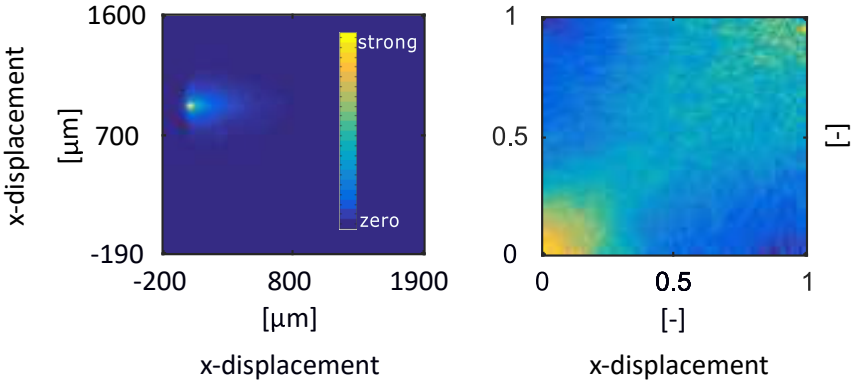

Figure 2.4: Bivariate distribution of particle displacements separated by a time lag τ_L in a) for the value space and in b) for the uniform space which represents an empirical copula density.

2.4 Digital Rock Physics

Studying particle trajectories during transport in natural rock is greatly facilitated by having detailed information on pore-scale geometry. Such

geometric information can be provided by X-ray tomography. The particle trajectories employed in this thesis are produced by the Royal School of Mines at Imperial College London. A detailed description of how this data is generated can be found, for instance, in *Bijeljic et al.*, *Blunt et al.*, *Raeini et al.*, *Pereira Nunes et al.* (2011, 2013, 2014, 2015) [20, 23, 103, 98].

The general workflow to obtain particle trajectories at (or even below) the size of the governing heterogeneity is:

1. Create a three-dimensional image of the pore geometry via a micro-CT scan.
2. Discretize the pore space.
3. Solve the Navier-Stokes equation to obtain the flow field inside the pore space.
4. Perform a PTRW-based transport simulation.
5. Track particle positions over time to obtain the trajectories.

In the following, I give the technical specifications of the DNS for pore-scale transport used throughout this thesis.

The pore-scale simulation of flow and transport for this thesis is conducted on a Doddington sandstone image. This comprises of 1000 cubed voxels per spatial direction (i.e., a total of $1 \cdot 10^9$ voxels) with 2.6929 μm voxel size, resulting in image lengths in each direction of $L_x = L_y = L_z = 2.6929\ mm$. The image is acquired by scanning a 5 mm diameter core in a micro-CT scanner Xradia Versa 500. The image processing is carried out using the Avizo Fire 7.0 program (VSG; www.vsg3d.com). The image porosity of $\phi = 0.195$ compares well with laboratory measurements using helium porosimetry ($\phi = 0.192$). Noise reduction has been achieved by using a non-local means edge-preserving filter [29] while segmentation into pore and solid voxels has been performed using the watershed seeded algorithm [4].

Each voxel created by image segmentation is a grid-block in the subsequent flow simulation. The volume conservation equation (2.52)(see below) and the Navier-Stokes equations (2.53) (see below) for incompressible viscous flow are solved in the pore space by the method presented in

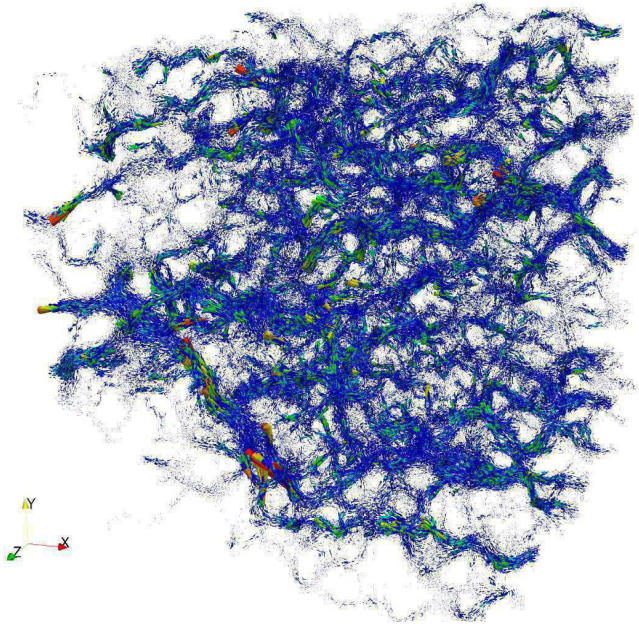

Figure 2.5: Visualization of the pore-scale velocity field of the Doddington sandstone sample.

Raeini et al. (2012) [102] and *Bijeljic et al.* (2013) [21]. This method is based on a finite-volume code implemented in OpenFoam [93]:

$$\nabla \cdot \mathbf{v} = 0 \tag{2.52}$$

$$\rho(\frac{\partial v}{\partial t} + \mathbf{v} \cdot \nabla \mathbf{v}) = -\nabla p + \mu_{\mathrm{L}} \nabla^2 \mathbf{v} \tag{2.53}$$

where $\mathbf{v}$ $\left[LT^{-1}\right]$ is the velocity vector, μ_{L} $\left[ML^{-1}T^{-1}\right]$ is the viscosity of the liquid (i.e., water), ρ $\left[ML^{-3}\right]$ is the density, and ∇p $\left[\mathrm{Pa}L^{-1}\right]$ is pressure. A unit pressure gradient is applied across the image with a constant-pressure boundary condition at the inlet and outlet image faces. No-slip boundary conditions are used at solid voxel boundaries.

The average pore velocity is calculated as $v_{\mathrm{av}} = \frac{q}{\phi}$, where $q = \frac{Q}{L_y L_z}$ is the Darcy velocity and Q $\left[L^3T^{-1}\right]$ is the volumetric flux. From flow simulation, the absolute permeability in the image flow direction using Darcy's law is $k = 3.23 \cdot 10^{-12} m^2$. Figure 2.5 presents the flow field based on voxel velocities in the resulting Doddington sandstone image. Transport is simulated on the image voxels by a particle tracking random walk method [20]. For the above velocity field, simulations are performed by tracking advective and diffusive displacements of particles in constant time steps $\Delta t_{\mathrm{sim}} = 1 \cdot 10^{-4} s$, so that the updated particle positions X_{t+1} given the current positions X_t is given by the Itô-Taylor expansion formulated in (2.11) and (2.12).

A total of 1000 particles are injected using flux-weighted injection and their particle trajectories are tracked until they cross the exit image face. To ensure that particles do not cross the inlet face by backward diffusion, the particles are injected sufficiently far from the inlet face. It turned out that injecting into the 30th image voxel layer as measured from the inlet is sufficient. In each time step, particles are moved advectively by $\mathbf{v}\left(X_t\right) \Delta t_{sim}$ along the streamlines, traversing one or more voxels using a modified Pollock's algorithm [99]. Then, they are moved diffusively by $\mathbf{B}\left(X_t\right) \Delta W_t = \sqrt{24 D_{\mathrm{m}} \Delta t_{\mathrm{sim}}}(U - 0.5)$ where $D_{\mathrm{m}} = 2.2 \cdot 10^{-9} \frac{m^2}{s}$ is the

molecular diffusion coefficient of water and U is a random number uniformly distributed between 0 and 1 [11]. Here, diffusive particle motion, typically represented as a Gaussian density, is approximated by a convolution of uniform densities, which is computationally more efficient and therefore used for the transport simulation [11]. Particles can hit solid boundaries only by diffusion - if this occurs, they are bounced back to the pore voxels in a random direction and traverse the remainder of the diffusive displacement for that time step.

Simulations are performed for two different transport conditions characterized by different Péclet numbers. The Péclet number is defined as $Pe = \frac{v_{\mathrm{av}} L}{D_{\mathrm{m}}}$ where the characteristic length L is obtained from the micro-CT image as $L = \frac{\pi V}{S}$, with porous medium volume$V$, and the area of the pore-grain interface S. Both is calculated from the micro-CT image [87]. The resulting characteristic length for Doddington sandstone is estimated as $L = 200.18\ \mu m$. For later comparison, simulations for $Pe = 10$ and $Pe = 100$ are performed that corresponds to average velocity values of $v_{\mathrm{av}} = 0.109896 \frac{mm}{s}$ and $v_{\mathrm{av}} = 1.09896 \frac{mm}{s}$, respectively.

Part II

Contributions

Chapter 3

Dependence Analysis of Three-Dimensional Particle Motion

Part II may contain similar and/or identical formulations from my publications *Most et al.* (2016) [86]. I omit a clear identification for readability and use parts of the article by kind permission of the publisher WRR.

Traditional formulations for transport in porous media that are founded on Fickian transport laws understand particle motion as an independent stochastic process. This is a very strong assumption and not always valid since dependence matters at some scales.

My main hypothesis of this thesis is that all information about process dependence is contained in the particle trajectories. To check whether process dependence is significant, I introduce an analysis framework to thoroughly analyze the statistics of particle motion through porous media based on the highly resolved trajectories obtained by DRP. This analysis is an essential step to better understand transport, which therefore addresses research objective one (**RO1**). The analysis is also an important component to answer one part of my research question:

How can we use latest advances in DRP best to better understand (and simulate) transport?

In the upcoming section, I elaborate on the relevance of dependence (section 3.1). In section 3.2, I give a detailed description of the preprocessing of the DNS-trajectories, which is a necessary step for the statistical

analysis of particle motion. In section 3.3, I introduce the copula-based analysis framework. In section 3.4 I discuss the results. Finally, I evaluate whether the proposed analysis framework fulfills research objective one. A summary of this chapter together with the conclusions can be found in part III.

3.1 The Relevance of Process Dependence

Recent advances in X-ray tomography made it possible to describe advective-diffusive transport in the pore space of micro-CT images with a high degree of accuracy [20, 24] (section 2.4). Such a highly accurate transport simulation through the pore space provides the input data for the upcoming analysis of process dependence. Analyzing the stochastic transport process in this manner adds new information on the nature of non-Fickianity (and how it depends on heterogeneity and on the Péclet number) by including improved descriptions of memory of speed and memory of direction.

To the best of my knowledge, there is no other study available that focuses so deeply on the complex dependence structure of pore-scale transport processes. That is an essential first step to more accurately simulate transport. The term *dependence structure* can be understood as the characteristic residence time a particle stays within a specific velocity quantile, for instance in a slow zone. This characteristic time can be very different for slow or fast particles, and for different angles of motions. In this chapter, I describe the dependence structure through transition probabilities from one to another velocity quantile in consecutive time increments.

To achieve a clearer understanding of the dependence structure, I will first analyze the memory effects in the longitudinal and transverse direction (memory of speed), and then expand my analysis to the cross-dependence *between* longitudinal and transversal direction (memory of direction). The main goal in this chapter is to provide a comprehensive analysis of the high-order dependence structure that encompasses the full 3D information of the pore-scale transport simulation (see research question and RO1).

I focus on the following four relevant issues:

(1) To date, there is no other study available that analyzes the statistics of transport in porous media in all directions in a joint manner. In specific, no other study analyses the evolution of the complex cross-directional (e.g., x- vs. y-direction or y- vs. z-direction) dependence of particle displacements over time. This is especially relevant for understanding mixing processes as the transverse spread controls the mixing behavior in natural systems (e.g., [40, 74]).

(2) Most studies (e.g., *Le Borgne et al.*, *Le Borgne et al.*, *Kang et al.*, *Kang et al.*, *Kang et al.*, *Sund et al.*, *Sund et al.* (2008, 2008, 2011, 2015, 2016, 2016, 2017) [72, 73, 62, 65, 66, 128, 129]) that address anomalous transport present an analysis or a simulation technique for a specific and/or simplified experimental set-up. All these methods contain a statistical description of the transport process up to their chosen degree of a-priori simplification. The current contribution will provide a statistical description of the spatial displacement dependence without simplifications and in full spatial complexity.

(3) I analyze process memory (in the temporal domain) under the influence of diffusion as a function of the sampling time dt, time lag τ_L and the Péclet number (parameters will be clarified below). Understanding process memory is essential to define the minimum duration and timescale that is required to return to a time-domain Markov process or to Fickian transport. In particular, the influence of diffusion on process memory is interesting, as diffusion alone can transport particles into and back out of stagnant zones. The inward process generates process memory while the outward process reduces memory, and both parts depend on the Péclet number.

(4) I conduct the analyses in a spherical coordinate system that moves with each particle. In specific, particle position increments are analyzed in terms of absolute lengths of displacements and two angles (azimuth and elevation), instead of looking at increments in each spatial direction (i.e., x, y, and z). I have found that this coordinate system is very close to the underlying physics and is better positioned to describe the complex dependence than the Cartesian coordinate system. Furthermore, an anal-

ysis of absolute displacements can directly be used to define stagnation or mobility of particles in respective zones of the flow field.

3.2 Preprocessing of the Simulation Data

The data for statistical analysis comes from a preprocessing step that is using the particle trajectories from the transport simulation (Figure 3.1 a). The preprocessing step extracts the data relevant to analyze particle increment distributions and their memory effects. I am interested in the dependence structure and the process memory as a function of time increment dt and time lag (between time increments) τ_{L} (Figure 3.1 b).

In this section, the process time t_p, the temporal discretization of the transport simulation Δt_{sim}, the time increment dt and the time lag τ_{L} are explained in detail as illustrated in Figure 3.1b). The process time t_p is the time passed from the initial injection of the particles into the flow field. It runs from $t = 0s$ to the end of the simulation 10 seconds later. This is the typical time coordinate used to describe time-dependent dispersion behavior. The parameter Δt_{sim} is the temporal discretization of the pore-scale transport simulation. It remains constant, and I assume that it is sufficiently small to neglect the discretization error, which has been validated in previous studies (e.g., *Bijeljic et al.*, *Mostaghimi et al.* (2004, 2012) [19, 87]).

However, the focus lies on dt and τ_{L}. I evaluate the absolute spatial increments of the particles within the time increment dt ($dt = n \cdot \Delta t_{\mathrm{sim}}$). The parameter dt is the temporal sampling window in which I sample the positions of particles moving through the porous medium according to the underlying velocity field. The spatial increments are defined as the Euclidean distances between the particles' position at t_i and the particles' position at $t_i + dt$, where the intervals for analysis run from $t_1 = 500$ to $t_n = 20000$. The time increment dt is varied as part of the analysis to see how particle increment statistics change with time resolution scale at which the transport is analyzed. As I am interested in the process dependence and its memory, I am, for instance, interested whether fast

particles in a current time step are still fast in a later time step. Therefore, I additionally derive a joint increment data set of all particle increments in time increments separated by a time lag τ_L, and vary τ_L to analyze the duration of memory.

The resulting data sets enter the copula-based analysis (section 2.3) to derive the dependence structure and memory of the transport process as a function of dt and τ_L. If we look only at fully advection-dominated transport, the ratio of particle position increments θ over time increments dt would be the particle velocities averaged over a temporal sampling window dt. However, as I analyze transport at a finite-Péclet regime, the position increments also contain diffusive contributions, and the analogy would not honor the full physics of the process.

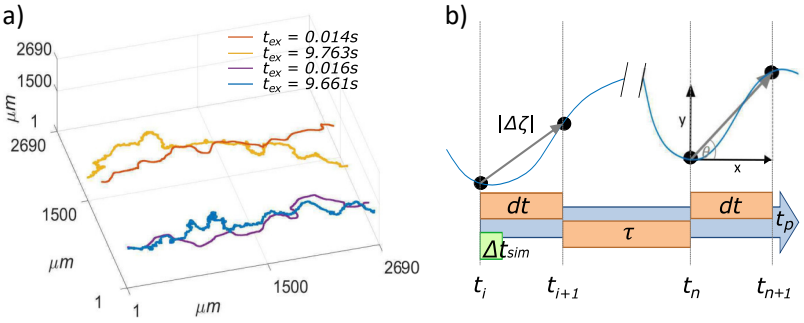

Figure 3.1: a) Trajectories of four particles in two transport regimes at Péclet=10 (yellow and blue) and Péclet=100 (orange and purple) and the time t_{ex} after which the particle's position exceed the sample boundary; b) exemplary sketch of the parameters used in the preprocessing procedure with $n = t_i + dt + \tau_L$.

3.3 Statistical Analysis

The statistical description of advective-diffusive particle motion and the interaction with the pore structure is essential to accurately parameterize stochastic processes (e.g., CTRW or SMM). In this chapter, I give a

detailed description of how I adapted the copula framework to extract processes understanding optimally.

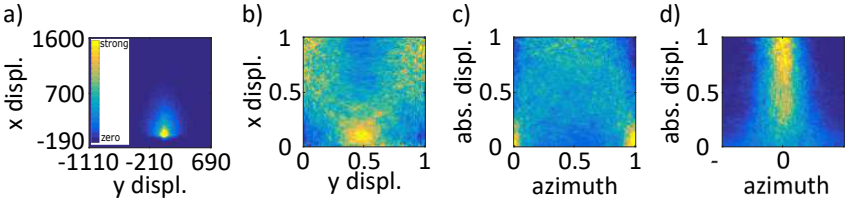

Figure 3.2: Advantages and disadvantages of several techniques for representing dependence. a) Bivariate density of particle displacements in μm. The color bar indicates the strength of dependence qualitatively from zero to strong. b) Copula of particle displacement in the rank space. c) Change to spherical coordinates: copula of absolute displacement vs. angle against main flow direction in the rank space d) hybrid depiction of absolute displacement in the rank space vs. angles against main flow direction in the value space.

Figure 3.2b shows the copula density of the displacement components in x and y direction within a given time increment dt. It is assessed by averaging all available increment data over process time t_p and over 1000 particle trajectories. The shown copula density describes the dependence structure of particle displacements for a given sampling window dt separated by a time lag τ_L. This is an analysis performed in the Cartesian coordinate system. We can see that large displacements in x-direction are often linked to small y-displacements. This cross-directional dependence is caused by particles moving fast at small angles to the flow direction (x). If we switch now to a spherical coordinate system, we can analyze the absolute displacements θ separated from the direction which is represented by two angles, azimuth and elevation (Figures 3.1b and 3.3). In Figure 3.2c, I show the dependence structure between absolute displacement θ and the azimuth Θ.

Small absolute values of the azimuth values represent displacements along the main flow direction, azimuth values close to $\pm 180^\circ$ represent displacements against the main flow.
Now that I have chosen the coordinate system for the analysis, we need

to re-visit the suitability of copulas as the analysis tool. Even if copulas reveal the pure dependence, it is very demanding to draw conclusions from the rank space that are valid and physically meaningful in the real world. For instance, if we consider the copula shown in Figure 3.2c, a naive interpretation might be that small displacements usually move against the main flow direction. Physical reasoning, however, reveals that small displacements occur mostly in regions with reduced or no flow, where diffusion is the controlling mechanism. Diffusion does not have a preferential direction, and this contradicts the results visually suggested by the copula analysis in Figure 3.2c.

This contradiction can only be resolved when understanding that dependence in the rank space as shown by the copula requires a careful and sometimes non-trivial interpretation before translating to conclusions on physics. As an alternative, I will choose a related but different way of representing the dependence. Copulas, as mentioned above, are most valuable if the marginals are heavily skewed. Therefore, they are very useful when analyzing absolute displacements. The distribution of azimuth values, however, is naturally constrained between -180° and 180°, which does not call for analysis in the rank space. During the analysis, I found that a hybrid representation of the dependence structure reveals an intuitive and physically correct perspective onto the transport physics that are the underlying cause of dependence among increments. The hybrid representation uses azimuth without transformation but treats absolute displacements in the rank space. The resulting analysis in Figure 3.2d reveals clearly that, for small absolute displacement, azimuth has a very high variance. This reflects the physical fact that, in stagnant or slow-flow zones, the diffusively driven transport component has no preferred direction. Hence, the hybrid representation of the dependence structure can provide an insightful and physically meaningful view on the process.

Throughout the whole analysis, the x-axis is always oriented along the overall mean flow direction. This gives us two possible transversal planes (x-y and-x-z plane) to analyze transversal effects of the transport process. I assume the porous medium to be isotropic in transverse directions and hence I do not expect new phenomena by analyzing the second

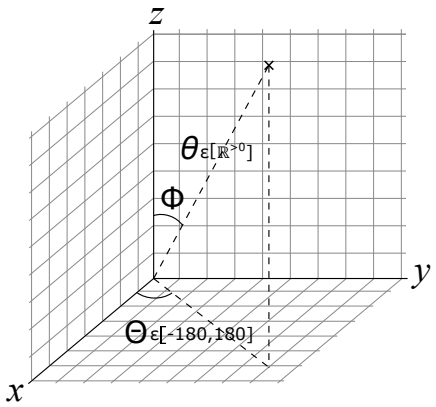

Figure 3.3: Spherical coordinate system with θ as the absolute displacement, Θ as the angle against the overall mean flow direction and ϕ as the second directional angle. The coordinate conversion is given by $\theta = \sqrt{(}x^2 + y^2 + z^2)$, $\Theta = arccos\frac{z}{\theta}$ and $\phi = arccos\frac{z}{\theta}$

transversal axis. Hence, I only analyze the dependence between absolute displacement θ and the azimuth Θ.

3.4 Results & Discussion

3.4.1 Univariate Analysis

I first focus on the univariate statistics of pore-scale transport by looking at displacement components in a traditional Cartesian coordinate system.

Figure 3.4 indicates that, for infinitesimal dt, pore-scale transport is likely to follow Fickian transport laws: the particle displacement distributions in all three spatial directions can be considered as Gaussian (Figure 3.4). Figure 3.4a shows that this finding is independent of process time t_p. I interpret this as a confirmation that the analysis of particle position *increments* is beneficial because statistics of particle positions (instead

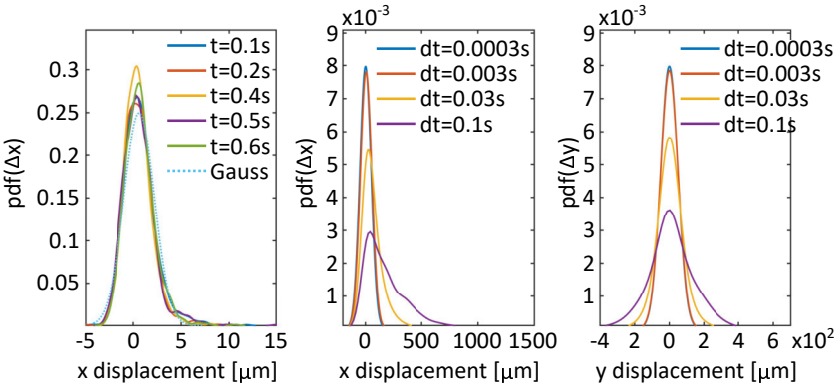

Figure 3.4: Empirical probability density functions for the Cartesian components of particles positions increments: a) longitudinal increments (x) for a very small time increment ($dt = 3 \cdot 10^{-4}s$) at different process times. b) longitudinal increments with increasing time increments dt c) same as b) but a transverse (y) component.

of increments) are known to be affected by time-increment-dependent scale effects [74].

However, we do not have access to infinitesimal dt and already for our smallest possible $dt = 3 \cdot 10^{-4}s$ the distributions are not perfectly symmetric. This is a first sign for the non-Fickianity evolving on larger time scales (dt). For larger dt (=larger Pe_{rel}), the skewness of the displacement distributions in longitudinal direction is increasing (Figure 3.4b). This is caused by fast advective forward motion of some particles, combined with slow or even stagnant motion of others. In transversal direction, the deviation from normality manifests itself in the kurtosis (Figure 3.4c)).

The increasing skewness and the non-normal kurtosis would not appear if the transport process could be described as an independent stochastic process based on normal increments for small dt as indicated in Figure 3.4a. In specific, the CLT dictates that, if the normal increments in Figure 3.4 were, in fact, independent, then increments for larger dt would again be normal. While diffusion is, per definition, a fully in-

dependent process, advection is a process with memory. The memory is induced by the physics of flow that induces the dependence. With higher Pe_{rel}, the dependence becomes stronger as advection becomes more dominant: the expected diffusive displacement scales with the square root of time, the expected advective displacement scales with time. As a result, the univariate distribution deviates more and more from normality with increasing dt, because the assumption of an independent process does not hold anymore.

In addition, the order of dependence must be higher than one, i.e., more complex than linear. If we assume for a moment that advection introduces only linear dependence, the resulting distributions for larger dt would again be Gaussian, because the appearing stochastic process would be an autocorrelated process [33] that remains Gaussian if the stochastic noise term is Gaussian. The non-linearity of dependence observable here must come from advection as diffusion cannot induce dependence.

3.4.2 Pearson Correlation

The Pearson-correlation plots in Figure 3.5 lead to similar conclusions about the dependence structure. The Figure shows the autocorrelation among x-components of particle position increments for a) $Pe = 10$ and b) $Pe = 100$ over increasing time lag τ_{L} for different values of time increment dt. For $Pe = 10$ and $dt = 3 \cdot 10^{-4}s$ the process is fully independent over all the time lags τ_{L} examined. This is the short-term regime of dt (small Pe_{rel}) in which diffusion dominates. If the transport process could be described as Taylor-Aris dispersion with a random yet constant-over-time velocity and without diffusion ($Pe \to \infty$), the correlation would be one over all τ_{L}. For $Pe = 100$ and $\tau_{\mathrm{L}} = 3 \cdot 10^{-4}s$, the correlation of 0.6 indicates that the process is not independent. Already at this scale, the dependence arising from advection influences the process (see also the slight asymmetry in Figure 3.4a). The correlation becomes one or very close to one for $\tau_{\mathrm{L}} = 3 \cdot 10^{-4}s$ as $dt \geq 30 \cdot 10^{-4}s$. The speed of gaining dependence depends strongly on the global flow regime. Under relatively diffusive conditions ($Pe = 10$) and dt below a specific flow-regime

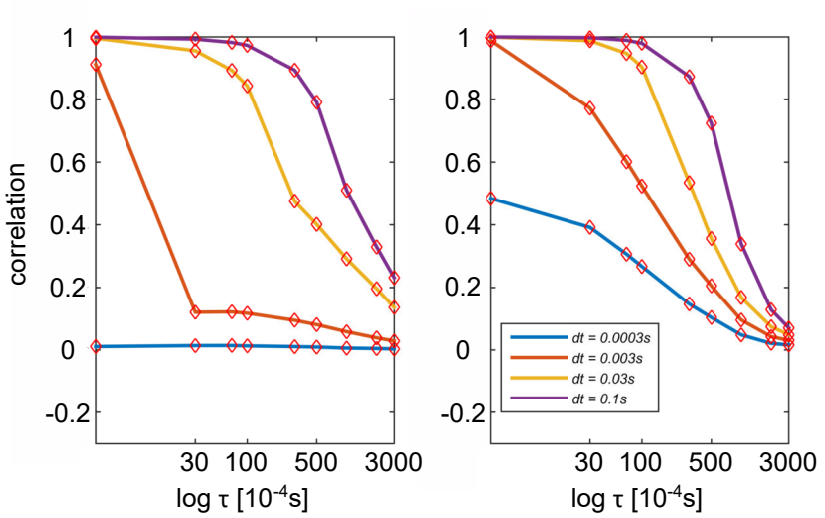

Figure 3.5: Auto correlation among x-components of particle position increments for a) $Pe = 10$ and b) $Pe = 100$ in longitudinal direction over increasing time lag τ_L for different values of time increment dt.

dependent constraint, the correlation is either zero or only present for very short time lags τ_L. This dt constraint decreases as the Péclet number increases. Above that constraint, the correlation decreases gradually with increasing τ_L. The correlation, however, does not decrease linearly with $log\ \tau_L$, and hence the memory causing the dependence must be beyond first order with increasing time lags τ_L, i.e., we have a Markov process of order higher than one. This conclusion can once again be drawn from comparison to an autoregressive model of order one (AR(1)), which would lead to an exponentially decaying correlation.

3.4.3 Analysis of Memory Effects in the Absolute Displacements (Pe=100)

We start with the bivariate dependence analysis between the absolute displacements recorded in consecutive time increments dt separated by

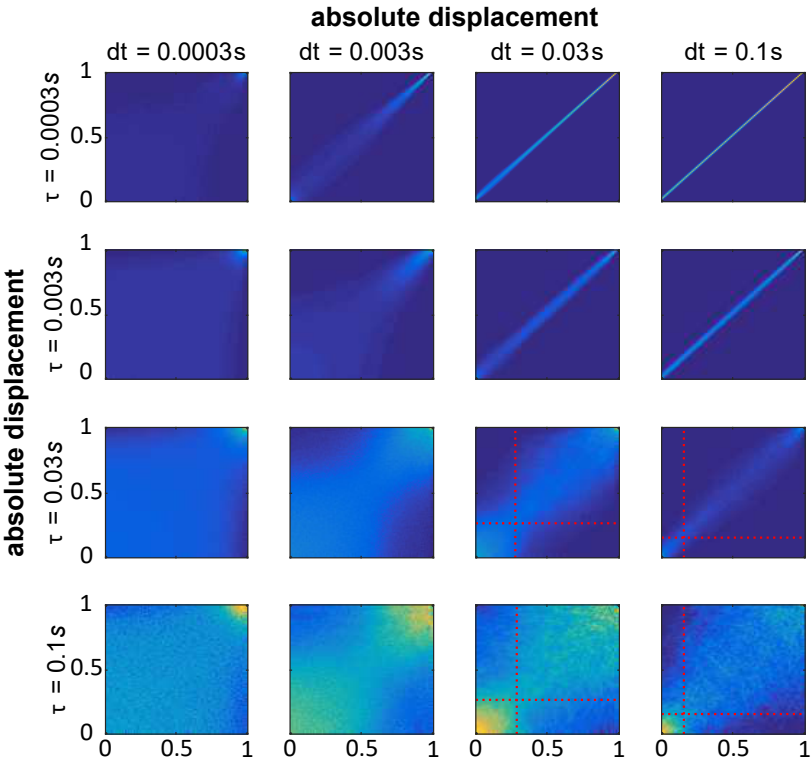

Figure 3.6: Copula densities for absolute displacements under advective and diffusive transport at $Pe = 100$ between increasing time increments dt separated by increasing time lags τ_L. The dashed-red lines mark the critical displacements that define the transition between the stagnant and the mobile zone.

a time lag τ_L. This means we look at the dependence between a displacement now versus a displacement later. As I deal with heavily skewed distributions, I use classical copulas. The bivariate copulas of the absolute displacements with increasing dt and τ_L are shown in Figure 3.6.

If we analyze Figure 3.6 from the left to the right column, we observe a process that is dominated more and more strongly by advection as dt increases. If we analyze from top to bottom, we are analyzing the persistence of process memory. For $dt = 3 \cdot 10^{-4}s$ and $\tau_L = 3 \cdot 10^{-4}s$, the copula density is occupied in the top right corner: There is already a small fraction of fast particles (in advection-dominated regions) that remain inside fast flow channels. For those particles, a small scale of time (dt) is already sufficient to induce dependence. The entire remaining area of the plot indicates complete independence, which is caused by diffusion that is dominant at this time scale. For increasing dt and $\tau_L = 3 \cdot 10^{-4}s$, advection becomes more influential as the relative Péclet number increases. The relative Péclet number is the Péclet number that is derived by the particles current velocity. In the first row of Figure 3.6, we can see the transition from a diffusion-dominated and nearly independent process towards an almost purely advective-dominated transport process with a nearly linear dependence between the states.

If we increase both parameters (dt and τ_L) and follow the plots on the diagonal of the Figure, we see a very interesting change of the dependence structure: For small dt and τ_L, the dependence is located only within the large-displacement quantiles. For increasing dt, the small displacement quantiles gradually gain dependence whereas, simultaneously, the large displacements continuously lose their dependence. Ergo, we can deduce that the dependence is non-linear and strongly scale-dependent. In other words, memory effects in non-Fickian transport come either from preferential flow when we analyze small-scale processes (small dt) or from the persistence of small displacements within stagnant zones at the larger scale. Hence, the root of non-Fickianity strongly depends on the considered scale (dt). This means that the stochastic process (or transition matrix) used in non-Fickian transport simulations to account for the inherent process dependence has only a limited validity range.

The square in the lower left corner of Figure 3.6 (red dotted lines) describe the transition probabilities of particle displacements that can be considered as mobile (upper right square) and the immobile particles (lower left square). The remaining two squares represent the transition

probability or exchange rate of particles from mobile to immobile or vice versa. The definition of a critical displacement that characterizes transport in stagnant velocity zones is derived by the χ^2-distribution, which is the sum of the squares of $k = 3$ independent standard normal random variables. Herein, the critical displacement is defined by the 95-quantile of a χ^2-distribution that scales with $D_m \times dt$. For $dt = 1000 \cdot 10^{-4} s$ (see right column), absolute displacements below $39.5193 \mu m$ are considered as stagnant.

3.4.4 Analysis of Memory Effects in the Azimuths (Pe=100)

In Figure 3.7, the bivariate densities of azimuths are illustrated, and we are looking at azimuths now versus azimuths later. Azimuth should be understood as deviation from the main flow direction. I do not use copulas in this case because the distribution is symmetric (Figure 3.7) and constrained between -180 and 180 degrees. If we start again with the smallest dt and τ_L, we can see from the ellipsoidal shape of this bivariate distribution that there is memory, and that the underlying dependence is linear. If we consider dt as the inverse frequency of evaluating the azimuth several times within a pore, the memory comes from the directed orientation of the streamlines within the individual pore geometries. As dt increases, two things change: first, the relative Péclet number increases, so that advection becomes more dominant and diffusive motion leads to less scattering relative to the advective drift. Second, the smaller geometries in the advective part get averaged out, so that the main flow direction becomes more pronounced. Together, the individual variances of the azimuth become smaller, leading to the density concentration around zero with increasing dt. With larger Pe_{rel}, the process memory of the azimuths becomes weaker before it vanishes fully. This happens because the deviations from the main flow direction start to lose their correlation after a specific τ_L which is increasing as dt increases (Figure 3.7).

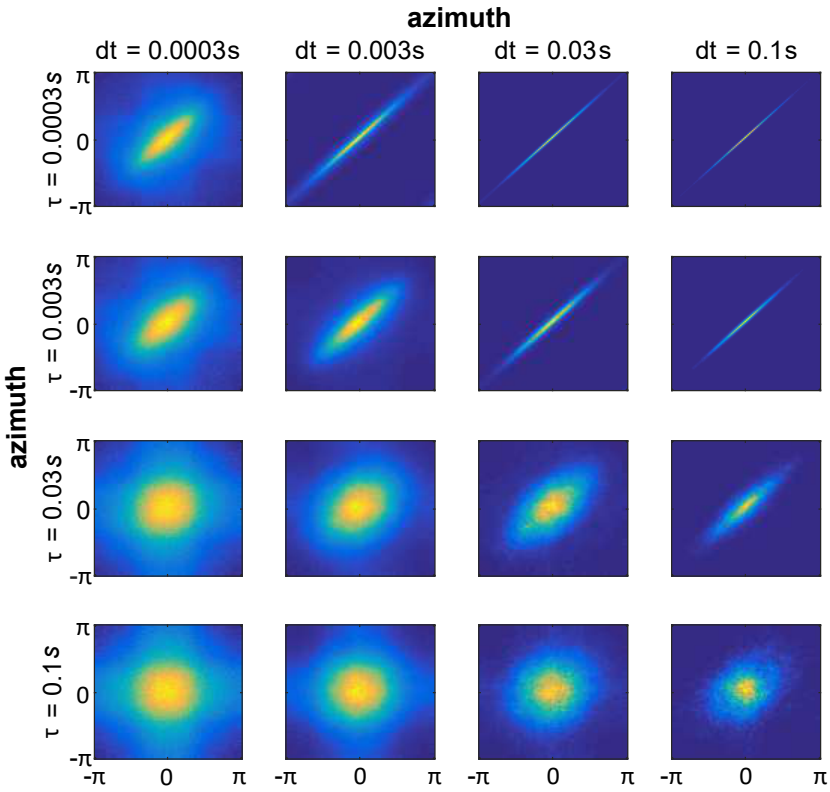

Figure 3.7: Bivariate densities of the azimuth under advective and diffusive transport at $Pe = 100$ between increasing time increments dt separated by increasing time lags τ_L.

3.4.5 Analysis of memory effects in the cross-dependence (Pe=100)

For analyzing the cross-dependence, I transform only the absolute displacements into uniform distributions and leave the respective azimuth

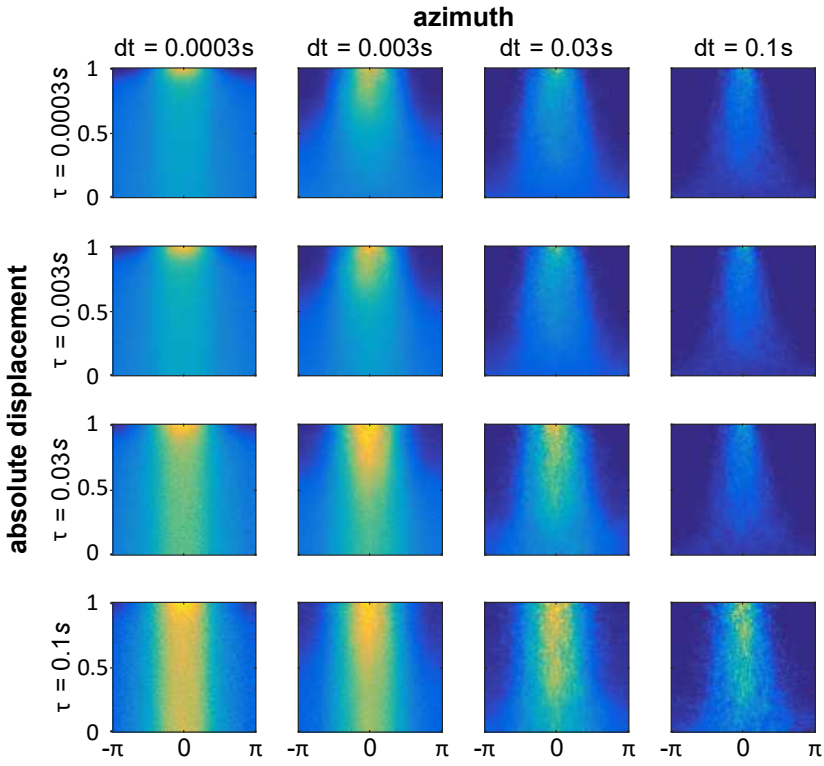

Figure 3.8: Copula densities between absolute displacements and azimuth under advective and diffusive transport at $Pe = 100$ between increasing time increments dt separated by increasing time lags τ_L.

in the value space. With my framework of representing the dependence, we can focus on the quantile-specific differences of dependence, i.e., we can observe how different ranges of velocities (now) restrict the freedom in angles (now and later) to different degrees. In Figure 3.8, we start the analysis in the top left for the lowest relative Péclet number ($dt = 3 \cdot 10^{-4}s$) and small time lags ($\tau_L = 3 \cdot 10^{-4}s$). Here, the depen-

dence is clearly concentrated between high displacements at the current state and small angles in the future state. Due to the low relative Péclet number, transport is mainly diffusive for small dt. However, there is a small fraction of cases where a particle experiences a large displacement as it currently resides in a fast flow conduit, and then it is very likely that the displacement is roughly aligned with the main flow direction. With increasing dt, we still observe a strong dependence between large displacements at the current state and small angles at later states for the upper displacement quantiles. If we consider the lower displacement quantiles instead, there is much less cross-dependence between displacement and angle, as we found it typical for diffusive processes. However, the particles that experience lower displacement quantiles are gaining dependence compared to lower dt values. This is caused by the increasing influence of advection even in the slower (even non-stagnant) regions of the pore space. The increasing dependence is the reason for the smaller azimuth variance at specific displacements quantiles, gradually intensive from upper to lower quantiles. In combination, I conclude that fast particles go straight, but particles that go straight can either be fast or slow.

For increasing time lags τ_L, the dependence between small angles and large spatial displacements is decreasing. Large displacements lead to gradually altering angles at later points in time, whereas small displacements trigger rapid angle changes, e.g., as a result of diffusion in stagnant zones. Throughout the complete analysis, the tendency for a particle to go straight is persistent over many scales of dt and τ_L. For even larger values of τ_L and dt beyond the ones we can investigate in the sandstone sample, we can expect that process dependence will vanish fully.

3.4.6 Analysis of Memory Effects in the Cross Dependence (Pe = 10)

All previous analyses are based on a Péclet number of 100 in the PTRW simulation. In the following, I characterize the cross-dependence and memory under a more diffusive transport regime characterized by a Péclet number of 10. The corresponding Figures showing the results are

provided in the appendix (appendix A). Just like in the previous results for $Pe = 100$, the process has almost no visible memory in the absolute displacements for very small dt. As the time increments dt increase (larger relative Péclet number), dependence establishes and can be found especially among the large displacements. For this Péclet regime, memory is increasingly limited to fast particles for increasing time lags τ_L with additional memory for stagnating particles at very large time lags.

Likewise, the cross-dependence between displacements and azimuth over time shows the same characteristics as for $Pe = 100$. For the most parts in a comparison between the two transport regimes, I can say that the memory and the dependence structures are similar. However, there are important differences: First, under more diffusive conditions ($Pe = 10$), the dependence does not appear as quickly with increasing dt as it occurs for the more advectively dominated transport regime ($Pe = 100$). When advection is less influential, the particle movements are slower and they need larger time increments to experience the pore-space geometry that establishes dependence and memory. Second, and the most crucial, the evolving dependence at $Pe = 10$ shows a lot more persistence compared to the dependence characterizing the process for $Pe = 100$, as the largest analyzed τ_L is five times larger than at $Pe = 100$ and we can still see persistent cross dependence. Hence, if the transport regime is heavily influenced by advection, dependence appears quickly and remains persistent over a certain time. If the transport regime is more diffusive, the process at work needs more time to establish dependence but the resulting memory effects also last longer.

3.5 Evaluation of Research Objective One

I proposed this copula-based analysis framework to gain process understanding (RO1), and whether or not the copula-based analysis framework succeeds in providing this better process understanding will be evaluated in this section.

The copula-based analysis framework enables a physically sound and intuitive analysis of particle motion in complex porous media flows.

Such an in-depth analysis of memory of speed and direction has not been done before. One reason for that is undoubtedly that classical copulas are very hard to interpret in spherical coordinates while other tools that make sense in spherical coordinates cannot reflect non-linear dependence. The framework I proposed reflects the non-linearities not only in Cartesian coordinates but also in spherical coordinates. This is why the proposed analysis tool is highly appropriate to extract process understanding. Based on the capabilities of the analysis framework I can conclude that I could fulfill my research objective one.

Overall, the analysis indicates that process dependence persists over the considered scales but also does not vanish throughout the whole simulation interval. The persistent process dependence strongly suggests to incorporate process dependence into our models which will be done in the following.

Chapter 4

Trajectories as Training Images to Simulate Non-Fickian Transport

Chapter 4 may contain similar and/or identical formulations from my publications *Most et al.* (2016) [86]. I omit a clear identification of individual phrases for readability. I am reusing parts of the article with kind permission of the publisher WRR.

In the previous chapter, I have shown that the dependence structure of particle motion through a real porous media persists over a particular scale and that the process dependence goes beyond linear correlation (chapter 3). Hence, the statistical analysis in chapter 3, but also other studies [80, 82], suggest that process dependence has to be reflected in the simulation scheme to accurately represent particle motion over time and space.

In this chapter, I address research objective two (**RO2**) and therefore I propose a fully data-driven approach with the objective to improve prediction. I present a fully data-driven modeling tool for three-dimensional particle motion in real porous media. It reflects process dependence with a technique that is inspired by geostatistics (i.e., training images). The training trajectory approach that is introduced in this chapter is a novel way to reflect process dependence beyond correlation but it also addresses of the research question:

How can we use latest advances in DRP best to better understand transport

and simulate transport in porous media?

In specific, I directly use the high-resolution trajectories derived from DRP, I apply the gained system understanding from the previous chapter (i.e., memory persists over a particular scale), and I enable the simulation of particle motion in three dimensions without having to make typical simplifications such as dimensionality reduction or neglecting diffusion.

In the next section, I give an introduction to the training trajectory approach (section 4.1) that is followed by a detailed description of the proposed training trajectory approach (section 4.2). Then, I briefly recapitulate the specifications of the direct numerical simulation (DNS) at the pore scale (section 2.4), which is used for parameterization and reference. I proceed with the results and discuss comparisons of the one-particle and particle-pair statistics (section 4.4). Finally, I evaluate whether the training trajectory approach fulfills research objective two. A summary of this chapter and some concluding remarks can be found in part III.

4.1 Introduction to the Training Trajectory Approach

In advectively dominated transport settings, spatial velocity contrasts control the spreading of a particle plume [73] and local velocities control particle residence times within slow or fast zones [42]. Within these zones, a Lagrangian particle's velocity fluctuation is small compared to the total velocity variation of the entire velocity field [27, 36, 42, 72]. We can interpret this piecewise constant velocity as *memory of speed* that persists over some characteristic correlation length λ_v. Likewise, the direction α of a particle's motion persists (memory of direction) over a characteristic correlation length λ_α. Both these correlation lengths are specific to a given medium, reflecting details of the pore-scale geometry, which ultimately controls particle flow paths. Such memory effects prohibit the assumption that particle motion is a stochastically independent process, an assumption inherent to classical Fickian transport laws, as well as many

state-of-the-art non-Fickian ones. Ideally, upscaled models should account for the influence of *memory of speed and direction* [80, 82, 86].

In order, I propose a data-driven Lagrangian approach to simulate non-Fickian transport in realistic porous media. I apply the method to the pore scale.

As introduced in section 2.2.2, spatial Markov models (SMMs) [26, 63, 128] are a family of models that represent memory of speed and direction through the use of a transition matrix. While these models have been applied to a broad range of systems [e.g. 27, 63, 64, 66, 72, 73, 125, 126, 127, 129], they typically rely on parameterizing a transition matrix, which can be difficult to do, although approaches applicable to real data have emerged recently [64, 114]. Another approach has involved sampling of particle trajectories [129], which in turn can be used for mixed upscaling and downscaling models. These models can estimate nonlinear measures such as the dilution index or scalar dissipation and even predict mixing-driven reactions [126]. However, such applications are to date limited to synthetic and idealized periodic systems.

Translating such approaches to more realistic and complex geologies and geometries will be key to their future success. Here I propose a trajectory-based method to model transport and mixing in a realistic complex porous medium. This method is largely inspired by ideas relating to *training images*, considered state of the art in the field of geostatistics [60]. Training images extend the classical representation of spatial dependence beyond (linear) correlation and are capable of reflecting highly complex structures [134]. Training images are chosen such that they contain all relevant information about the spatial dependence one wishes to impose. Then they are *cut*, *copied*, and *pasted* in a suitable random fashion to simulate realizations of random space functions.

Instead of using an actual image, I replace the idea of a training image with an archive of fine-scale particle trajectories that contain all information about memory of speed and direction. These trajectories are obtained from highly resolved direct numerical simulations in a small sample of the medium of interest. The key idea to this approach is to randomly sample, cut and then suitably re-arrange segments of these

trajectories to construct larger-scale random trajectories that naturally reflect the required dependence structure. The overall hypothesis of this thesis is that all aspects of dependence are contained in the trajectories and hence an appropriate rearrangement of trajectory segments should reveal trajectories that resemble the original dependence structure. The ensemble of such trajectories represents the transport process. Unlike other SMM approaches, I no longer require a transition matrix. The manner in which I cut, copy, and paste the trajectories is conceptually similar to how training images are used to generate spatial random fields and therefore I call my method the training trajectory approach (TTA).

Continuous-time random walk (CTRW) models are widely and often implemented to model anomalous transport processes in porous media as an independent stochastic process [16, 121]. For this to be representative of heterogeneous systems, each spatial displacement must be larger than the length scales λ_{ind} over which velocities or transit times are statistically dependent (e.g., correlated).

Yet, in many instances, the scale λ_{ind} exceeds scales we are interested in, so that we cannot meaningfully use an uncorrelated model [35, 112]. One can overcome such restrictions by incorporating dependence, e.g., a SMM in which the subsequent transit time depends on the current one [26, 63, 128]. Even though SMMs refine spatial resolution, there are still limitations on the smallest possible scale at which they are valid. For a valid spatial Markov process, the autocorrelation of velocity must decrease exponentially [44, 128, 132] and hence the resolution of an SMM cannot be finer than one over which this holds.

Another challenge with SMMs is the parameterization of the transition matrix that describes dependence. The complex parameterization of this transition matrix might be why, to date, spatial Markov models are seldom applied to build effective three-dimensional models of finite-Péclet transport. As such, most applications to date are of reduced dimensional order, typically one dimension aligned with the principle direction of flow. In this case, parameterization of the transition matrix is substantially easier (while not trivial). However, I argue that the ultimate goal should be still to simulate three-dimensional particle motion. For this I propose an alternative parameterization of a SMM.

The proposed training trajectory approach extends state-of-the-art SMMs as follows: (a) it is a model that can upscale three-dimensional finite-Péclet transport, incorporating high-order process memory of speed and direction. (b) Training trajectories do not require a high-dimensional transition matrix and (c) I can represent particle motion at scales below the validity scale of spatial Markov models as I use segments of real trajectories to describe the particle path between states instead of a linear interpolation (the average location) as used in other SMMs. This last point is relevant for phenomena that are driven by details at small scales, such as dilution [69], mixing [74] and mixing-limited reaction kinetics [126]. An accurate representation of such small-scale processes requires more than just the average location of a particle as they are nonlinear processes for which one must be able to resolve subscale variability in concentrations accurately (Figure 4.2).

Therefore, I will test the performance of my approach not only against metrics that depend on mean concentrations or one-particle statistics such as arrival time distributions (e.g. breakthrough curves), but also against higher-order nonlinear metrics such as the dilution index [69]. I also analyze particle-pair statistics, e.g., the temporal evolution of the separation distance of particle-pairs conditioned on their initial separation.

4.2 The Training Trajectory Approach

Advances in digital rock physics together with direct numerical simulation (DNS) of pore-scale flow and transport in porous media can simulate highly realistic particle trajectories [20, 87, 98]. The details of the DNS are outlined in section 2.4 but, to summarize, I have to conduct thee major steps to produce trajectories: (i) discretize the pore geometry obtained from micro CT-imaging, (ii) solve the Navier-Stokes equations to obtain the flow field, and (iii) run a particle tracking random walk simulation. By tracking particle positions over time, I build what I refer to as the *training trajectories*. Full trajectories can then be divided into smaller trajectory segments of length λ_v (Figure 4.1). These segments are then used

to build a database (or archive) from which the increments within my SMM model are sampled. The full training trajectories inherently contain the processes that form a "larger-scale" perspective. To take advantage of this information, I propose an SMM that cuts, copies and pastes segments of the training trajectories in a manner that imposes continuity of velocity and direction, so that the resulting simulated trajectories inherit relevant properties and statistics from the full DNS-based trajectories, resulting in an upscaled model true to the small-scale physics.

A critical part of this model is the resampling approach (cut, conditional copy and randomized paste) that I propose. To avoid unphysical features at the intersections of trajectory segments (e.g., sharp edges and infinite accelerations; Figure 4.2 top) subsequent segments should be sampled conditional to the previous one, typically based on correlating consecutive velocities. This results in smoother transitions between sim-

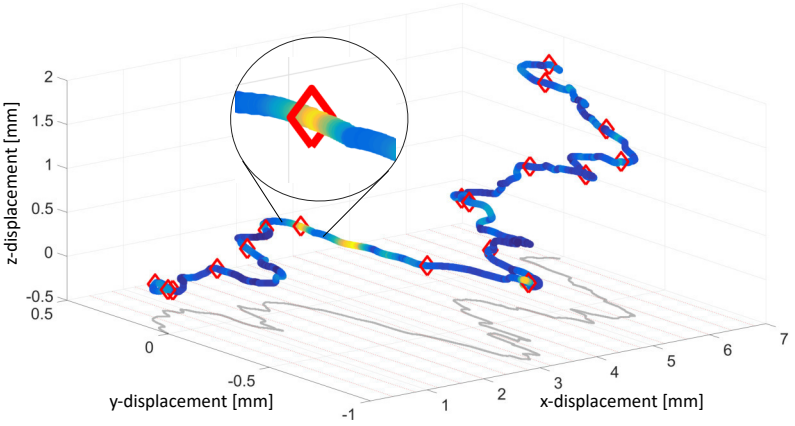

Figure 4.1: Resampled trajectory: The red diamonds subdivide the full trajectory into trajectory segments of length λ_v. The magnified area focuses on the intersection between two segments which is smooth in speed and direction. The red dotted lines on the ground indicate spatial intervals of length λ_v.

ulation steps (Figure 4.2 bottom). Doing this with average velocities per segment, however, would not yet ensure total smoothness because the average velocity need not align with the velocity at the end of a specific segment. It is this final part of the segment, which is important if I want to ensure physically realistic continuity of trajectory segments that are pasted together. Here I propose a methodology that reflects this.

I can subdivide my simulation scheme in three major steps: cut, conditional copy, and paste. First, from the full-length trajectories I cut out trajectory segments so that the series of appropriately merged segments can reflect the original process dependence (Figure 4.1 and more details given in section 4.2.1). Second, I choose (conditional copy) the upcoming trajectory segment such that I avoid sharp transitions in speed

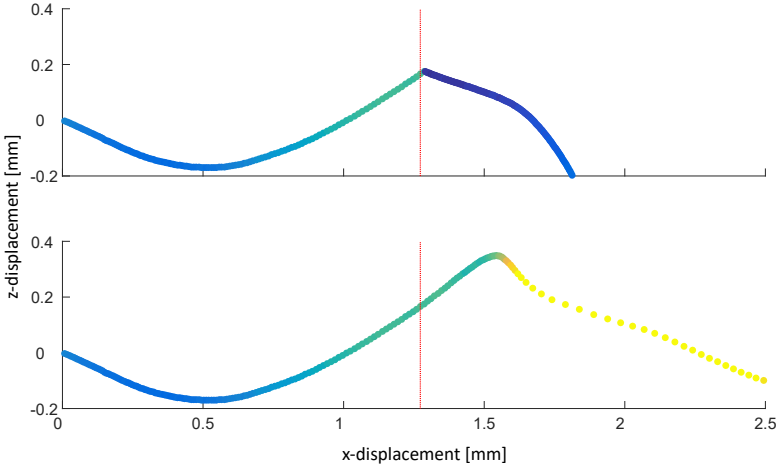

Figure 4.2: Upper: Unconditioned transition between trajectory segments results in a sharp transition in speed and direction at the intersection (red dotted line). Lower: Smooth transitions between trajectory segments generated by the TTA. The TTA represents particle motion at the resolution of the input data while other SMM and CTRW methods resolve transport only at spatial resolution of the upscaled model.

and direction between two segments (details in section 4.2.2). I ensure smooth transitions (i.e. smooth transitions in velocity and direction) by randomly selecting the upcoming segment (from the training trajectory archive) conditioned on the Cartesian velocity triplet of the current segment end. Third, I append (paste) the selected trajectory segment (details in section 4.2.3). I sequentially repeat this procedure many times to generate long trajectories. For the generation of an ensemble of full trajectories, I repeat the procedure multiple times.

These three steps require me to identify two characteristic lengths to form a valid Markov process that generates physically reasonable trajectories: a) the segment length λ_v and b) the length of the segment end λ_α that is relevant for the conditional random selection of the next segment (Figure 4.3).

4.2.1 Step 1 - Cutting: identifying the relevant scales

For a valid spatial Markov process two assumptions must hold: (1) the spatial correlation structure must be statistically stationary and (2) the particles next velocity state depends solely on the current state [105, 106, 123, 129]. In this chapter I follow the methodology of *Sund et al.* (2016) [128] and define the scale over which these two assumptions are valid by making use of a less commonly used metric - the autocorrelation K of the particles' velocity along the trajectory,

$$\mathrm{K}(j,i) = \frac{\mathrm{Cov}\left(v_i(\lambda), v_j(\lambda)\right)}{\sqrt{\mathrm{Cov}\left(v_i(\lambda), v_i(\lambda)\right) \cdot \mathrm{Cov}\left(v_j(\lambda), v_j(\lambda)\right)}} \tag{4.1}$$

where $\mathrm{Cov}\left(v_i(\lambda), v_j(\lambda)\right)$ is the covariance of $v_i(\lambda)$ and $v_j(\lambda)$. $v_i(\lambda)$ and $v_j(\lambda)$ are the velocities averaged along trajectory segments i and j with the length λ. As I assume statistical stationarity, $K(j,i) = K(|j-i|)$, all possible pairs of segments separated by $|j-i| \cdot \lambda$ for $|j-i| \in \mathbb{N}$ along the full-length trajectories have the same correlation. The velocity $v_i = \frac{\lambda}{\tau_i}$ with the transit time τ comes from the direct numerical simulations (DNS).

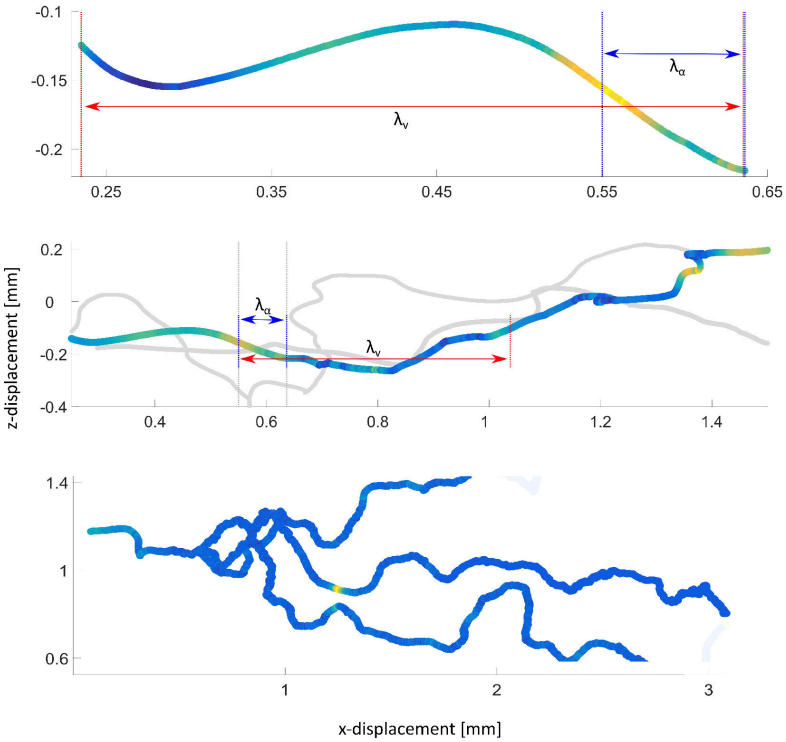

Figure 4.3: Upper: Trajectory segment of length λ_v over which the velocity process forms a spatial Markov process. Sub-segment length λ_α is the scale over which the component-wise velocity correlation is maximal. Middle: Sketch of the merging procedure between trajectory segments. At the juncture of two segments, I always exchange the first part (λ_α) of the next segment by the last part (λ_α) of the current segment. This ensures smoothness. The merging of all other trajectory segments (e.g., the grey trajectories) occurs in the same spatial intervals ($I = [n \cdot (\lambda_v - \lambda_\alpha) \quad n \cdot \lambda_v]$). Lower: Three trajectories evolving from the very same initial trajectory segment to show that the TTA does not simply copy the original trajectory based on the chosen initial segment.

To make use of the autocorrelation as an indicator, I exploit that particle motion is a normal process controlled by the local velocity and diffusivity. The spatial coordination of the velocity field defines the number of simulation steps a particles stays within a certain velocity class. The autocorrelation of a particle's velocity $v(\lambda)$ is a function of the averaging length λ. For very small λ, we can observe an independent process ($K \approx 0$) for all $i, j \in \mathbb{N}$ as particle motion on very small scales is dominated by diffusion. From there, the autocorrelation K increases with increasing λ as advection takes over process control and introduces memory into the velocity process. For even larger λ, the particle loses its memory and the particle motion can be considered again as independent (K converges back to zero) [128]. For a certain intermediate λ_v, however, advective-diffusive particle motion follows a Gauss-Markov process if the autocorrelation decays exponentially [44, 128, 132]. A Gauss-Markov process can be expressed as an autoregressive model with an one-step memory (AR(1)) in which the noise term is Gaussian. Hence, to express the velocity process as an AR(1), I require the autocorrelation function K between velocities averaged over a distance λ and separated by a distance $|j - i| \cdot \lambda$ to be exponential, such that

$$K(j, i)|_\lambda = K(|j - i|)|_\lambda = \exp(a_\lambda |j - i|) \tag{4.2}$$

where $a_\lambda \in \mathbb{R}^-$ can be related to the second largest eigenvalue of the (doubly stochastic) transition matrix $T(|j - i|)$. This eigenvalue describes the convergence of T towards the uniform stationary matrix [64, 65]. Parameter a_λ therefore uniquely parameterizes the transition matrix of the underlying Gauss-Markov process.

Now I need to relate $K(i, j)|_\lambda$ to $K(\lambda_v)|_{1,2}$ in order to define the scale λ_v over which we obtain the valid spatial Markov process. While $K(i, j)|_\lambda$ is the velocity autocorrelation in the proper sense, $K(\lambda)|_{1,2}$ is simply the velocity correlation between two adjacent trajectory segments of averaging length λ, but it is calculated the same way (equation (4.1)). *Sund et al.* (2016) [128] provide this link by analyzing $K(\lambda_v)|_{1,2}$ as a function of multiples of (a small) λ. They found that a_λ is in $\mathbb{R}^-$ and therefore parameterizes the transition matrix T only if $K(\lambda_v)|_{1,2}$ decreases mono-

tonically and with a positive second derivative. These are the fundamental requirements that I am subject to as well.

4.2.2 Step 2 - Conditional Copy: identifying the transition probabilities between segments

A second characteristic length λ_α is essential to determine the transition probabilities between consecutive trajectory segments in my SMM approach. Under advective influence, particle trajectories become smooth in direction and velocity after a scale smaller than λ_v. This is the scale, λ_α, at which the Péclet number indicates that advection dominates over diffusion, but well before larger-scale dispersion becomes relevant. I identify this scale by determining the peak of the autocorrelation function in (4.1) [129]. I ensure smooth transitions in direction and velocity by merging trajectory segments only if the Cartesian velocities at the contact faces are similar in velocity and direction over that scale. Therefore, I average the velocities $\bar{v}_\alpha \in \mathrm{R}^{d\times 1}$ component wise (x-,y-, and, z-direction; $d = 3$) over each segment end and beginning over length λ_α. Note, the averaging length λ_α in the main flow direction is a constant, and as a result the respective time (τ_α) over which I average varies for each subsegment I analyze.

Process memory is induced by advection, as diffusion is a fully memoryless process. Therefore, I store only the advective components s^l_A of the trajectory start-segments (averaged over length λ_α) in an archive with $l = 1 \ldots n_{\mathrm{arc}}$ entries. As mentioned before, I ensure smoothness by merging segments with similar Cartesian velocities $\bar{v}_\alpha\,(s)$.

Hence, the transition probability $p(s^l_{\mathrm{A}}|s_{\mathrm{AD}})$ of appending trajectory segments with start s^s_{A} must be proportional to the similarity between the velocity triplet of the current advective-diffusive subsegment s_{AD} and all candidate subsegments s^l_{A}. Here, similarity will be defined based on the tolerance introduced by diffusion within the time it takes advection to cover the distance λ_α. An example for a low transition probability $p(s^l_{\mathrm{A}}|s_{\mathrm{AD}})$ can be found in Figure 4.2 (upper). The velocities averaged over λ_α at the left (s_{AD}) and the right (s^l_{A}) of the red-dotted line results in

two vectors that point in very different directions. The same averaging applied to another potential upcoming trajectory segment shown in Figure 4.2 (lower) results in two vectors that point much more in the same direction which indicates a much higher transition probability $p(s_{\mathrm{A}}^{l}|s_{\mathrm{AD}})$.

To define the transition probability $p(s_{\mathrm{A}}^{l}|s_{\mathrm{AD}})$ based on the physics of the system, I must quantify the likelihood that the discrepancy between purely advective velocities in s_a and advective-diffusive velocities s_{AD} comes from diffusion alone which acts for a certain amount of time $\tau_\alpha = \frac{\lambda_\alpha}{\bar{v}_\alpha}$ a particle needs to pass λ_α. I quantify this likelihood by exploiting that molecular diffusion follows a Gaussian process. Hence I can quantify the likelihood of diffusion being the cause for the velocity discrepancies via the expression of the Gaussian likelihood:

$$p\left(s_{\mathrm{AD}}|s_{\mathrm{A}}^{l}\right) = \left(2\pi\sigma^2\right)^{-\frac{d}{2}} \cdot \exp\left(-\frac{1}{2\sigma^2}\sum_{i=1}^{d}\left(s_{\mathrm{AD,i}} - s_{\mathrm{A,i}}^{l}\right)^2\right) \tag{4.3}$$

where $\sigma(\tau_\alpha) = \frac{d}{2} D_{\mathrm{m}} \tau_\alpha$ describes the standard deviation of diffusive particle displacement in three dimensions ($d = 3$) over a time τ_α [47].

I derive the transition probabilities $p\left(s_{\mathrm{A}}^{l}|s_{\mathrm{AD}}\right)$ between the current segment s_{AD} and all candidate segments s_{A}^{l} by applying Bayes rule

$$p\left(s_{\mathrm{A}}^{l}|s_{\mathrm{AD}}\right) \propto p\left(s_{\mathrm{AD}}|s_{\mathrm{A}}^{l}\right) \cdot p\left(s_{\mathrm{A}}^{l}\right) \tag{4.4}$$

where $p\left(s_{\mathrm{A}}^{l}\right)$ is the prior probability of s_{A}^{l} being the best-fitting upcoming trajectory segment. Here, s_A^l is the candidate segment (of length λ_v) defined by the l-th purely-advective (subscript A) velocity triplet in the archive where $l \in (1, n_{arc})$. s_{AD} is the start of the current segment that contains advection and diffusion indicated by the subscripted AD. With this expression, I condition all potential upcoming segments on the last part (of length λ_α) of segment s_{AD}. The prior probability $p\left(s_{\mathrm{A}}^{l}\right)$ is uniformly distributed over the archive as, before relating s_{AD} to s_{A}^{l}, all candidate subsegments from the training trajectory archive are equally likely.

As a consequence and without loss of generality, I can erase $p\left(s_{\mathrm{A}}^{l}\right)$ from equation (4.4).

Altogether, I determine the transition probabilities of the spatial Markov process by applying Bayes rule together with the likelihood of a normal process. The transition procedure between consecutive trajectory segments can be understood as a classical conditional sampling in which the upcoming segment is drawn conditional to the velocity observed in the end part of the current trajectory segment (i.e. one-step memory). This random conditional sampling ensures that I do not simply copy trajectories starting from the initial trajectory segment as I show in Figure 4.3 (lower).

4.2.3 Step 3 - Paste: generating the simulated trajectories

In the remaining step, I merge the trajectory segments. Here, I exchange the first part (λ_α) of the next segment with the last part (λ_α) of the current segment (Figure 4.3). By doing so, I generate smooth trajectories that inherently encode the full memory of speed and direction of the underlying pore-scale transport process.

4.3 Obtaining the Training Trajectories by Direct Numerical Simulation

To demonstrate my approach, I use the same set of DNS-trajectories that is used to perform the dependence analysis in chapter 3. These trajectories provide the necessary archive of training trajectories and also acts as a benchmark.

For filling the archive and for performing the reference transport simulation, the volume-averaged velocity of the PTRW simulation is set to $v_{av} = 1.09896 \cdot 10^{-3} \frac{m}{s}$ which results in a $Pe = 100$ regime. In total I have again a set of 1000 DNS-trajectories that end at the downstream image

face. The particles are injected flux-weighted into the 30th image voxel layer to avoid backwards-directed diffusion across the upstream image face. A more detailed description of the flow and transport simulation is given in section 2.4 and in *Most et al.* (2016) [86].

4.4 Results & Discussion

4.4.1 Velocity Autocorrelation

First, I determine the characteristic length λ_v, the length (in the main flow direction) over which I have to average the velocities along the trajectories so that the autocorrelation $\mathrm{K}(j,i)\,|_{\lambda_v}$ decays exponentially. The measured correlation as a function of increasing averaging length λ for $Pe = 100$ is shown in Figure 4.4. For $\mathrm{K}(j,i)\,|_{\lambda_v}$ to decay exponentially, the velocity correlation $K(\lambda)|_{1,2}$ between two adjacent trajectory segments averaged over λ at least has to decay monotonically with a positive second derivative (section 4.2.1 or *Sund et al.* (2016) [128]). The correlation function $K(\lambda)$ appears to start being convex ($K''(\lambda) > 0$) at $\lambda \geq 6 \cdot 10^{-5}$m and is clearly convex at $\lambda_\mathrm{v} = 8 \cdot 10^{-4}$m, which represents 3 % of the total sample length. I keep λ_v as small as possible in order to merge as many trajectory segments as possible (roughly 34).

Second, I determine the characteristic length λ_α, required to ensure smooth transitions (section 4.2.2) by identifying the interval over which the autocorrelation is maximum; here $\lambda_\alpha = 1.6 \cdot 10^{-5}$m. This represents 0.6 % of the total sample length. Given these values, I can now run my proposed training trajectory model.

In the advectively dominated scenario ($Pe = 100$), diffusion is the reason why we have a peak in the autocorrelation function at λ_α (please note the logarithmic scale). The location of the peak λ_α and of the inflection point λ_v (of $K''(\lambda)|_{1,2}$) move in positive direction with increasing influence of diffusion. Therefore, the characteristic lengths λ_α and λ_v are shorter when derived from an in-average faster trajectory than when derived from a slow trajectory where diffusion has more time to act. Note,

I derive λ_α and λ_v by averaging over all trajectories and for this reason I potentially underestimate characteristic lengths for "slow" trajectories.

Next, I describe and compare several benchmark metrics to test and validate the proposed modeling approach.

4.4.2 Breakthrough Curves

I simulate the arrival time statistics at three control planes for a Péclet = 100 transport process. Breakthrough curves (BTCs) are measured at downstream distances corresponding to 30%, 60% and 100% of the total simulation domain. For testing, I use 5000 trajectories generated by the

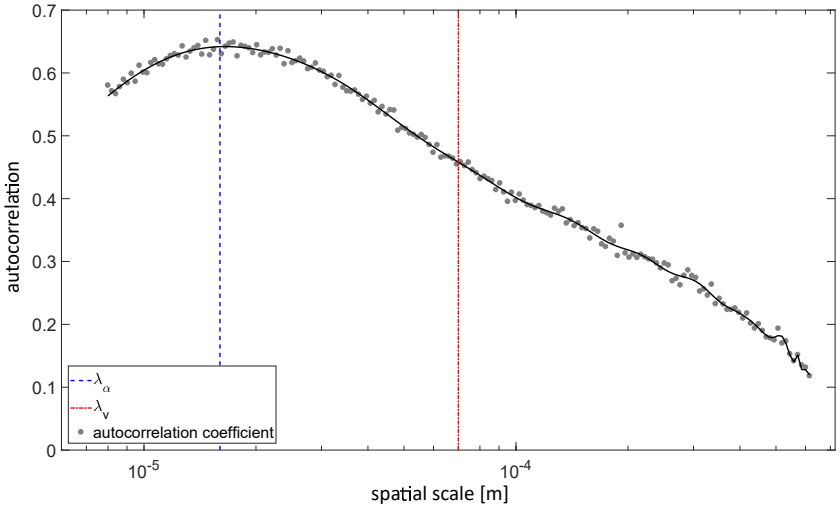

Figure 4.4: Evolution of the autocorrelation over space in longitudinal direction. The blue dashed line indicates the highest correlation and hence defines λ_α. The red dashed line lies in the range in which $K(\lambda)|_{1,2}$ decays monotonically with a positive second derivative and indicates my choice of λ_v. The full length of the trajectories is 2.69mm and the λ_v lies between 1 and 2 typical grain sizes.

proposed training trajectory approach. For comparison, I produce 5000 trajectories for which I select the consecutive trajectory segments randomly (*unconditional sampling*) from the archive of trajectory segments. The BTCs predicted by the training trajectories and by the DNS-based reference solution (1000 trajectories) show good agreement at all three control planes (Figure 4.5). There are no major deviations between model and benchmark in either early or late arrivals. These are typically the aspects where those strong non-Fickian transport signatures emerge that are the hardest to capture. The predicted BTCs deviate, as might be expected, from the benchmark when I select consecutive trajectory segments unconditionally.

To accurately predict arrival times at control planes in the longitudinal direction, the model has to reflect typical residence times in low-velocity (leads to tailing) and high-velocity zones (leads to early arrivals). Memory of speed is nothing else than these typical residence times that I aim to mimic. Hence, the BTC results indicate that I am realistically representing memory of speed with my training trajectory approach. The comparison between the conditional and unconditional TTA predictions versus the benchmark clearly suggest that the spatial Markov approach (i.e., conditional sampling) is the key step that introduces the required process memory to reflect the characteristic residence times in low- or high-velocity zones.

Even if the agreement of the arrival times is very good, I slightly underestimate the late-time arrivals. This is presumably an effect of underestimating λ_α, but especially λ_v, for the "slow" trajectories (section 4.4.1), which control the late-time behavior of the particle plume. To test this hypothesis, I increase λ_v by a factor of 3 and 6 (constant λ_α), which clearly improves the match, particularly in the late time behaviors (appendix B). The observed improvement suggests that perhaps λ_α and λ_v should not be derived from averaging over all trajectories but rather accounting for the slow ones in particular.

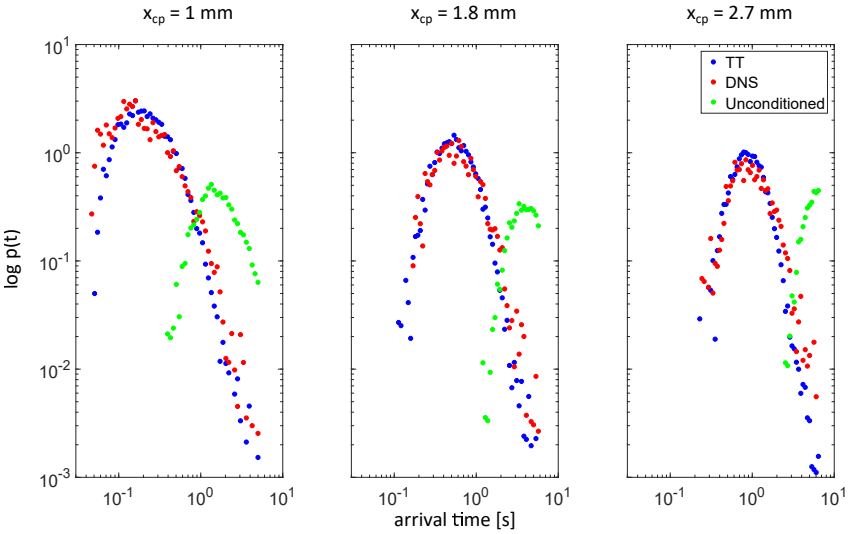

Figure 4.5: Comparison of the arrival time densities between the reference simulation (DNS) and the training trajectory approach (TTA) at three control planes at 30%, 60%, and 100% of the simulation domain ($\approx$ 2.7mm).

4.4.3 The Dilution Index

Matching BTCs indicate that the model does a good job of representing particle motion in direction of mean flow. Yet, it tells us nothing about the ability of the model to upscale more complex nonlinear behaviors that depend on the full three-dimensional nature of the particle plume. I will now further test the TTA's ability to accurately model such behaviors.

To this end, I will compare the evolution of the dilution index [69] over time as measured from the DNS and predicted by the TTA. The dilution index is a metric that describes how dilute a plume is, or in other words measures the total volume occupied. It is based on the concept of entropy that classically describes the disorder in a system. Dilution is controlled by spreading and mixing, both of which are tightly coupled [74]. I estimate the dilution index in discrete form. That means, I perform a histogram-type analysis where I count the number of particles in each cubic bin of $10 \times 10 \times 10$ voxels which relates to a typical pore size. For the histogram-type estimation, the dilution index is defined as

$$E = \Delta V \cdot \exp\left(- \sum_{k=1}^{r} P_k \cdot ln\left(P_k\right) \right) \tag{4.5}$$

where ΔV is the volume of a voxel and P_k is the fraction of particles in histogram bin k divided by the total number of particles. The dilution index is an excellent metric for testing the veracity of an upscaling procedure as it is highly sensitive to the full-dimensional nature of the plume and subtly reflects the complex interplays between spreading and mixing [69], which most upscaling approaches fail to capture.

In Figure 4.6 I plot the temporal evolution of the dilution index based on the TTA predictions, its unconditioned counterpart, and based on the DNS reference. In general, again, the agreement between the TTA and the DNS reference is close while we see clear a deviation when I merge trajectory segments unconditionally.

However, the agreement between TTA and DNS for this benchmark is less good than for the BTCs. The reason is that, in contrast to the DNS,

the TTA does not account for reflection at no-flow boundaries and the accessible space (number of bins) for particles is therefore unconstrained. Also, the dilution index is a nonlinear measure that is very sensitive to low concentrations (P_k enters equation (4.5) with $ln(P_k)$). Therefore, minor deviations between TTA- and DNS-based particle motion already lead to visible deviations in the dilution index. Again, as for the BTCs, the agreement is better for larger λ_v.

In Figure 4.6, the dilution index decreases after approximately 0.7 seconds. This seemingly unphysical behavior (re-appearance of order) comes from particles that exit the simulation domain and are thus removed from the system. However, DNS and TTA, especially for larger λ_v where the Gauss-Markov assumption also holds for slow particles, show this behavior in a very similar way. This fact still demonstrates the veracity of the TTA approach and suggests that I capture the desired memory processes also in three dimensions where particle motion is controlled by memory of speed and direction plus diffusion. Again, the results indicate that conditional sampling is significant to correctly incorporate memory of speed and memory of direction, necessary to accurately predict full three-dimensional transport processes.

4.4.4 Particle-Pair Statistics

Both BTCs and the dilution index are measures derived from the evolution of an ensemble of individual particles. Next, we look at the interaction between particles by analyzing the separation distance of two particles (i.e., particle pairs). This particle-pair perspective of transport is important because it provides insights on how particles diverge and converge, which can play an important role in understanding mixing and reaction processes. Additionally, it is a further and robust test of my approach to capture nontrivial dynamics that go beyond just predicting mean behaviors.

My key analysis metric is the probability density function $p(s^t|s^0)$ of the Euclidean separation distance s^t (at discrete time steps t) conditioned on the initial separation distances s^0. In the following, I will refer to

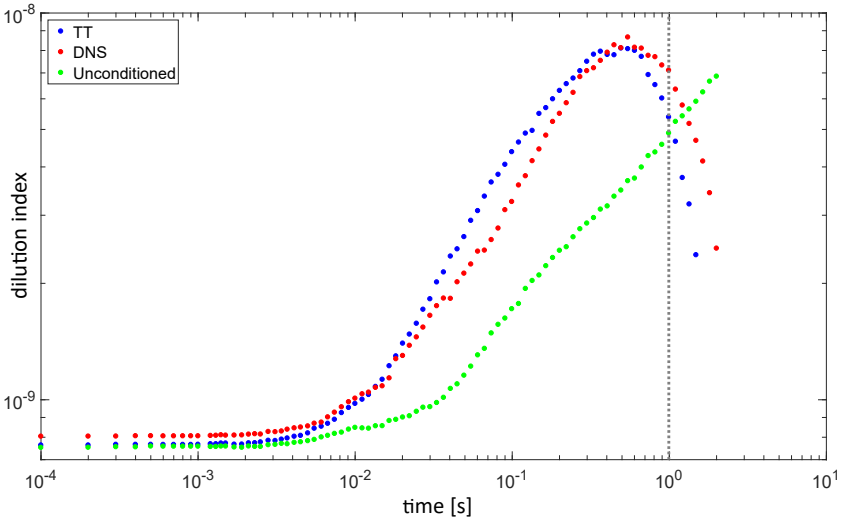

Figure 4.6: Temporal evolution of the dilution index derived by the reference simulation (DNS) and the training trajectory approach (TTA).

$p(s^t|s^0)$ as the *fingerprint of dilution*. In Figure 4.7 (a), I plot an example of this metric for an individual particle separation of 1.0mm $< s_0 <$ 1.1mm. Each cross-section orthogonal to the time axis (e.g., white dashed lines at $t = 0.05$, $t = 0.1$, and $t = 0.7$sec) represents a separation density $p(s^t|s_0)$ of particle pairs at these points in time. The horizontal line indicates the distance (s_{reac}) below which I assume potential reaction of particles, chosen as half of a typical pore size (0.13mm) for my sample [46].

Figure 4.7 (b)-(d) highlights three important measures related to the fingerprint of dilution, comparing results measured from DNS to predictions made by the TTA. These three metrics are

- The separation distance densities $p(s^t|s^0)$, shown at three different times for an initial separation distance 1mm $< s_0 <$ 1.1mm, which as noted correspond to the white vertical lines in Figure 4.7 (a).
- The evolution of entropy $H(s) = -\sum_{i=1}^{d} p(s^t|s^0) \cdot \log_2 p(s^t|s^0)$ over time for three initial separation distances $s^0 \approx 0.1$mm, $s^0 \approx 1.1$mm and $s^0 \approx 2.2$mm. I choose these relatively small and large separations to span a broad range of relevant separation distances.
- The reaction probability, defined here as the waiting time distribution of initially separated particles to fall below a fixed distance (here $s_{\text{reac}} = 0.13$mm), as discussed above. Results are shown for three initial separation distances $s^0 \approx 0.5$mm, $s^0 \approx 1.1$mm and $s^0 \approx 1.6$mm

Across all three metrics, the agreement between measurements from DNS simulations and predictions with the TTA are excellent, further solidifying the veracity of the proposed TTA, and suggesting that the TTA is capable of accurately simulating the rich dynamics of 3D particle motion in a complex porous medium flow.

Specifically, the agreement with the separation distance density suggests that the TTA captures characteristic convergence and divergence (i.e. interaction) mechanisms of particles. The agreement on entropy suggests that not only are characteristic diverging and converging mechanisms of particle pairs well captured, but also associated mixing dynamics. The results here also suggest that the TTA captures the complex inter-

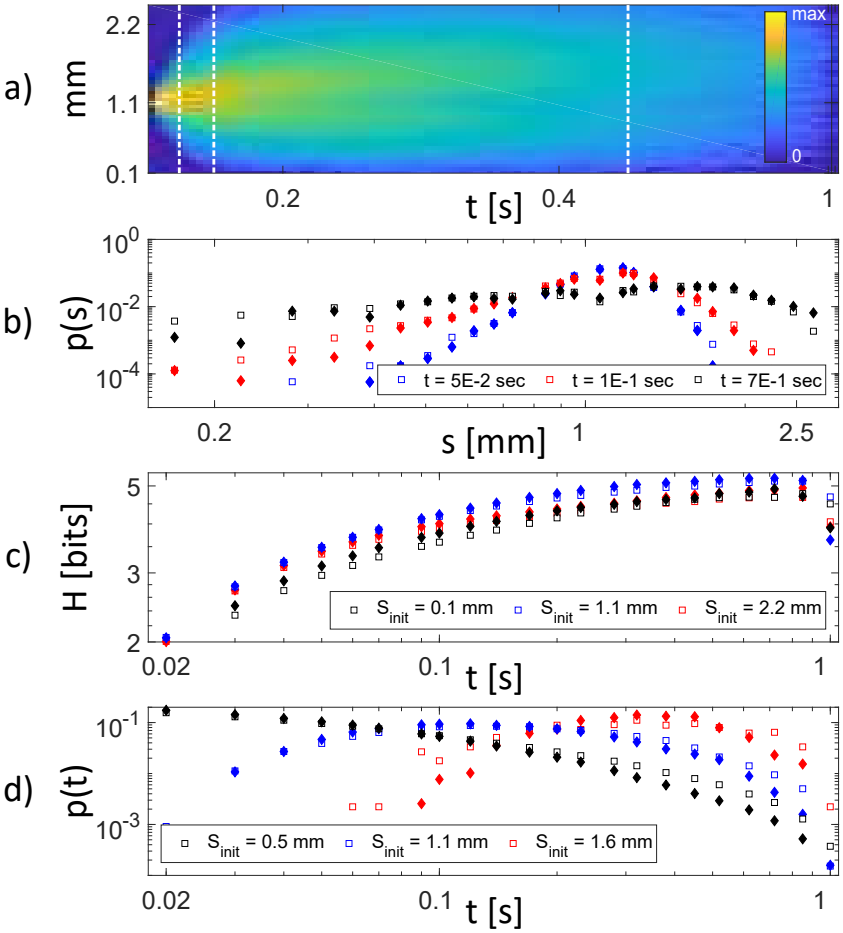

Figure 4.7: In general, the filled symbols represent the results for the training trajectory approach and the outlined symbol represent the results from the DNS. (a): Fingerprint of mixing: This Figure shows the temporal evolution of separation distance density function $p(s^t|s^0)$ of particle pairs conditioned on an initial separation of $s^0 \approx 1.1$mm (b): Pair-wise separation-distance density $p(s^t|s^0)$ with initial separation $s^0 \approx 1.1$mm at three different points in time. (c): Entropy over time as a measure for similarity between reference separation-distance density and the according pdf derived from the training trajectories. (d): Reaction potential over time given an initial pair-wise separation distance.

action of particles independent of the initial condition, given the broad range of initial separation distances. Reactions are strongly dictated by how close reacting particles can get and the probability of reaction increases dramatically when particle distances falls below a given threshold [45, 97]. The agreement here between DNS and TTA suggests that the TTA may be well suited to modeling not only conservative transport, but reactive transport processes as well. Thus it may be coupled with reactive random walk approaches, e.g., *Benson and Meerschaert*, *Bolster et al.*, *Edery et al.*, *Engdahl et al.* (2008, 2016, 2010, 2017) [11, 28, 45, 49].

4.4.5 Challenges and Opportunities

All of the tests that I performed against the benchmarks demonstrate good agreement between TTA predictions and reference DNS measurements, suggesting promise for the TTA approach. However, the way I parameterize the proposed spatial Markov process, while novel, is certainly not comprehensive and still necessitates further work. In my view, remaining research questions for TTA are:

Data Requirements: The approach (as I have implemented) it has quite demanding computational expense. It requires high-resolution simulation of flow and transport for the DNS simulation from which the trajectories are extracted. While the ultimate goal is expend this computational cost to simulate transport in a single REV to achieve upscaling over scales much larger than this, any ability to reduce computational demands at the REV-scale will be essential. In the context of previous SMM advances, such gains have been made by more efficient numerical models of small-scale processes (e.g., [129]) or by using simplified analytical models (e.g.,[66, 42]). At this stage I do not have a clear vision of what such approaches might be for the TTA approach. However, I am hopeful that similar advances are possible here and should be pursued in future research efforts.

Parameterization: I defined the scale over which I describe transport as a Gauss-Markov process by the correlation between the veloc-

ities averaged over consecutive trajectory segments. As I do that for all trajectories, the correlation function $\mathrm{K}(\lambda)_{1|2}$ I obtain reveals the peak location λ_α for an "average" trajectory. The characteristic length scales λ_α and λ_v obtained like this, however underestimate the lengths that are required to obtain optimal simulation results, presumably due to the slowest trajectories in the system. As shown, tripling this length scale leads to much better results. Thus, while my approach yields a decent first estimate, an improved and rigorous approach for obtaining these length scales should be sought.

Optimization: The conditional sampling procedure that finds the upcoming trajectory segment, is currently computationally intensive and increases with the number of archive entries. Thus, it can become a computational bottleneck in effectively implementing the method. This step, however, can be accelerated by implementing more efficient search algorithms; e.g. a k-d tree supported search algorithm that acts on equation (4.4). Currently, all trajectories have the same prior probability of being the upcoming segment. This is inefficient as the velocity triplet of many candidates deviates strongly from the current reference so that we could exclude them immediately before the conditional sampling through a non-naive efficient search. This could improve the search on average from being an $O(n)$ to an $O(\log n)$ operation.

Validation: Here, I have used the same sample to generate the trajectories for TTA parameterization and for the DNS validation. Admittedly, this makes the validation somewhat circular in nature, although this is not uncommon for many transport models, particularly in their first implementation. I openly admit that this is not ideal, but computational limitations restrict my efforts to go further. For now, I accept this compromise, but future efforts must go further. Ideally, if staying at small scales, I would have two distinct sandstone samples (which are statistically similar) and use one to infer the trajectories and the other to validate the simulation, e.g., via tracer tests or another DNS. Similarly, to test the true upscaling potential of this approach, it will be essential to compare to larger-

scale transport experiments through larger sandstone samples such as column experiments (e.g., [115]) and ultimately field-scale data (e.g., [66]).

Sufficient Statistics: Similar to the previous comments, it will also be important to analyze what properties (e.g., number, length, initial condition) characterize an ideal set of training trajectories? In the ergodic limit, one very long trajectory cut into segments should be sufficient to fill the archive. Most likely, the number of trajectories is less important than their initial condition, especially when the domain is limited. It seems that, in my case, 1000 trajectories are sufficient. But a thorough convergence study will be necessary to better validate this and identify potential error sources and uncertainties.

Generalization: Here, I have applied the TTA only to one 2.6mm^3 Doddington sandstone and the resulting velocity field is subject to the real pore geometry. While I see no obvious reasons why the TTA cannot be applied to other porous media than sandstones (e.g., carbonates or unconsolidated media) this remains to be truly validated.

Practical Use: If we can overcome some of the identified hurdles and validate the TTA across a diverse range of complex flows, I believe that this approach holds great success in effectively and efficiently predicting large-scale transport in complex porous media flows. In particular, the fact that the TTA can provide a three-dimensional upscaled picture of transport is key as many effective models of transport are of reduced dimensionality, which can limit their ability to predict nonlinear processes without further complex closures. This is relevant to better represent dilution or reaction process that occur at such fine scales.

4.5 Evaluation of Research Objective Two

Chapter 3 suggest that process dependence has to be incorporated into our modeling frameworks. The training trajectory approach incorporates process dependence very differently to any other spatial Markov models as we no longer parameterize dependence via transition matrices.

Nonetheless, different does not mean automatically better, but the modeling results are very promising. I compared DNS measurements of a broad range of benchmark metrics (e.g., arrival times or dilution index) against predictions made with our proposed TTA. Additionally, I analyze particle pair statistics based on the evolution of separation distances of particle pairs over time. From these tests, I can conclude that we can simulate particle motion and its interaction in a three-dimensional porous media. It would be interesting to see how the TTA performs in comparison to another three dimensional SMM, but unfortunately, there is no other SMM that simulates transport in three dimensions. Hence, the extension of SMM to three-dimensions itself significantly improves the existing set of prediction tools (RO2) that are based on spatial Markov processes.

Additionally, the TTA represents particle motion at scales below the validity scale of spatial Markov models as I use a segment of a real trajectory to describe the particle path between states instead of a linear interpolation (the average location) as used in other SMMs. This is relevant for phenomena that are driven by details at small scales, such as dilution [69], mixing [74] and mixing-limited reaction kinetics [126].

Overall, the TTA is a fully predictive data-driven simulation tool that extends spatial Markov models to three dimensions, and that represents particle motion below the scale of other SMMs. This clearly improves the family of spatial Markov models, and hence I can conclude that the TTA fulfills research objective two.

Chapter 5

Scaling Transport across Péclet Regimes

In chapter 3, I have shown that process understanding and dependence is the key to better models. The training trajectory approach, introduced in chapter 4, incorporates process dependence to accurately predict three-dimensional particle motion. Nevertheless, the training trajectory approach (such as almost all other SMMs) requires a highly accurate transport simulation for its parameterization. Such spatial Markov models are particularly tailored to the Péclet regime of the reference simulation that is used for parameterization.

In this chapter, I address research objective three: To obtain a generalized model formulation. Therefore I propose an adaptive time-domain random walk model that scales transport across Péclet regimes. The key to this generalization is that the adaptive time-domain random walk model is parameterized only by information obtained from the velocity field, which can easily be scaled across transport regimes [20].

In the upcoming section, I introduce the adaptive time-domain random walk. Then, I briefly recapitulate the DNS specifications used in this chapter (section 5.2.1). This is followed by the description of methods including a detailed description of the adaptive TDRW (sections 5.2.2 - 5.2.4). In section 5.3, I present and discuss the application of the models to finite-Péclet transport ($Pe = 10$ and $Pe = 100$) for a sample of Doddington sandstone. Finally, I evaluate whether the adaptive TDRW fulfills research objective three. The summary of this chapter and some concluding remarks can be found in part III.

5.1 Introduction to the Adaptive Time-Domain Random Walk Approach

In porous media, non-Fickian transport processes are usually caused by spatial fluctuations of the fluid velocity field at the pore scale [21, 63, 74]. The local velocity of slow or fast velocity zones controls the particle residence time in these zones. Within these zones, the particle velocity remains fairly constant during the respective residence time, which I refer to as memory of speed. *Le Borgne et al.* (2008) [73] summarize that local velocity contrasts control the spread of particles in general, but these contrast also trigger characteristic non-Fickian features like a strong tailing of the particle arrival time or non-Gaussian spatial particle distributions mainly as a result of memory of speed along particle trajectories. The question arises on how to parameterize memory as a function of space or time. Usually, memory of speed expresses itself in long intervals of slow velocities interrupted by short intervals of fast velocities, known as intermittency [36, 63]. This suggests that memory of speed persists over a certain spatial distance rather than over a certain amount of time. Based on these arguments, *Dentz et al.* (2016) [42] conclude that it is more appropriate to describe non-Fickian transport as spatially correlated velocity process.

The existence of such a characteristic length scale suggests the application of a continuous-time random walks (CTRW) method [13, 14, 39, 79, 83, 90] with equidistant displacements, also known as time-domain random walks (TDRW). As mentioned before, classical CTRWs (for which the spatial transition distribution can be a random variable as well) and TDRWs have been successfully applied many times to simulate non-Fickian transport at pore scale [5, 18, 41, 63, 73], at Darcy scale [16, 39, 46, 72, 107, 109], in fractured porous media [10, 37, 64, 90] and also in turbulent flows [116, 131]. CTRW methods model non-Fickian transport as an independent stochastic process by assigning a random transit time to a spatial transition greater than the correlation length scale [16].

The key to a generalized model formulation (RO3), however, is a parameterization of the simulation tool only via properties of the ve-

locity field. This is important as it is the velocity field, and not the advective-diffusive particle trajectories, that can easily be scaled across Péclet regimes. However, this kind of parameterization is not straightforward with current CTRW tools:

(a) The intention of directly using the pore-scale velocity field, obtained from DRP, demands for displacements equal to the spatial resolution of the pore-scale velocity field. Any other displacement would incorporate an averaging (e.g., [43, 84, 109]), which adds inaccuracy, especially for heterogeneous media. At that scale, however, consecutive velocities are correlated and thus not directly applicable to classical CTRWs or TDRWs.

(b) Spatial Markov models (section 2.2), also known as correlated CTRW models, incorporate correlation and thus allow displacements at the resolution of the DNS-simulation. But to date, with some exceptions (e.g., [114]), we need a high-resolution, pore-scale transport model as a prerequisite to parameterize the transition matrix.

(c) Therefore, such spatial Markov models are particularly tailored to the Péclet regime of the (computationally expensive) reference simulation, which prohibits the efficient scaling of the SMM surrogate across Péclet regimes.

(d) *Dentz et al.* (2016) [42] propose a TDRW that incorporates velocity correlation along streamlines by a Markovian velocity process solely parameterized by a unique (stationary) velocity distribution. Even if promising, this study omits diffusion, which is the second mechanism that controls the correlation pattern of the velocity process.

For a fully diffusively-driven process, *Dentz et al.* (2012) [41] show convergence for a TDRW with exponentially distributed transit times to the heterogeneous diffusion equation. *Russian et al.* (2016) [109] extended this TDRW to simulate advective-dispersive transport with independent exponentially distributed transit times that are parameterized by the particles' local advective and diffusive mass exchange rate.

Physically, however, we have to solve a first passage time problem under advection and diffusion, which follows an inverse Gaussian and

not an exponential distribution [5, 53]. Exponentially distributed transit times solely approximate the underlying physics of particle motion. This introduces inaccuracy that becomes relevant for transport within moderate and high Péclet regimes (e.g., $Pe = 10$, and $Pe > 100$, more details in sections 5.2.4 and 5.3).

Below I introduced the adaptive TDRW approach that does not anymore suffer from the four (i.e., a-d) difficulties because:

The proposed adaptive TDRW reflects process memory via correlated consecutive transit times (a), which allows a parameterization only via properties of the velocity field. (b) This simplifies the non-trivial parameterization of existing CTRW as we no longer have to run a costly transport simulation. In particular, I account for memory of speed by piecewise constant velocities with random jumps to new values at random points in time. The random jumps in velocity are equally probable in each simulation step and occur in average after particles pass the correlation length λ.

(d) The first novelty I present in this chapter is that I account for the effect of diffusion by drawing transit times either from an inverse Gaussian or from an exponential distribution according to the local particles' velocity. (c) As second novelty I scale transport across Péclet regimes by explicitly model the effects of advection and diffusion, not only its effects. This includes the evolution and decay (i.e., the asymptotic return to Fickianity) of non-Fickian transport and so my TDRW approach - herein referred to as adaptive TDRW - is valid from local to pre-asymptotic to asymptotic scales.

5.2 Methods

5.2.1 The Reference Simulations

To assess the quality of the adaptive TDRW transport simulation, I use again the direct numerical simulation (DNS) of flow and transport

through a sample of Doddington sandstone thoroughly described in section 2.4. The velocity field that I use to derive the velocity distribution function is the same that is used to perform the PTRW from which I obtain the reference trajectories for comparison.

5.2.2 The Inverse Gaussian Distribution

In this study, I focus on CTRW simulation tools and asses their accuracy in predicting arrival times at certain control planes. As an alternative to numerical models, the inverse Gaussian distribution provides the analytical solution for the arrival times under the assumptions of Fickian transport laws and hence for advective-diffusive particle motion in a homogeneous porous medium [70],

$$p(\tau_a; x_{cp}, \bar{v}, D_e) = \frac{x_{cp}}{\sqrt{4 \cdot D_e \cdot \tau_a^3}} \cdot \exp\left(\frac{-\left(x_{cp} - (\bar{v} \cdot \tau_a)\right)^2}{4 \cdot D_e \cdot \tau_a}\right) \tag{5.1}$$

where $\bar{v}$ and D_e are mean particle velocity and hydrodynamic dispersion coefficient. Parameter x_{cp} is the location of the control plane, $\bar{v}$ is the mean of the velocity field and D_e can be derived from the temporal evolution of the mean squared particle displacement.

Non-Fickian transport is characterized by arrival times, which deviate from the inverse-Gaussian distribution. The purpose of the comparison between the measured arrival times (e.g., tracer or as here a DNS) and its Fickian reference is to show that the pore geometry of the sandstone samples affects transport in a non-Fickian way (Figure 5.2).

5.2.3 The Purely Advective Continuous-Time Random Walk

Continuous-time random walk models have been applied successfully to simulate transport in highly heterogeneous porous media [17, 63, 36, 74].

In the CTRW context, particle motion along trajectories over time and space can be formulated by the recursion relations,

$$s_i^{n+1} = s_i^n + \theta, \qquad t_i^{n+1} = t_i^n + \tau_i^n \tag{5.2}$$

where s is a point in space and t is a point in time.

While the displacements θ can follow an arbitrary distribution $\Phi(\theta)$, for transport in porous media the displacements θ are often kept constant (e.g., [63, 128]). In such an *equidistant* CTRW (also known as TDRW), each displacement θ has to exceed the medium-specific correlation length λ to ensure stochastic independence between consecutive displacements which is an inherent assumption to CTRWs [14, 13, 39, 112, 128]. By claiming $\theta \geq \lambda$, we ensure independence and for $\theta = \lambda$ we also ensure the highest possible spatial resolution of particle motion.

The transit time τ follows a probability distribution $\Psi(\tau)$ and the challenge in the design of a CTRW is to map all important aspects of particle motion within the complex porous medium onto Ψ. The identification of Ψ in order to represent the trapping and release of particles in slow velocity zones lies at the heart of CTRWs [15].

In order to emphasize the significance to incorporate diffusion into the simulation scheme, I parameterize the transit time distribution $\Psi(\tau)$ simply as the inverse of p_s,

$$\Psi(\tau) = \frac{\lambda}{p_\mathrm{s}(v)} \tag{5.3}$$

where p_s is the s-Lagrangian velocity distribution that will be introduced below.

This parameterization deliberately ignores the effect of diffusion on particle motion, which will affect primarily the late-time behavior of the breakthrough curves (e.g., exaggerated tailing). Other CTRWs that reflect diffusion via an appropriate choice of the transit time distribution $\Psi(\tau)$ accurately represent particle motion. However, this parameterization requires, for instance, DNS of pore-scale transport and is thus valid

only for the Péclet regime under consideration. This parameterization cannot be scaled to represent transport across different Péclet regimes.

The velocity statistics

In this chapter, I aim to parameterize all employed equidistant CTRW models (i.e., purely advective CTRW and in the following two TDRWs) only by the velocity distribution of the underlying velocity field. Hence, the underlying velocity distribution must reflect the statistics of equidistant particle transitions. According to *Dentz et al.* (2016) [42] this is the s-Lagrangian velocity density $p_{\mathrm{s}}(v)$ that can be derived by sampling the velocities along the particles' trajectories at fixed spatial intervals (*equidistant sampling*).

The counterpart of s-Lagrangian velocity statistics are t-Lagrangian velocity statistics $p_{\mathrm{t}}(v)$ for which the velocities are sampled at fixed temporal intervals along particle trajectories (*isochronal sampling*). Assuming Lagrangian ergodicity, the t-Lagrangian velocity density $p_{\mathrm{t}}(v)$ is equal to the ensemble velocity density $p_{\mathrm{e}}(v)$ and this is what we can derive directly from the DNS based pore-scale velocity field as the empirical density of the voxel velocities. *Dentz et al.* (2016) [42] show that we obtain s-Lagrangian velocity density simply by flux-weighting the ensemble velocity density $p_{\mathrm{e}}(v)$ as:

$$p_{\mathrm{s}}(v) = \frac{v}{\langle v_{\mathrm{e}} \rangle} \cdot p_{\mathrm{e}}(v) \tag{5.4}$$

with $\langle v_{\mathrm{e}} \rangle$ as the mean absolute velocity:

The relation between t-Lagrangian and s-Lagrangian velocity statistics allows us to directly use the pore-scale velocity field (e.g., obtained with methods from section 2.4) to parameterize all CTRW models that will be used in this chapter.

For scaling transport across Péclet regimes, we need to adapt the initial $p_{\mathrm{s}}(v)$ (here: from DNS for $Pe = 100$) so that it represents the advective conditions of an arbitrary transport regime. In order to scale transport

from $Pe = 100$ to $Pe = 10$, I divide $p_s(v)$ by a factor of 10 to correct for the average velocity (section 2.4: $Pe = \frac{u_{av} \cdot L}{D_m}$). This is very similar to how pore-scale transport simulations (DNS) are scaled across Péclet regimes [18].

We do not have to modify λ as the correlation length is an intrinsic property of the pore geometry and is not affected by varying Péclet conditions. For Doddington sandstone, I assume the correlation length λ to be at the range of one typical grain size which is $d_{grain} = \lambda = 269.29 \cdot 10^{-6} m$. *Bijeljic et al.* (2013) [21] show that it is a reasonable assumption as the correlation lengths derived from variograms for porosity and velocity for several rock samples lie (in most cases) in the range of one typical grain size.

The velocity process

Now, that I have derived the physically correct velocity statistics, I introduce the velocity process used for all CTRW methods that will be compared in this chapter.

The direct application of the grid-based velocity field used in the DNS suggests the use of a CTRW framework with constant spatial particle transitions equal to the spatial resolution of the velocity field d_{voxel}. The intention of using the velocity field directly demands for displacements equal to the spatial resolution of the velocity field (d_{voxel}) as any bigger length would incorporate an averaging that adds avoidable inaccuracy. The formulation of the velocity process is therefore similar to the classical CTRW formulation in equation (5.2) but in equation (5.5) the equidistant particle displacements d_{voxel} is distinctively smaller than λ:

$$s_i^{n+1} = s_i^n + d_{voxel}, \qquad t_i^{n+1} = t_i^n + \tau_i^n. \tag{5.5}$$

As a consequence of $d_{\text{voxel}} \ll \lambda$, we have to incorporate process memory, and I do that by correlating consecutive particle velocities over a λ-dependent number of equidistant simulation steps, which is controlled

by a random Bernoulli process. Therefore, I draw a Bernoulli-distributed random number $\xi_n(\alpha)$ in each simulation step n. While $\xi_{n\ldots m} = 0$, I generate a series of spatially fully correlated velocities, as $v_{\mathrm{Adv}}^{n+1} = v_{\mathrm{Adv}}^{n}$. Once the particles exceed λ ($\xi_{m+1} = 1$), we draw a new advective velocity v_{Adv}^{n+1} from p_{S}. In this scheme, the Bernoulli process controls the number of equidistant displacements that is equal to the number of simulation steps up to which consecutive velocities are correlated. According to the medium-specific correlation length λ , the Bernoulli process $\xi_n(\alpha)$ can be parameterized by $\alpha = \frac{d_{\mathrm{voxel}}}{\lambda}$ such that $\xi = 1$ once the particles cross λ (in average).

The generation of the series of correlated velocities is described by:

$$v_{\mathrm{Adv}}^{n} = \begin{cases} P_{\mathrm{s}}^{-1}(U) & \text{if } \xi(\alpha) = 1 \\ P_{\mathrm{s}}^{-1}\left(P_{\mathrm{s}}\left(v_{\mathrm{Adv}}^{n-1}\right)\right) = v_{\mathrm{Adv}}^{n-1} & \text{if } \xi(\alpha) = 0. \end{cases} \tag{5.6}$$

Here, U is a uniformly distributed random number between 0 and 1. This design of the velocity process ensures that particle velocities are correlated over the medium-specific correlation length.

Keep in mind, the velocity statistics (p_{s}) and velocity process, which we employ in the purely-advective CTRW framework, are used in the same way in the upcoming two TDRW frameworks. The three methods (i.e., purely-advective CTRW, the exponential TDRW and the adaptive TDRW) are different in that each method parameterizes its transit times differently (i.e., purely-advective CTRW as $\tau = \frac{\lambda}{v}$). A detailed description of how the TDRWs are parameterized, is given in the following.

5.2.4 Time-Domain Random Walk with Exponentially Distributed Transit Times

Generating the transit time distribution $\Psi(\tau)$ simply as the ratio of transition length θ and the pure advective particle velocity v_{adv} is problematic when v_{adv} is infinitesimal because transit times become infinite. The particle residence time within a nearly-zero velocity zone is controlled

by diffusion and leave low-velocity zones by diffusion rather than by advection.

Dentz et al. (2012) [41] and *Russian et al.* (2016) [109] propose a time-domain random walk (TDRW), which reflects that slow particles leave zero-velocity zones via diffusion. Central to the TDRW approaches is the derivation of expected particles' advective-diffusive transit time κ at a distance θ that parameterizes an exponential transit time distribution. Especially, for a diffusively dominated particle motion, the exponential distribution is the physically correct distribution as diffusion is per definition a memoryless process [41].

For parameterization of the exponentials, we define the advective-diffusive rate b_{ij} for particles that move from node j to node i as:

$$b_{ij} = \frac{D_\mathrm{e}}{\theta^2} + \frac{v_{ij}^{n-1}}{\theta} \cdot \frac{1}{2} \left(\frac{v_{ij}^{n-1}}{|v_{ij}^{n-1}|} + 1 \right). \tag{5.7}$$

Term one represents a diffusive rate where D_e is the effective diffusion coefficient and term two represents an advective rate where v_{ij}^{n-1} is the local advective velocity in the previous simulation step $n-1$. The probability w_{ij} of moving from node j to node i and the expected local transit time κ_j can be expressed as:

$$w_{ij} = \frac{b_{ij}}{\sum_{[jk]} b_{kj}} \qquad \kappa_j = \frac{1}{\sum_{[jk]} b_{kj}}. \tag{5.8}$$

We define $v_{ij} > 0$ and hence node i is always downstream of node j. As a consequence, $b_{ij} \neq b_{ji}$ as b_{ij} is finite-Péclet, whereas $b_{ji} = b_{ij}$ in case of pure diffusion. The notation $[jk]$ indicates the summation over the two rates in drift and against drift direction (hence k indicates a neighboring cell), which results in $\sum_{[ij]} w_{ij} = 1$.

With κ_j as the expected local transit time of particle j we can parameterize an exponential transit time distribution:

$$\tau_j \sim \kappa^{-1} \exp\left(-t \cdot \kappa^{-1}\right). \tag{5.9}$$

Exponentially distributed transit times, in contrast to the inverse of the velocity distribution, account for the diffusive cut-off of the arrival time distribution and limits the residence time of particles in no-flow zones.

Nonetheless, the arrival times of an advective-diffusive transport as a normal process with drift follow an inverse Gaussian distribution and the exponential distribution solely acts as an approximation. The transit times of an advective-diffusive process over a specific distance follow an inverse Gaussian distribution [5, 53]. As said before, the approximation works well for diffusive Péclet regimes where the transit times demonstrably converge to the analytic solution of the heterogeneous diffusion equation [41]. However, for transport in intermediate Péclet regimes, the exponential transit times deviate strongly from those drawn from an inverse Gaussian distribution (Figure 5.10 for $Pe = 1$). Another critical point is than, when we apply exponentially distributed transit times, the transit times remain random, even under fully advective ($Pe = \infty$) and hence deterministic conditions.

5.2.5 Time-Domain Random Walk with Adaptive Transit Times

The inverse Gaussian distribution provides the physically correct arrival time distribution for a Gaussian process with drift at a control plane - however, only for a control plane in drift direction [5, 53]. As a consequence, we do not track particles that go beyond the characteristic length d_{voxel} against drift direction where they also lose their memory of speed.

Hence, neither inverse Gaussian nor exponentially distributed transit times represent transit times of particles sufficiently accurate across the full Péclet range. I propose a TDRW approach that exploits the advantages of exponential and inverse-Gaussian transit times by choosing the physically appropriate distribution according to the local Péclet number. In advectively dominated zones, particles are unlikely to effectively

move against drift direction, and we apply inverse Gaussian distributed transit times. If diffusion is strong, the effective motion against drift is likely, and we apply exponentially distributed transit times to approximate the arrival times at the control plane in and against main flow direction. Hence, we apply inverse Gaussian distributed transit times if advection controls transport ($Pe \geq 1$) and if diffusion controls transport ($Pe < 1$,) we apply exponentially distributed transit times to approximate particle motion.

Both, exponential and inverse Gaussian distributed transit times are parameterized by the current particle velocity v_{adv} and the effective diffusion coefficient D_e. We parameterize the local transit time distribution τ according to:

$$\tau^n\left(t, d_{\mathrm{voxel}}, v_{\mathrm{adv}}^{n-1}, D_{\mathrm{e}}\right) = \begin{cases} \frac{d_{\mathrm{voxel}}}{\sqrt{4D_{\mathrm{e}}t^3}} \exp \frac{-\left(d_{\mathrm{voxel}} - \left(v_{\mathrm{adv}}^{n-1} t\right)\right)^2}{4D_{\mathrm{e}}t} & \text{for Pe} \geq 1 \\ \kappa^{-1} \exp\left(-t\kappa^{-1}\right) & \text{for Pe} < 1. \end{cases} \tag{5.10}$$

In equation (5.10), parameter t is the time and κ is the expected transit time (section 5.2.4). The parameters v_{adv}^{n-1} and D_{e} act as scaling and shape parameters.

Previously, I claimed that the simulation scheme has to (a) reflect the chosen Péclet regime and (b) the spatial correlation of the velocity field. The former is done by applying inverse Gaussian transit times when we can assume a Gaussian process with drift and by applying exponentially distributed transit times when transport is governed by diffusion. Hence, the transit times adapt automatically to the local transport regime, and this is what allows us to scale across Péclet numbers (RO3: generalization). I incorporate the spatial correlation of the velocity field by employing a Bernoulli process to sample the s-Lagrangian velocity distribution P_{s} systematically to generate correlated transit-time series drawn from a Péclet-dependent transit time distribution. With that scheme, I exploit the advantages of the Markov Chain CTRW presented in *Dentz et al.* (2016) [42], and I extend this approach to apply it to any finite-Péclet transport regime.

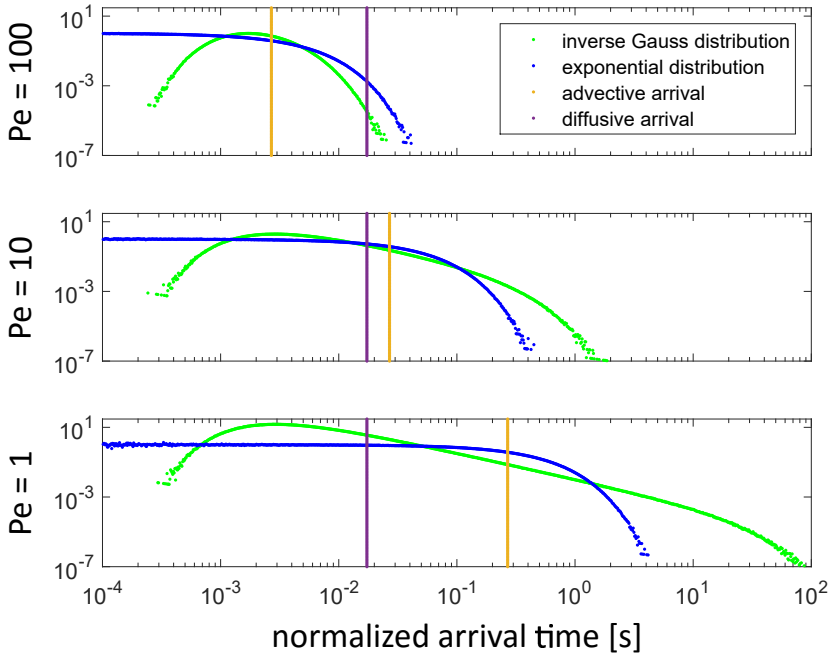

Figure 5.1: Exponential and inverse Gaussian distributed waiting times normalized by the respective advective mean arrival at three different Péclet regimes.

To facilitate the understanding, I give a stepwise summary of the adaptive TDRW scheme for one particle:

Input: the flux-weighted Eulerian velocity distribution function P_s and a correlation length λ (RO3: parameterization only via the velocity field).

1. We start with the initial advective-only particle velocity v^n_{Adv}.
2. According to a Bernoulli random number $\xi(\lambda, d_{\mathrm{voxel}})$, we decide either to draw a new advective velocity from P_s (if $\xi = 1$) or to leave the particles advective velocity unchanged (if $\xi = 0$).
3. We determine the local Péclet number ($Pe = \frac{v^n_{\mathrm{Adv}} d_{\mathrm{voxel}}}{D_e}$) and draw the particle transit time to pass d_{voxel} from an inverse Gaussian distribution if $Pe < 1$ or from an exponential distribution if $Pe \geq 1$. We obtain the particle transit time τ^{n+1} for a finite Péclet transport process.
4. Now, the scheme recursively starts from step 1 with v^{n+1}_{Adv} as the new initial advective-only particle velocity.

5.3 Results & Discussion

In this section, I show that transport through the pore space of the Doddington sandstone reveals non-Fickian characteristics by comparing the DNS arrival times to the analytic solution of the inverse Gaussian distribution. Then, I assess the accuracy of the applied CTRW models (i.e., adaptive TDRW, the purely-advective CTRW (section 5.2.3), and the exponential TDRW (section 5.2.4) by comparing the modeled arrival times based on 10^5 particles against the DNS reference (10^3 particles). Similarly, I assess the scaling of the transport from a Péclet 100 to a Péclet 10 transport regime.

Comparison between DNS and the inverse Gaussian

In Figure 5.2, the tailing of the DNS-based arrival times at Péclet 100 deviate from the fitted inverse Gaussian distribution. Non-Fickianity is

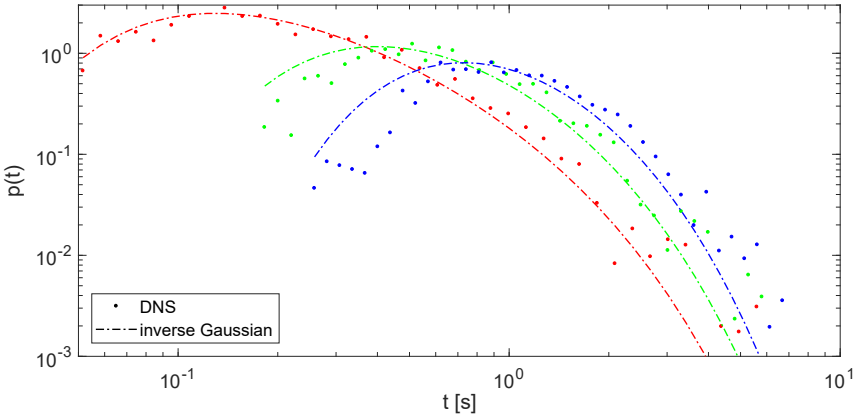

Figure 5.2: Comparison of particle arrival times at $Pe = 100$ between DNS arrival times and a fitted inverse Gaussian distribution at three control planes (30% (red), 60% (green), and 100% (blue) of the total domain length).

therefore triggered predominately by anomalously long residence times in low-velocity zones of the pore space. This behavior is typical for non-Fickian transport processes and shows that particle motion through the pore space of the Doddington sandstone sample goes beyond the Fickian description of transport.

Comparison of the simulation tools at Péclet 100

In the left column of Figure 5.3, I show the three CTRW-based and the DNS-based breakthrough curves for a Péclet 100 transport process and control planes at $x_{\mathrm{CP}} = 1.08mm$, $x_{\mathrm{CP}} = 1.89mm$, and $x_{\mathrm{CP}} = 2.69mm$ (30%, 60% and 100% of the total modeling domain). For visualization, I choose histograms to represent the tailing of the arrival times as direct as possible. As I am interested in tailing, I employ a double logarithmic axis to generate the histograms.

The adaptive TDRW-based BTCs coincide well with the DNS-based

reference. However, there are (small) differences regarding the early arrivals. I suspect the root of these deviations in the DNS of the transport process. Here, the particle injection plane is close to the boundary condition. In such a setting, boundary effects can influence the velocity evolution in a non-physical manner. Due to limitations in sample size, I am not able to prove this hypothesis ($d \gg \lambda$).

Nevertheless, the overall accordance between the model and the reference BTCs is convincing - especially when we recall that the whole simulation scheme is fully predictive. Hence, the accuracy of results suggests that the herein presented adaptive TDRW scheme is capable of representing the underlying transport process.

For the early arrivals at Péclet 100, all three CTRW models provide similar results. This is expected for this model set-up with relatively small displacements ($d_{voxel} = 2.6 \cdot 10^{-6}$m) under strong advection. Here, inverse Gaussian and exponential transit times do not deviate much from the expected advective arrival time ($\tau_{\mathrm{a}} = d_{\mathrm{voxel}} / v^{n}_{\mathrm{Adv}}$).

The three CTRWs differ, however, if we consider the tailing of the arrival times. The purely-advective CTRW, by design, overestimate the tailing. The exponential TDRW and especially the adaptive TDRW particularly simulate diffusion and thus provide the desired diffusive cutoff. The comparison of the respective arrival times against the DNS-reference shows that the adaptive TDRW represents the tailing accurately while the exponential TDRW overestimates the late arrival times. At Péclet 100, advection is the dominating mechanism that controls particle motion. Under these conditions transit times follow an inverse Gaussian and not an exponential distribution. In this setting, the adaptive TDRW represents particle motion closer to the underlying physics, and this results in the higher modeling accuracy.

Comparison of the simulation tools after scaling transport from Péclet 100 to Péclet 10

The right column of Figure 5.3 shows the arrival times after scaling a $Pe = 100$ transport process to a $Pe = 10$ transport process. The mod-

eled evolution of the adaptive TDRW arrival times coincides well with the DNS-based reference at $Pe = 10$, within the simulation window of the reference data. The deviations in the early arrivals are weaker compared to the Péclet 100 simulations and reduce, due to stronger diffusion, comparably fast (no visible effects at control plane two and three). This fact supports the hypothesis that the initial condition affects the arrival times at control planes close to the particles origin. Nevertheless, the results shown in both columns of Figure 5.3 indicate that by, individually simulating advection and diffusion, we are capable of scaling a transport process across Péclet regimes.

For $Pe = 10$, all CTRW models provide very different results. The deviation between the advective CTRW from the TDRW simulations is expected. Yet, I illustrate the results to highlight the significance of diffusion. The two TDRWs, however, deviate even if they should represent the very same transport process. Due to limitations in the reference data, there is no way to assess the quality of the TDRW models especially in their ability to represent the late-time behavior of particle motion. Nonetheless, it seems that the diffusive cut-off in the reference simulation is earlier and more abrupt than simulated by the exponential TDRW. The adaptive TDRW seems to more accurately represent this cut-off and hence the late-time behavior of particle motion. The reason for the deviation is the difference in the exponential and inverse Gaussian distributions. They are very different for moderate Péclet numbers, e.g., $Pe = 1$ or $Pe = 10$ (Figure 5.1). Here, especially the tailing of the exponential distribution is much stronger than for the inverse Gaussian distribution, which causes the deviations in the later arrival times (exponential vs. adaptive).

These differences in the distributions do not only affect the late-time behavior. The exponential TDRW also overestimates the behavior of the early arrivals, especially at control planes two and three where we can assume that the influence of the initial condition has vanished. Even under moderate Péclet conditions (i.e., $Pe = 10$), particle motion is dominated by advection and the arrival times at a control plane should be distributed, according to the inverse Gaussian distribution, around the expected advective arrival time. This is different for exponentially dis-

tributed arrival times because infinitesimal arrival times (instead of the expected advective arrival time) are always those with the highest probability (Figure 5.1). This property of exponential distributions is the reason why the exponential TDRW, in contrast to the adaptive TDRW, overestimates the early particle arrivals. Even under relatively strong diffusion, the early arrivals are predominately controlled by advection and therefore given by inverse Gaussian distribution. Note, the early-time behavior of particle motion is much better represented in the reference data, as fast particles are very likely to pass the control planes even within the relatively narrow temporal simulation window of the reference. Hence, I can conclude that the adaptive TDRW is the more reliable modeling tool to predict the early-time behavior of particle motion.

Overall, the simulation results indicate that the Péclet-dependent interplay between inverse-Gaussian and exponentially distributed transit times of the adaptive TDRW reflects particle motion under advection and diffusion much better than the exponential TDRW. The adaptive TDRW is close to the underlying physics and this is why it is a reasonable assumption that the adaptive TDRW also better represents the late-time behavior of particle motion in moderate Péclet regimes. Of course, this has to be proven by comparison with a DNS reference simulation that reflects the late-time behavior of particle motion as well.

5.4 Evaluation of Research Objective Three

In chapter 3, I have shown that process understanding and dependence is significant. In chapter 4, I then proposed a simulation tool that reflects process dependence, which requires a highly accurate transport simulation for its parameterization.

In this chapter, I addressed research objective three: Obtain a generalized model formulation (chapter 5). The adaptive time-domain random walk model provides this generalization in that it enables the simulation of particle motion across Péclet regimes. The parameterization of the adaptive TDRW, only by properties of the velocity field, enables the simulation of advection and diffusion as two individual processes, which is

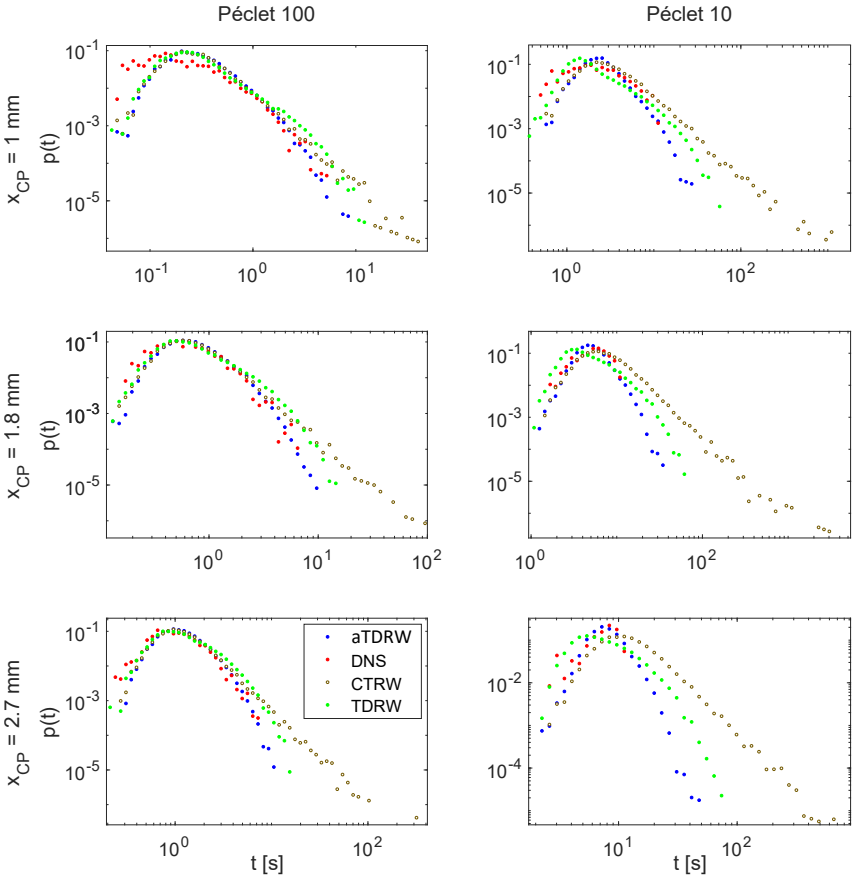

Figure 5.3: Distribution of the arrival times at 3 control planes at 30% ($\approx 3 \cdot \lambda$), 60% and 100% of the total domain. The left column shows the arrival times at $Pe = 100$. The right column shows the arrival times for the down-scaled transport simulation at $Pe = 10$.

the key to the scaling of transport across Péclet regimes and hence the key to the generalization.

Overall, the adaptive time-domain random walk provides an accurate, predictive, and generalized model formulation. Hence I can conclude that the adaptive time-domain random walk fulfills research objective three.

Part III

Summary & Conclusions

5.4.1 Motivation & Objectives

Traditionally transport in porous media is described by Fickian transport laws, which assume transport to be a stochastic process with independent increments. This means that dissolved particles do not reveal any kind of memory, neither memory of speed nor memory of direction, while they move through a porous medium. This assumption is invalid at many scales as dissolved particles keep their speed and direction over a material-specific temporal and spatial scale.

Digital rock physics, a relatively new technique in the geosciences, provides excellent insights into particle motion far below the pore scale and even below the size of the governing heterogeneities of the velocity field. Recent advances in X-ray tomography made it possible to describe advective-diffusive transport in the pore space of highly resolved computer tomography images. From these simulations, we obtain particle trajectories in great detail that are assumed to contain all information about process dependence and memory.

Having access to such highly-resolved data about particle motion enabled me to test the **main hypothesis** of this work: Extracting and reflecting process dependence is the key to understand and simulate transport in porous media. Closely linked to this hypothesis is my **overall research question**: How can we use latest advances in digital rock physics best to better understand and simulate transport? In this thesis I provide a framework to answer this question by addressing my **three research objectives**: (1) Gain detailed process understanding, (2) improve predictions with data-driven techniques, and (3) obtain a generalized model formulation.

5.4.2 Approaches

Copula-based Analysis Framework

First, I have performed a full statistical analysis of advective-diffusive pore-scale transport in a real pore geometry, adopting the Lagrangian

(here: particle based) view and choosing a copula-based method to assess memory of speed and direction in the motion of virtual particles through porous media (chapter 3). With this framework, I studied the evolution of non-Fickian transport and the return to Fickian transport as a function of increasing time increments in observing particle positions and as a function of time lags τ_L between time increments dt. The data (particle trajectories) for this analysis are provided through direct numerical simulation (DNS) of advection and diffusion in the pore space of a sandstone rock image. The main findings are:

1. I found that a statistical analysis in a spherical coordinate system results in a clear description of the underlying physics. In this coordinate system, particle motion is described by the absolute displacement and two angles. This has two advantages: (a) stagnant and mobile zones can easily be distinguished by the absolute displacement. (b) The provided view onto the underlying physics is much more intuitive and allows more meaningful analysis compared to analyses in a Cartesian system.

2. At very small time increments, only fast particles tend to stay fast whereas, at larger time increments, only the slow particles tend to remain slow. The slow particles at small time increments and the fast particles at larger time increments do not reveal such a tendency. Hence, at the small scale, non-Fickianity is triggered by fast-flow channels whereas, at larger scales, non-Fickianity is triggered by stagnant velocity regions. This means that (a) the root of non-Fickianity strongly depends on the considered scale (dt) and (b) the stochastic process descriptions currently used in non-Fickian transport simulations to account for the inherent process dependence only have a limited range of validity with respect to numerical time step sizes.

3. Large particle displacements are aligned with the main flow direction, whereas stagnant particles can move in an arbitrary direction. This memory of direction, the cross-dependence between longitudinal and transversal displacements, is highly nonlinear and persistent over time. The cross dependence is usually neglected in

other studies and in non-Fickian, continuous-time random walk simulations but appears to be significant.

4. The lower the Péclet number of the transport regime becomes, the weaker is the general dependence and memory of the transport process. Even if the general dependence is weaker at smaller Péclet numbers, the involved (weaker) memory effects show a stronger persistence over time than in transport processes characterized by larger Péclet numbers.

Overall, I have shown in chapter 3 that, for pore-scale transport, the dependence is persistent in all directions, that the dependence is highly nonlinear, that the dependence behaves differently on different temporal scales, and that the persistence of the dependence changes with the Péclet-number of the transport regime.

The majority of studies that analyze non-Fickian transport perform simplifications; either with respect to the pore geometry or to the analyzed direction. This analysis framework provides an extension of all these studies, as I have analyzed the transport process without doing any a priori simplifications.

Training Trajectory Approach

Building on the gained process understanding, I have proposed a trajectory-based spatial Markov approach to simulate three-dimensional transport in porous media through a Doddington sandstone sample at $Pe = 100$ (chapter 4). The proposed method borrows ideas from state-of-the-art non-Fickian spatial Markov transport models and blends them with ideas from the concepts of training images. Training images are commonly used in geostatistics and are known for their ability to model highly complex spatial dependence structures that go well beyond linear correlation. This feature is highly desirable in the context of upscaling pore-scale non-Fickian transport as this is often tied to process dependence beyond linear correlation [36].

Instead of a training image, for my proposed method, I use highly-resolved particle trajectories, obtained from direct numerical simulation of pore-scale transport. These trajectories inherently contain all relevant information about the dependence structure of the velocity process at the pore scale. The main idea is to subdivide particle trajectories into trajectory segments (*cut*) and then re-sample these to build simulated trajectories. Key to my approach is that I only allow subsequent segments to add to the previous ones in a way that ensures smooth transitions of direction and speed at the intersections (*conditional copy*). By recursively merging (*paste*) trajectory segments, I can generate trajectories of arbitrary length. This way, I can generate trajectories that reflect the same dependence structure as the original trajectories. I use the trajectories to represent the dependence structure of the velocity process in a similar manner than training images are used to describe spatial dependence. Therefore I call the method training trajectory approach.

With the training trajectory approach I overcome three frequent drawbacks of other spatial Markov models:

1. I do not require simplifications that have often been invoked in other studies such as dimensionality reduction or neglecting diffusion.
2. I do not require an explicit parameterization of process dependence, i.e., a high-dimensional transition matrix. I incorporate process dependence directly by a merging procedure that ensures transitions are smooth in speed and direction.
3. I represent particle motion at the resolution of the training trajectory and hence can accurately make inferences at scales smaller than other spatial Markov models. This is relevant when we consider smaller-scale processes (e.g., dilution, mixing, or reaction).

These benefits do come at a price as discussed in section 4.4.5, including, in particular, computational costs both in parameterizing and implementing the models. However, as advances in spatial Markov models from the original work of *Le Borgne et al.* (2008) [73] have shown, I am hopeful that similar advances can be made to the training trajectory approach.

To test the training trajectory approach, I compared the direct numerical simulation measurements of a broad range of benchmark metrics against predictions made with the proposed training trajectory approach. First, I analyzed statistics of a particle plume including arrival time distributions and the temporal evolution of the dilution index. Additionally, I analyzed a slew of particle pair statistics based on the evolution of separation distances of particle pairs over time. In all cases, the agreement between measurements and predictions was good, demonstrating the veracity of the training trajectory approach and demonstrating that the training trajectory approach can accurately capture the fully-dimensional nature of transport along with the complex interplays between spreading and mixing dynamics. Based on the outcomes, I am confident that this method can accurately model the complex three-dimensional dynamics of a particle plume and the interaction between the particles within the plume.

Adaptive Time-Domain Random Walk

Existent continuous-time random walk models with correlated consecutive simulation steps demand for a highly resolved and therefore computationally more expensive transport simulation to parameterize the model. Then, the parameterization is only valid for the applied transport regime, represented by its Péclet number.

To overcome this limitation, I presented a time-domain random walk approach that incorporates velocity correlation, that is (a) predictive (no fitting involved), (b) relatively easy to parameterize and that (c) scales across different Péclet regimes (chapter 5). I parameterized the model only with information provided by a DNS-based velocity field by deriving an (equidistant) velocity distribution and a correlation length of the velocity. Then, I sampled the velocity CDF in such a way so that particles keep their advective velocity over a distance that is, on average, as long as the correlation length (roughly a typical pore size). Finally, I drew the respective advective-diffusive transit time from an inverse Gaussian distribution if the particle is driven predominately by advection ($Pe > 1$) or from an exponential ($Pe \leq 1$) distribution if the particle is predominately

driven by diffusion. The transit time distributions can be parameterized by the local advective velocity and the molecular diffusion coefficient.

I tested the modeling framework by comparing the simulated arrival times against a direct numerical simulation of pore-scale transport. Based on this comparison I can conclude that the presented time-domain random walk approach is capable of successfully representing the complex pore-scale transport process. The Péclet 100 velocity distribution was then re-scaled to model a Péclet 10 transport process. The accordance between the scaled transport simulation and the DNS-based reference indicates that, by specifically representing advection and diffusion as separate processes, the approach is capable of scaling transport across Péclet regimes.

I also compared the adaptive time-domain random walk against a purely advective continuous-time random walk and a time-domain random walk with exponentially distributed transit times. The continuous-time random walk and the exponential time-domain random walk perform worse, especially at moderate Péclet conditions. The proposed adaptive time-domain random walk scheme selects the transit time distribution according to the underlying Péclet scheme and is therefore very close to the governing physics. This is why the adaptive time-domain random walk provides good simulation results across the full range of Péclet regimes.

5.4.3 Prospective Work

There is further work necessary to establish the herein proposed methods in science and practice:

All proposed methods should be applied to more challenging porous media such as carbonates to test whether their performance remains convincing. Furthermore, I am hopeful to get access to a direct numerical simulation that is performed with more than 1000 particles and also performed over larger temporal and spatial scales (this, however, is yet limited by computational power). More particles and a larger domain enable

a better convergence check and the exclusion of boundary effects (in the training trajectory approach and adaptive time-domain random walk).

In particular, the copula-based analysis, or more specifically copulas, are closely related to transition matrices. Therefore, it will be interesting to see how copulas and hybrid copulas can help to parameterize transition matrices for three-dimensional particle motion which are yet hard to fill.

The training trajectory approach is a very powerful tool but comes at the price of a high computational burden. Nonetheless, the results look very promising. The methods developed and tested here are proofs of concept, and hence, there are numerous opportunities to optimize the scheme (e.g., exchanging the conditional sampling by a non-trivial kd-tree search). The most intriguing aspect for future studies is to exploit the high resolution of the produced trajectory in reactive-transport simulations as reaction occurs on very small scales.

A key step for upcoming work is to asses the quality of the model against a reference simulation that covers a sufficiently long interval, so that all particles arrive at the control planes. Moreover, the adaptive time-domain random walk is yet implemented for a one-dimensional transport problem only but I do not see (apart from a larger data demand) obvious reasons why we could not extend to three dimensions.

5.4.4 Key contributions and conclusions

Each of the three proposed methods addresses one particular research objective (sections 3 - 5). From the results, I can conclude, that (1) the copula-based analysis framework reveals an intuitive and physically sound way to gain process understanding, (2) the training trajectory approach improves prediction as it accurately models particle motion and the interactions without commonly made simplifications, and (3) the adaptive time-domain random walk scales transport across Péclet regimes, which is a major generalization.

Each method for itself does not provide an satisfying answer to my research question. In combination, however, the developed methods provide the answer to the question of how can we use digital rock physics best to better understand and simulate transport. The proposed framework employs the DNS-based data in a novel way and results in analysis and simulation tools that overcome major shortcomings of current analysis and simulation tools. From the results of the analysis and the simulation tools, I can draw the following overall conclusions:

1. Process dependence does not vanish during the simulation interval considered here and must therefore be incorporated into the models. This conclusion supports other studies that also found that the assumption of independence is seldom true (e.g., [35, 113]).

2. Incorporating process dependence directly via the proposed resampling scheme (not via transition matrices) successfully reflects the process dependence and it describes transport at the scale of the training data. Hence, even though the training trajectory approach is merely a surrogate, its resolution is fine enough to represent small-scale processes such as dilution, mixing, and reaction.

3. Separating advection from diffusion is the key to scale transport across Péclet regimes as the velocity field, which parameterizes the whole model, can easily be scale across the transport regimes.

My findings confirm the hypothesis that the key to understanding and simulate transport in porous media is to extract and reflect process dependence. With this thesis I demonstrated that we obtain better models and more reliable predictions if we implement detailed process understanding. I proposed an advanced analysis, a modeling tool, and a generalized modeling framework for particle motion through complex three-dimensional porous media. None of these techniques demand for an a-priory simplification of the medium and this is why we can apply them directly to real word solute transport problems. Hence, these methods enable us to better safeguard our subsurface water quality and therefore this thesis can contribute to protecting our safe drinking water resources.

Appendix A

Supporting Information for "Dependence Analysis of Three-Dimensional Particle Motion"

This supporting information contains the illustration of the same statistical analysis as presented in chapter 3. First, figure A.1 shows the cross-dependence for $\tau = 0$. Second, figures A.2 and A.3 show the copula analysis of the transport simulation under more diffusive conditions (Péclet = 10). The interpretations can be found in chapter 3.

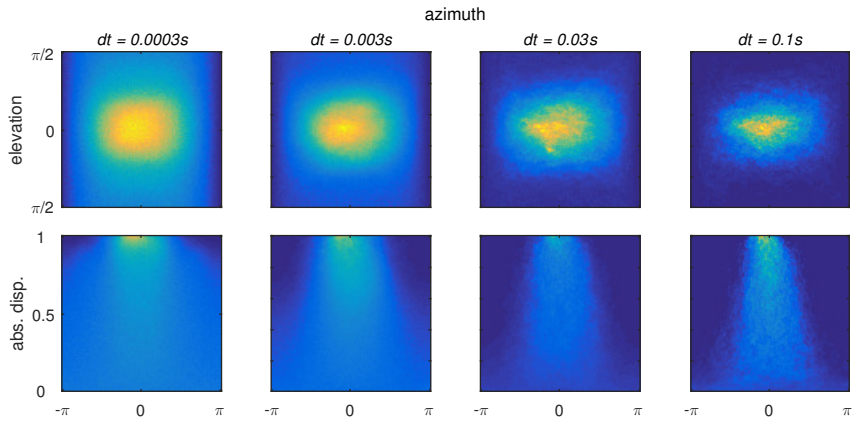

Figure A.1: Cross-dependence for $\tau = 0$. Top row: azimuth versus elevation; Bottom row: absolute displacement versus azimuth.

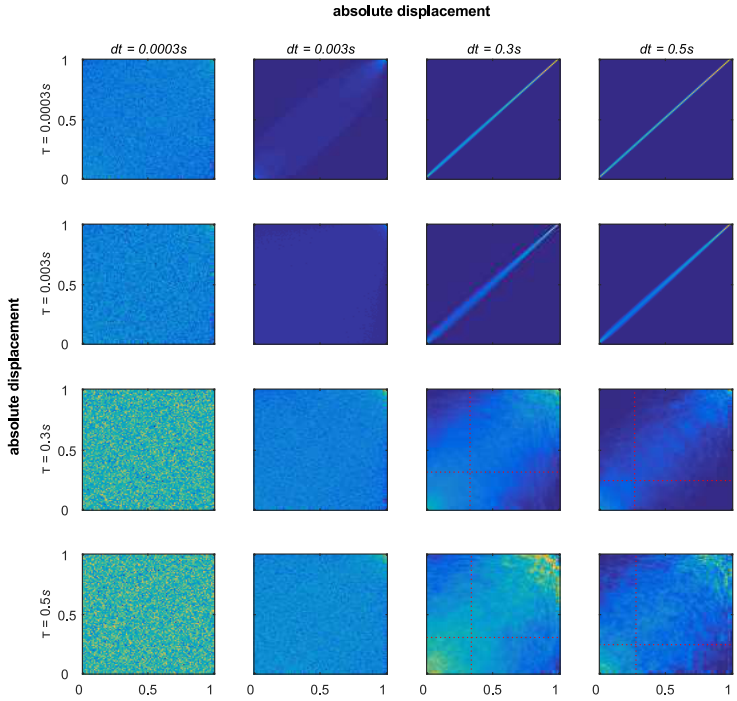

Figure A.2: Copula densities for absolute displacements under advective and diffusive transport at $Pe = 10$ between increasing time increments dt separated by increasing time lags τ. The dashed-red lines mark the critical displacements that define the transition between the stagnant and the mobile zone.

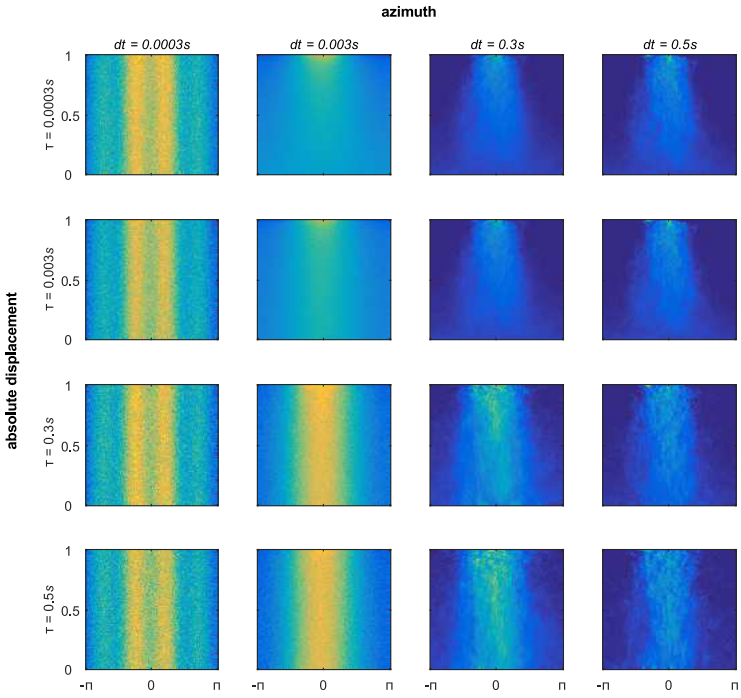

Figure A.3: Copula densities between absolute displacement and azimuth under advective and diffusive transport at $Pe = 10$ between increasing time increments dt separated by increasing time lags τ.

Appendix B

Supporting Information for "Trajectories as Training Images to Simulate Advective-Diffusive, Non-Fickian Transport"

In this section I show how a larger λ_{v} improves the overall model accuracy. By increasing the scale of the underlying Gauss-Markov process I make sure that the process assumption also hold for slow particles. From the increasing accuracy, I can conclude that $K(j,i)\,|_{\lambda}$ should be derived from the in-average slower trajectories as this improves the modeling accuracy. The definition of "in-average slower" goes beyond this work and is something that has to be analyzed in upcoming studies.

In the following, I visualize the modeling results for the breakthrough curves (see B.1 and B.2) and the dilution index (see B.3 and B.4) for $\lambda_v = 2.4 \cdot 10^{-4}$m and $\lambda_v = 4.8 \cdot 10^{-4}$m. I do not show the results of the two-particle statistics for this λ_{v} specification as even for smaller λ_{v} the accordance between model and reference is high.

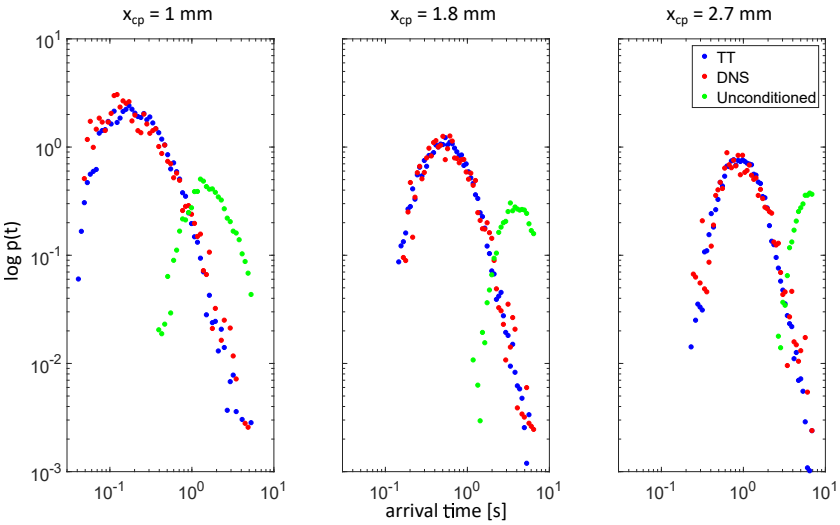

Figure B.1: Comparison of the arrival time densities between the reference simulation (DNS) and the training trajectories approach (TT) for $\lambda_v = 2.4 \cdot 10^{-4}$m at three control planes at 30%, 60%, and 100% of the simulation domain ($\approx$ 2.7mm).

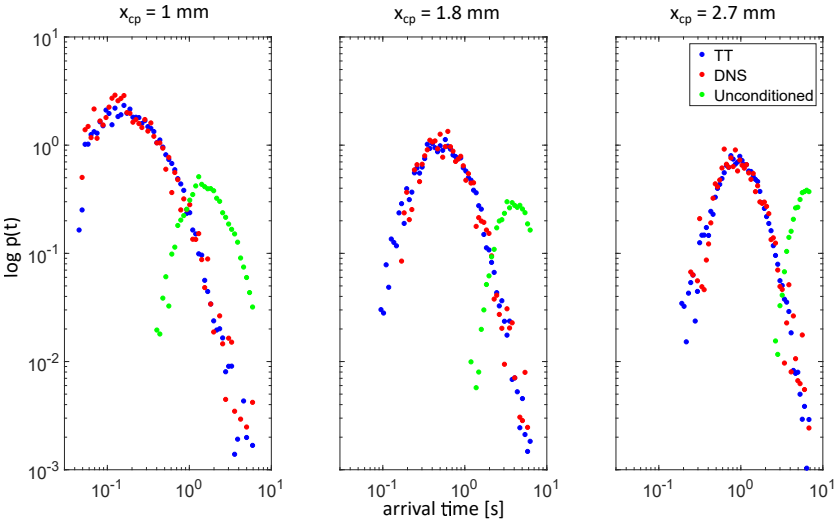

Figure B.2: Comparison of the arrival time densities between the reference simulation (DNS.eps) and the training trajectories approach (TT) for $\lambda_v = 4.8 \cdot 10^{-4}$m at three control planes at 30 %, 60 %, and 100 % of the simulation domain ($\approx$ 2.7mm).

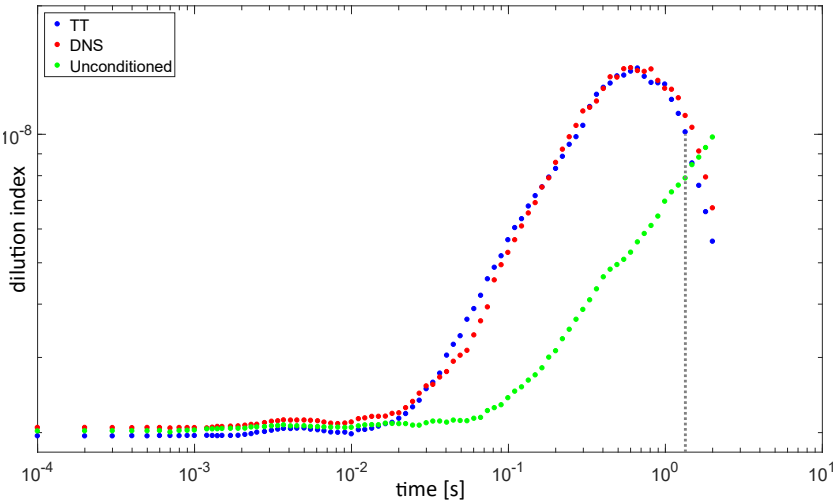

Figure B.3: Comparison of the evolution of the dilution index between the reference simulation (DNS) and the training trajectories approach (TT) for $\lambda_v = 2.4 \cdot 10^{-4}$m at three control planes at 30%, 60%, and 100% of the simulation domain ($\approx$ 2.7mm).

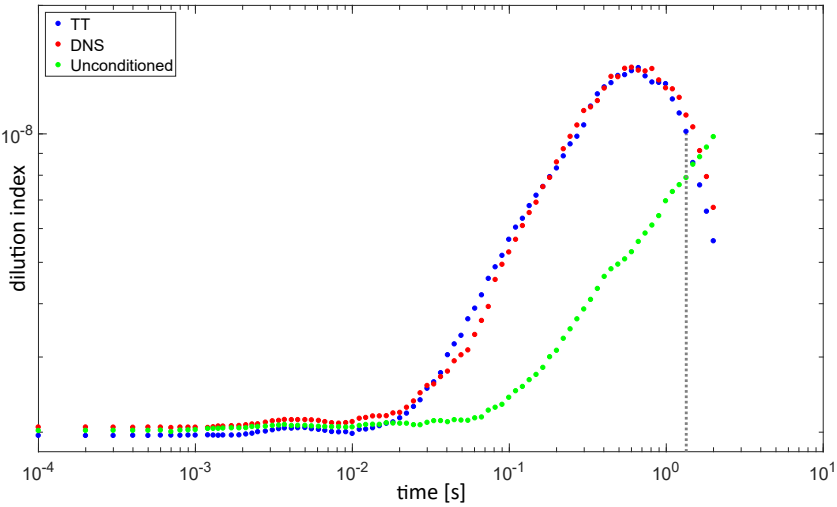

Figure B.4: The evolution of the dilution index between the reference simulation (DNS) and the training trajectories approach (TT) for $\lambda_v = 4.8 \cdot 10^{-4}$m at three control planes at 30%, 60%, and 100% of the simulation domain ($\approx$ 2.7mm).

Bibliography

[1] Ahmed, M. A., E. Kroener, M. Holz, M. Zarebanadkouki, and A. Carminati (2014), Mucilage exudation facilitates root water uptake in dry soils, *Functional Plant Biology*, *41*(11), 1129–1137.

[2] Alt-Epping, P., P. Wersin, and B. Gilbert (2017), Diffusive transport and reaction in clay rocks: A storage (nuclear waste, CO2, H2), energy (shale gas) and water quality issue, *Advances in Water Resources*, *106*, 39–59, doi:10.1016/ j.advwatres.2017.03.019.

[3] Andrä, H., N. Combaret, J. Dvorkin, E. Glatt, J. Han, M. Kabel, Y. Keehm, F. Krzikalla, M. Lee, C. Madonna, M. Marsh, T. Mukerji, E. H. Saenger, R. Sain, N. Saxena, S. Ricker, A. Wiegmann, and X. Zhan (2013), Digital rock physics benchmarks-Part I: Imaging and segmentation, *Computers & Geosciences*, *50*, 25–32, doi: 10.1016/J.CAGEO.2012.09.005.

[4] Andrew, M., B. Bijeljic, and M. J. Blunt (2014), Pore-scale imaging of trapped supercritical carbon dioxide in sandstones and carbonates, *International Journal of Greenhouse Gas Control*, *22*, 1–14, doi: 10.1016/j.ijggc.2013.12.018.

[5] Aquino, T., and M. Dentz (2018), A coupled time domain random walk approach for transport in media characterized by broadly-distributed heterogeneity length scales, *Advances in Water Resources*, *119*, 60–69, doi:10.1016/ j.advwatres.2018.07.009.

[6] Aronofsky, J. S., and J. P. Heller (1957), A diffusion model to explain mixing of flowing miscible fluids in porous media, *Transactions of the Metallurgical Society of AIME*, *210*(12), 345–349.

[7] Bakangura, E., L. Wu, L. Ge, Z. Yang, and T. Xu (2016), Mixed matrix proton exchange membranes for fuel cells: State of the art and perspectives, *Progress in Polymer Science*, *57*, 103–152, doi: 10.1016/j.progpolymsci.2015.11.004.

[8] Bárdossy, A. (2006), Copula-based geostatistical models for groundwater quality parameters, *Water Resources Research*, *42*(11), W11,416, doi:10.1029/2005WR004754.

[9] Bear, J. (1972), *Dynamics of Fluids in Porous Media*, 589 pp., Elsevier, New York.

[10] Benke, R., and S. Painter (2003), Modeling conservative tracer transport in fracture networks with a hybrid approach based on the Boltzmann transport equation, *Water Resources Research*, *39*(11), doi:10.1029/2003WR001966.

[11] Benson, D. A., and M. M. Meerschaert (2008), Simulation of chemical reaction via particle tracking: Diffusion-limited versus thermodynamic rate-limited regimes, *Water Resources Research*, *44*(12), W12,201, doi:10.1029/2008WR007111.

[12] Benson, D. A., R. Schumer, M. M. Meerschaert, and S. W. Wheatcraft (2002), Fractional dispersion, Lévy motion, and the MADE tracer tests, in *Dispersion in Heterogeneous Geological Formations*, pp. 211–240, Springer, Dordrecht, doi:10.1007/978-94-017-1278-1_1.

[13] Berkowitz, B. (2002), Characterizing flow and transport in fractured geological media: A review, *Advances in Water Resources*, *25*(8-12), 861–884, doi:10.1016/S0309-1708(02)00042-8.

[14] Berkowitz, B., and H. Scher (1998), Theory of anomalous chemical transport in random fracture networks, *Physical Review E*, *57*(5), 5858–5869, doi:10.1103/PhysRevE.57.5858.

[15] Berkowitz, B., J. Klafter, R. Metzler, and H. Scher (2002), Physical pictures of transport in heterogeneous media: Advection-dispersion, random-walk, and fractional derivative formulations, *Water Resources Research*, *38*(10), 9–1, doi:10.1029/2001WR001030.

[16] Berkowitz, B., A. Cortis, M. Dentz, and H. Scher (2006), Modeling non-Fickian transport in geological formations as a continuous time random walk, *Reviews of Geophysics*, *44*(2), W11,416, doi:10.1029/2005RG000178.

[17] Berkowitz, B., S. Emmanuel, and H. Scher (2008), Non-Fickian transport and multiple-rate mass transfer in porous media, *Water Resources Research*, *44*(3), doi:10.1029/2007WR005906.

[18] Bijeljic, B., and M. J. Blunt (2006), Pore-scale modeling and continuous time random walk analysis of dispersion in porous media, *Water Resources Research*, *42*(1), doi:10.1029/2005WR004578.

[19] Bijeljic, B., A. H. Muggeridge, and M. J. Blunt (2004), Pore-scale modeling of longitudinal dispersion, *Water Resources Research*, *40*(11), n/a–n/a, doi:10.1029/2004WR003567.

[20] Bijeljic, B., P. Mostaghimi, and M. J. Blunt (2011), Signature of non-Fickian solute transport in complex heterogeneous porous media, *Physical review letters*, *107*(20), 204,502, doi: 10.1103/PhysRevLett.107.204502.

[21] Bijeljic, B., P. Mostaghimi, and M. J. Blunt (2013), Insights into non-Fickian solute transport in carbonates, *Water Resources Research*, *49*(5), 2714–2728, doi:10.1002/wrcr.20238.

[22] Bijeljic, B., A. Raeini, P. Mostaghimi, and M. J. Blunt (2013), Predictions of non-Fickian solute transport in different classes of porous media using direct simulation on pore-scale images, *Physical Review E*, *87*(1), 13,011, doi:10.1103/PhysRevE.87.013011.

[23] Blunt, M. J., B. Bijeljic, H. Dong, O. Gharbi, S. Iglauer, P. Mostaghimi, A. Paluszny, and C. Pentland (2013), Pore-scale imaging and modelling, *Advances in Water Resources*, *51*, 197–216, doi:10.1016/ j.advwatres.2012.03.003.

[24] Blunt, M. J., B. Bijeljic, H. Dong, O. Gharbi, S. Iglauer, P. Mostaghimi, A. Paluszny, and C. Pentland (2013), Pore-scale imaging and modelling, *Advances in Water Resources*, *51*, 197–216, doi:http://dx.doi.org/10.1016/j.advwatres.2012.03.003.

[25] Bode, F., W. Nowak, and M. Loschko (2016), Optimization for Early-Warning Monitoring Networks in Well Catchments Should Be Multi-objective, Risk-Prioritized and Robust Against

Uncertainty, *Transport in Porous Media*, *114*(2), 261–281, doi: 10.1007/s11242-015-0586-6.

[26] Bolster, D., and M. Dentz (2012), Anomalous dispersion in chemically heterogeneous media induced by long-range disorder correlation, *Journal of Fluid Mechanics*, *695*, 366–389, doi: 10.1017/jfm.2012.25.

[27] Bolster, D., Y. Méheust, T. Le Borgne, J. Bouquain, and P. Davy (2014), Modeling preasymptotic transport in flows with significant inertial and trapping effects - The importance of velocity correlations and a spatial Markov model, *Advances in Water Resources*, *70*, 89–103, doi:10.1016/j.advwatres.2014.04.014.

[28] Bolster, D., A. Paster, and D. A. Benson (2016), A particle number conserving Lagrangian method for mixing-driven reactive transport, *Water Resources Research*, *52*(2), 1518–1527, doi: 10.1002/2015WR018310.

[29] Buades, A., B. Coll, and J.-M. Morel (2005), A non-local algorithm for image denoising, in *Computer Vision and Pattern Recognition, 2005. CVPR 2005. IEEE Computer Society Conference on*, vol. 2, pp. 60–65, IEEE, doi:10.1109/CVPR.2005.38.

[30] Carrera, J., X. Sánchez-Vila, I. Benet, A. Medina, G. Galarza, and J. Guimerà (1998), On matrix diffusion: formulations, solution methods and qualitative effects, *Hydrogeology Journal*, *6*(1), 178–190, doi:10.1007/s100400050143.

[31] Carton, J., and A. Olabi (2017), Three-dimensional proton exchange membrane fuel cell model: Comparison of double channel and open pore cellular foam flow plates, *Energy*, *136*, 185–195, doi: 10.1016/j.energy.2016.02.010.

[32] Class, H., and R. Helmig (2002), Numerical simulation of non-isothermal multiphase multicomponent processes in porous media.: 2. Applications for the injection of steam and air, *Advances in Water Resources*, *25*(5), 551–564, doi:10.1016/S0309-1708(02)00015-5.

[33] Craig, R. G. (1984), Sampling an autocorrelated process: The AR(1), *Journal of the International Association for Mathematical Geology*, *16*(8), 745–751, doi:10.1007/BF01036702.

[34] Crank, J. (1979), *The mathematics of diffusion*, Oxford university press.

[35] Cushman, J. H., and D. O'Malley (2015), Fickian dispersion is anomalous, *Journal of Hydrology*, *531*, 161–167, doi:10.1016/j.jhydrol.2015.06.036.

[36] De Anna, P., T. Le Borgne, M. Dentz, A. M. Tartakovsky, D. Bolster, and P. Davy (2013), Flow intermittency, dispersion, and correlated continuous time random walks in porous media, *Physical review letters*, *110*(18), 184,502, doi:10.1103/PhysRevLett.110.184502.

[37] Delay, F., and J. Bodin (2001), Time domain random walk method to simulate transport by advectionâĂŘdispersion and matrix diffusion in fracture networks, *Geophysical Research Letters*, *28*(21), 4051–4054, doi:10.1029/2001GL013698.

[38] Dentz, M., and B. Berkowitz (2003), Transport behavior of a passive solute in continuous time random walks and multirate mass transfer, *Water Resources Research*, *39*(5), 1111, doi:10.1029/2001WR001163.

[39] Dentz, M., A. Cortis, H. Scher, and B. Berkowitz (2004), Time behavior of solute transport in heterogeneous media: Transition from anomalous to normal transport, *Advances in Water Resources*, *27*(2), 155–173, doi:10.1016/j.advwatres.2003.11.002.

[40] Dentz, M., T. Le Borgne, A. Englert, and B. Bijeljic (2011), Mixing, spreading and reaction in heterogeneous media: A brief review, *Journal of Contaminant Hydrology*, *120*, 1–17, doi:10.1016/j.jconhyd.2010.05.002.

[41] Dentz, M., P. Gouze, A. Russian, J. Dweik, and F. Delay (2012), Diffusion and trapping in heterogeneous media: An inhomogeneous continuous time random walk approach,

Advances in Water Resources, *49*(Supplement C), 13–22, doi:https://doi.org/10.1016/j.advwatres.2012.07.015.

[42] Dentz, M., P. K. Kang, A. Comolli, T. Le Borgne, and D. R. Lester (2016), Continuous time random walks for the evolution of Lagrangian velocities, *Physical Review Fluids*, *1*(7), 74,004.

[43] Dentz, M., M. Icardi, and J. J. Hidalgo (2018), Mechanisms of dispersion in a porous medium, *Journal of Fluid Mechanics*, *841*, 851–882, doi:DOI: 10.1017/jfm.2018.120.

[44] Doob, J. L. (1942), The Brownian Movement and Stochastic Equations, *Annals of Mathematics*, *43*(2), 351–369, doi:10.2307/1968873.

[45] Edery, Y., H. Scher, and B. Berkowitz (2010), Particle tracking model of bimolecular reactive transport in porous media, *Water Resources Research*, *46*(7), doi:10.1029/2009WR009017.

[46] Edery, Y., A. Guadagnini, H. Scher, and B. Berkowitz (2014), Origins of anomalous transport in heterogeneous media: Structural and dynamic controls, *Water Resources Research*, *50*(2), 1490–1505, doi:10.1002/2013WR015111.

[47] Einstein, A. (1905), INVESTIGATIONS ON THE THEORY OF THE BROWNIAN MOVEMENT, *Ann. der Physik*.

[48] Ejaz, M., Y. Tsujii, and T. Fukuda (2001), Controlled grafting of a well-defined polymer on a porous glass filter by surface-initiated atom transfer radical polymerization, *Polymer*, *42*(16), 6811–6815, doi:10.1016/S0032-3861(01)00192-6.

[49] Engdahl, N. B., D. A. Benson, and D. Bolster (2017), Lagrangian simulation of mixing and reactions in complex geochemical systems, *Water Resources Research*, *53*(4), 3513–3522, doi:10.1002/2017WR020362.

[50] Feller, W. (1968), *An introduction to probability theory and its applications*, vol. 1, Wiley New York.

[51] Fischer, H. (2011), *A History of the Central Limit Theorem: From Classical to Modern Probability Theory*, Sources and Studies in the History of Mathematics and Physical Sciences, Springer New York, New York, doi:10.1007/978-0-387-87857-7.

[52] Flament, F., G. Francois, H. Qiu, C. Ye, T. Hanaya, D. Batisse, S. Cointereau-Chardon, M. D. G. Seixas, S. E. Dal Belo, and R. Bazin (2015), Facial skin pores: a multiethnic study, *Clinical, Cosmetic and Investigational Dermatology*, *8*, 85–93, doi:10.2147/CCID.S74401.

[53] Folks, J. L., and R. S. Chhikara (1978), The Inverse Gaussian Distribution and Its Statistical Application–A Review, *Journal of the Royal Statistical Society. Series B (Methodological)*, *40*(3), 263–289.

[54] Gardiner, C. W. (1985), *Handbook of stochastic methods*, vol. 4, Springer Berlin, Berlin.

[55] Gelhar, L. W., C. Welty, and K. R. Rehfeldt (1992), A critical review of data on field-scale dispersion in aquifers, *Water Resources Research*, *28*(7), 1955–1974, doi:10.1029/92WR00607.

[56] Gleeson, T., Y. Wada, M. F. P. Bierkens, and L. P. H. van Beek (2012), Water balance of global aquifers revealed by groundwater footprint, *Nature*, *488*(7410), 197–200, doi:10.1038/nature11295.

[57] Haggerty, R., and S. M. Gorelick (1995), Multiple-rate mass transfer for modeling diffusion and surface reactions in media with pore-scale heterogeneity, *Water Resources Research*, *31*(10), 2383–2400, doi:10.1029/95WR10583.

[58] Harvey, C. F., C. H. Swartz, A. B. M. Badruzzaman, N. Keon-Blute, W. Yu, M. A. Ali, J. Jay, R. Beckie, V. Niedan, and D. Brabander (2002), Arsenic mobility and groundwater extraction in Bangladesh, *Science*, *298*(5598), 1602–1606, doi:10.1126/science.1076978.

[59] Heinemann, N., R. Stewart, M. Wilkinson, G. Pickup, and R. Haszeldine (2016), Hydrodynamics in subsurface CO2 storage: Tilted contacts and increased storage security, *Inter-*

national Journal of Greenhouse Gas Control, *54*, 322–329, doi:10.1016/J.IJGGC.2016.10.003.

[60] Hu, L. Y., and T. Chugunova (2008), Multiple - point geostatistics for modeling subsurface heterogeneity: A comprehensive review, *Water Resources Research*, *44*(11), doi:10.1029/2008WR006993.

[61] Jackson, R. B., J. S. Sperry, and T. E. Dawson (2000), Root water uptake and transport: using physiological processes in global predictions, *Trends in Plant Science*, *5*(11), 482–488, doi:10.1016/S1360-1385(00)01766-0.

[62] Kang, P. K., M. Dentz, T. Le Borgne, and R. Juanes (2011), Spatial Markov model of anomalous transport through random lattice networks, *Physical review letters*, *107*(18), 180,602, doi:10.1103/PhysRevLett.107.180602.

[63] Kang, P. K., P. Anna, J. P. Nunes, B. Bijeljic, M. J. Blunt, and R. Juanes (2014), Pore-scale intermittent velocity structure underpinning anomalous transport through 3D porous media, *Geophysical Research Letters*, *41*(17), 6184–6190, doi:10.1002/2014GL061475.

[64] Kang, P. K., T. Le Borgne, M. Dentz, O. Bour, and R. Juanes (2015), Impact of velocity correlation and distribution on transport in fractured media: Field evidence and theoretical model, *Water Resources Research*, *51*(2), 940–959, doi:10.1002/2014WR015799.

[65] Kang, P. K., M. Dentz, T. Le Borgne, and R. Juanes (2015), Anomalous transport on regular fracture networks: Impact of conductivity heterogeneity and mixing at fracture intersections, *Physical Review E*, *92*(2), 22,148.

[66] Kang, P. K., S. Brown, and R. Juanes (2016), Emergence of anomalous transport in stressed rough fractures, *Earth and Planetary Science Letters*, *454*, 46–54, doi:10.1016/J.EPSL.2016.08.033.

[67] Kenkre, V. M., E. W. Montroll, and M. F. Shlesinger (1973), Generalized master equations for continuous-time random walks, *Journal of Statistical Physics*, *9*(1), 45–50, doi:10.1007/BF01016796.

[68] Kissinger, A., R. Helmig, A. Ebigbo, H. Class, T. Lange, M. Sauter, M. Heitfeld, J. Klünker, and W. Jahnke (2013), Hydraulic fracturing in unconventional gas reservoirs: risks in the geological system, part 2, *Environmental earth sciences*, *70*(8), 3855–3873, doi: 10.1007/s12665-013-2578-6.

[69] Kitanidis, P. K. (2010), The concept of the Dilution Index, *Water Resources Research*, *30*(7), 2011–2026, doi:10.1029/94WR00762.

[70] Kreft, A., and A. Zuber (1978), On the physical meaning of the dispersion equation and its solutions for different initial and boundary conditions, *Chemical Engineering Science*, *33*(11), 1471–1480, doi: 10.1016/0009-2509(78)85196-3.

[71] LaBolle, E. M., G. E. Fogg, and A. F. B. Tompson (1996), Random-walk simulation of transport in heterogeneous porous media: Local mass-conservation problem and implementation methods, *Water Resources Research*, *32*(3), 583–593, doi:10.1029/95WR03528.

[72] Le Borgne, T., M. Dentz, and J. Carrera (2008), Spatial Markov processes for modeling Lagrangian particle dynamics in heterogeneous porous media, *Physical Review E*, *78*(2), 26,308, doi: 10.1103/PhysRevE.78.026308.

[73] Le Borgne, T., M. Dentz, and J. Carrera (2008), Lagrangian statistical model for transport in highly heterogeneous velocity fields, *Physical review letters*, *101*(9), 90,601, doi: 10.1103/PhysRevLett.101.090601.

[74] Le Borgne, T., M. Dentz, D. Bolster, J. Carrera, J.-R. de Dreuzy, and P. Davy (2010), Non-Fickian mixing: Temporal evolution of the scalar dissipation rate in heterogeneous porous media, *Advances in Water Resources*, *33*(12), 1468–1475, doi: 10.1016/J.ADVWATRES.2010.08.006.

[75] Levy, M., and B. Berkowitz (2003), Measurement and analysis of non-Fickian dispersion in heterogeneous porous media, *Journal of Contaminant Hydrology*, *64*(3), 203–226, doi:10.1016/S0169-7722(02)00204-8.

[76] Li, J. (2010), Application of copulas as a new geostatistical tool, Ph.D. thesis.

[77] Marco, D., and B. Brian (2003), Transport behavior of a passive solute in continuous time random walks and multirate mass transfer, *Water Resources Research*, *39*(5), doi:10.1029/2001WR001163.

[78] Meerschaert, M. M., D. A. Benson, and B. Bäumer (1999), Multidimensional advection and fractional dispersion, *Physical Review E*, *59*(5), 5026–5028, doi:10.1103/PhysRevE.59.5026.

[79] Metzler, R., and J. Klafter (2000), The random walk's guide to anomalous diffusion: a fractional dynamics approach, *Physics Reports*, *339*(1), 1–77, doi:10.1016/S0370-1573(00)00070-3.

[80] Meyer, D. W., and B. Bijeljic (2016), Pore-scale dispersion: Bridging the gap between microscopic pore structure and the emerging macroscopic transport behavior, *Physical Review E*, *94*(1), 13,107, doi:10.1103/PhysRevE.94.013107.

[81] Meyer, D. W., and H. A. Tchelepi (2010), Particle - based transport model with Markovian velocity processes for tracer dispersion in highly heterogeneous porous media, *Water Resources Research*, *46*(11), doi:10.1029/2009WR008925.

[82] Meyer, D. W., H. A. Tchelepi, and P. Jenny (2013), A fast simulation method for uncertainty quantification of subsurface flow and transport, *Water Resources Research*, *49*(5), 2359–2379, doi:10.1002/wrcr.20240.

[83] Montroll, E. W., and G. H. Weiss (1965), Random Walks on Lattices. II, *Journal of Mathematical Physics*, *6*(2), 167–181, doi:10.1063/1.1704269.

[84] Morales, V. L., M. Dentz, M. Willmann, and M. Holzner (2017), Stochastic dynamics of intermittent pore-scale particle motion in three-dimensional porous media: Experiments and theory, *Geophysical Research Letters*, *44*(18), 9361–9371, doi:10.1002/2017GL074326.

[85] Moroni, M., N. Kleinfelter, and J. H. Cushman (2007), Analysis of dispersion in porous media via matched-index particle tracking velocimetry experiments, *Advances in Water Resources*, *30*(1), 1–15, doi:10.1016/j.advwatres.2006.02.005.

[86] Most, S., B. Bijeljic, and W. Nowak (2016), Evolution and persistence of cross-directional statistical dependence during finite-Péclet transport through a real porous medium, *Water Resources Research*, *52*(11), 8920–8937, doi:10.1002/2016WR018969.

[87] Mostaghimi, P., B. Bijeljic, and M. Blunt (2012), Simulation of flow and dispersion on pore-space images, *SPE Journal*, *17*(04), 1–131, doi:10.2118/135261-PA.

[88] Murphy, C. M., and F. J. O'Brien (2010), Understanding the effect of mean pore size on cell activity in collagen-glycosaminoglycan scaffolds, *Cell Adhesion & Migration*, *4*(3), 377–381, doi:10.4161/cam.4.3.11747.

[89] Nelsen, R. B. (2013), *An introduction to copulas*, vol. 139, 1–272 pp., Springer Science & Business Media, New York, doi:10.1007/0-387-28678-0.

[90] Nœtinger, B., and T. Estebenet (2000), Up-Scaling of Double Porosity Fractured Media Using Continuous-Time Random Walks Methods, *Transport in Porous Media*, *39*(3), 315–337, doi:10.1023/A:1006639025910.

[91] Oladyshkin, S., H. Class, R. Helmig, and W. Nowak (2011), A concept for data-driven uncertainty quantification and its application to carbon dioxide storage in geological formations, *Advances in Water Resources*, *34*(11), 1508–1518, doi:10.1016/J.ADVWATRES.2011.08.005.

[92] Oladyshkin, S., H. Class, R. Helmig, and W. Nowak (2011), An integrative approach to robust design and probabilistic risk assessment for CO2 storage in geological formations, *Computational Geosciences*, *15*(3), 565–577, doi:10.1007/s10596-011-9224-8.

[93] OpenFOAM (2011), The open source CFD toolbox [Available at: http://www.openfoam.com].

[94] Orr, F. M., and J. J. Taber (1984), Use of carbon dioxide in enhanced oil recovery, *Science*, *224*(4649), 563–569.

[95] Page, J. S., J. G. Reynolds, T. M. Ely, and G. A. Cooke (2018), Development of a carbonate crust on alkaline nuclear waste sludge at the Hanford site, *Journal of Hazardous Materials*, *342*, 375–382, doi: 10.1016j.jhazmat.2017.08.033.

[96] Pandey, R. P., G. Shukla, M. Manohar, and V. K. Shahi (2017), Graphene oxide based nanohybrid proton exchange membranes for fuel cell applications: An overview, *Advances in Colloid and Interface Science*, *240*, 15–30, doi:10.1016/J.CIS.2016.12.003.

[97] Paster, A., D. Bolster, and D. A. Benson (2014), Connecting the dots: Semi-analytical and random walk numerical solutions of the diffusionm - reaction equation with stochastic initial conditions, *Journal of Computational Physics*, *263*, 91–112, doi: 10.1016/J.JCP.2014.01.020.

[98] Pereira Nunes, J. P., B. Bijeljic, and M. J. Blunt (2015), Time-of-Flight Distributions and Breakthrough Curves in Heterogeneous Porous Media Using a Pore-Scale Streamline Tracing Algorithm, *Transport in Porous Media*, *109*(2), 317–336, doi:10.1007/s11242-015-0520-y.

[99] Pereira-Nunes, J. P., B. Bijeljic, and M. J. Blunt (2015), Time-of-flight distributions and breakthrough curves in heterogeneous porous media using a pore-scale streamline tracing algorithm, *Transport in Porous Media*, *109*(2), 317–336, doi:10.1007/s11242-015-0520-y.

[100] Peters, A., W. Durner, and S. C. Iden (2017), Modified Feddes type stress reduction function for modeling root water uptake: Accounting for limited aeration and low water potential, *Agricultural Water Management*, *185*, 126–136, doi: 10.1016/J.AGWAT.2017.02.010.

[101] Printz Ringbæk, T., Y. Simeonov, M. Witt, R. Engenhart-Cabillic, G. Kraft, K. Zink, and U. Weber (2017), Modulation power of porous materials and usage as ripple filter in particle therapy, *Physics in Medicine and Biology*, *62*(7), 2892–2909, doi:10.1088/1361-6560/aa5c28.

[102] Raeini, A. Q., M. J. Blunt, and B. Bijeljic (2012), Modelling two-phase flow in porous media at the pore scale using the volume-of-fluid method, *Journal of Computational Physics*, *231*(17), 5653–5668, doi:10.1016/j.jcp.2012.04.011.

[103] Raeini, A. Q., M. J. Blunt, and B. Bijeljic (2014), Direct simulations of two-phase flow on micro-CT images of porous media and upscaling of pore-scale forces, *Advances in Water Resources*, *74*, 116–126, doi:10.1016/j.advwatres.2014.08.012.

[104] Rasmuson, A., and I. Neretnieks (2018), Migration of radionuclides in fissured rock: The influence of micropore diffusion and longitudinal dispersion, *Journal of Geophysical Research: Solid Earth*, *86*(B5), 3749–3758, doi:10.1029/JB086iB05p03749.

[105] Renner, C., J. Peinke, and R. Friedrich (2001), Evidence of Markov properties of high frequency exchange rate data, *Physica A: Statistical Mechanics and its Applications*, *298*(3-4), 499–520, doi:10.1016/S0378-4371(01)00269-2.

[106] Renner, C., J. Peinke, and R. Friedrich (2001), Experimental indications for Markov properties of small-scale turbulence, *Journal of Fluid Mechanics*, *433*, 383–409, doi:DOI:10.1017/S0022112001003597.

[107] Rhodes, M. E., B. Bijeljic, and M. J. Blunt (2008), Pore-to-field simulation of single-phase transport using continuous time random walks, *Advances in Water Resources*, *31*(12), 1527–1539, doi:10.1016/j.advwatres.2008.04.006.

[108] Rubin, Y., and J. Gomez-Hernandez (1990), A stochastic approach to the problem of upscaling of conductivity in disordered media:

Theory and unconditional simulations, *Water Resources Research*, *22*(4), 691–701, doi:10.1029/WR026i004p00691.

[109] Russian, A., M. Dentz, and P. Gouze (2016), Time domain random walks for hydrodynamic transport in heterogeneous media, *Water Resources Research*, *52*(5), 3309–3323, doi:10.1002/2015WR018511.

[110] Salamon, P., D. Fernàndez-Garcia, and J. J. Gómez-Hernández (2006), A review and numerical assessment of the random walk particle tracking method, *Journal of Contaminant Hydrology*, *87*(3), 277–305, doi:10.1016/j.jconhyd.2006.05.005.

[111] Scher, H., and M. Lax (1973), Stochastic Transport in a Disordered Solid. I. Theory, *Physical Review B*, *7*(10), 4491–4502, doi:10.1103/PhysRevB.7.4491.

[112] Schumer, R., D. A. Benson, M. M. Meerschaert, and S. W. Wheatcraft (2001), Eulerian derivation of the fractional advection-dispersion equation, *Journal of Contaminant Hydrology*, *48*(1âĂŞ2), 69–88, doi:http://dx.doi.org/10.1016/S0169-7722(00)00170-4.

[113] Schumer, R., D. A. Benson, M. M. Meerschaert, and B. Baeumer (2003), Fractal mobile/immobile solute transport, *Water Resources Research*, *39*(10), doi:10.1029/2003WR002141.

[114] Sherman, T., A. Fakhari, S. Miller, K. Singha, and D. Bolster (2017), Parameterizing the Spatial Markov Model From Breakthrough Curve Data Alone, *Water Resources Research*, *53*(12), 10,888–10,898, doi:10.1002/2017WR021810.

[115] Sherman, T., A. Foster, D. Bolster, and K. Singha (2018), *Predicting downstream concentration histories from upstream data in column experiments*, doi:10.1029/2018WR023420.

[116] Shlesinger, M. F., B. J. West, and J. Klafter (1987), Levy dynamics of enhanced diffusion: Application to turbulence, *Physical Review Letters*, *58*(11), 1100–1103.

[117] Sidle, R. C., B. Nilsson, M. Hansen, and J. Fredericia (1998), Spatially varying hydraulic and solute transport characteristics of a

fractured till determined by field tracer tests, Funen, Denmark, *Water Resources Research*, *34*(10), 2515–2527, doi:10.1029/98WR01735.

[118] Silliman, S. E., and E. S. Simpson (1987), Laboratory evidence of the scale effect in dispersion of solutes in porous media, *Water Resources Research*, *23*(8), 1667–1673, doi:10.1029/WR023i008p01667.

[119] Silliman, S. E., L. F. Konikow, and C. I. Voss (1987), Laboratory investigation of longitudinal dispersion in anisotropic porous media, *Water Resources Research*, *23*(11), 2145–2151, doi:10.1029/WR023i011p02145.

[120] Sklar, A. (1973), Random variables, joint distribution functions, and copulas, *Kybernetika*, *9*(6), 449–460.

[121] Sokolov, I. M. (2012), Models of anomalous diffusion in crowded environments, *Soft Matter*, *8*(35), 9043–9052, doi:10.1039/C2SM25701G.

[122] Sternberg, S. P. K., J. H. Cushman, and R. A. Greenkorn (1996), Laboratory observation of nonlocal dispersion, *Transport in Porous Media*, *23*(2), 135–151, doi:10.1007/BF00178123.

[123] Strumik, M., and W. M. Macek (2008), Testing for Markovian character and modeling of intermittency in solar wind turbulence, *Physical Review E*, *78*(2), 26,414, doi:10.1103/PhysRevE.78.026414.

[124] Sudicky, E. A., J. A. Cherry, and E. O. Frind (1983), Migration of contaminants in groundwater at a landfill: A case study: 4. A natural-gradient dispersion test, *Journal of Hydrology*, *63*(1), 81–108, doi:10.1016/0022-1694(83)90224-X.

[125] Sund, N., D. Bolster, S. Mattis, and C. Dawson (2015), Pre-asymptotic Transport Upscaling in Inertial and Unsteady Flows Through Porous Media, *Transport in Porous Media*, *109*(2), 411–432, doi:10.1007/s11242-015-0526-5.

[126] Sund, N., G. Porta, D. Bolster, and R. Parashar (2017), A Lagrangian Transport Eulerian Reaction Spatial (LATERS) Markov Model for

Prediction of Effective Bimolecular Reactive Transport, *Water Resources Research*, *53*(11), 9040–9058, doi:10.1002/2017WR020821.

[127] Sund, N. L., D. Bolster, and C. Dawson (2015), Upscaling transport of a reacting solute through a peridocially converging-diverging channel at pre-asymptotic times, *Journal of Contaminant Hydrology*, *182*, 1–15, doi:10.1016/j.jconhyd.2015.08.003.

[128] Sund, N. L., D. Bolster, and D. A. Benson (2016), Testing the limits of the spatial Markov model for upscaling transport: The role of nonmonotonic effective velocity autocorrelations, *Physical Review E*, *94*(4), 43,107.

[129] Sund, N. L., G. M. Porta, and D. Bolster (2017), Upscaling of dilution and mixing using a trajectory based Spatial Markov random walk model in a periodic flow domain, *Advances in Water Resources*, *103*, 76–85, doi:10.1016/j.advwatres.2017.02.018.

[130] Szulczewski, M. L., C. W. MacMinn, H. J. Herzog, and R. Juanes (2012), Lifetime of carbon capture and storage as a climate-change mitigation technology, *Proceedings of the National Academy of Sciences*, *109*(14), 5185–5189, doi:10.1073/pnas.1115347109/-/DCSupplemental.

[131] Thalabard, S., G. Krstulovic, and J. Bec (2014), Turbulent pair dispersion as a continuous-time random walk, *Journal of Fluid Mechanics*, *755*, doi:DOI: 10.1017/jfm.2014.445.

[132] Wang, L.-P., and D. E. Stock (1992), Stochastic trajectory models for turbulent diffusion: Monte Carlo process versus Markov chains, *Atmospheric Environment. Part A. General Topics*, *26*(9), 1599–1607, doi:10.1016/0960-1686(92)90060-X.

[133] Wen, X.-H., and J. Gómez-Hernández (1996), Upscaling hydraulic conductivities in heterogeneous media: An overview, *Journal of Hydrology*, *183*(1-2), ix–xxxii, doi:10.1016/S0022-1694(96)80030-8.

[134] Wen, X.-H., and J. Gómez-Hernández (1996), Upscaling hydraulic conductivities in heterogeneous media: An overview, *Journal of Hydrology*, *183*(1-2), ix–xxxii, doi:10.1016/S0022-1694(96)80030-8.

[135] Wu, C., A. L. Spongberg, J. D. Witter, M. Fang, and K. P. Czajkowski (2010), Uptake of Pharmaceutical and Personal Care Products by Soybean Plants from Soils Applied with Biosolids and Irrigated with Contaminated Water, *Environmental Science & Technology*, *44*(16), 6157–6161, doi:10.1021/es1011115.

[136] Xie, Y., H. Dong, G. Zeng, L. Tang, Z. Jiang, C. Zhang, J. Deng, L. Zhang, and Y. Zhang (2017), The interactions between nanoscale zero-valent iron and microbes in the subsurface environment: A review, *Journal of Hazardous Materials*, *321*, 390–407, doi: 10.1016/j.jhazmat.2016.09.028.

[137] Yoshida, N., and Y. Takahashi (2012), Land-surface contamination by radionuclides from the Fukushima Daiichi Nuclear Power Plant accident, *Elements*, *8*(3), 201–206, doi:10.2113/gselements.8.3.201.

[138] Zhan, H. (1999), On the Ergodicity Hypothesis in Heterogeneous Formations, *Mathematical Geology*, *31*(1), 113–134, doi: 10.1023/A:1007549532023.

[139] Zhang, Y., and D. A. Benson (2008), Lagrangian simulation of multidimensional anomalous transport at the MADE site, *Geophysical Research Letters*, *35*(7), L07,403, doi:10.1029/2008GL033222.

Institut für Wasser- und Umweltsystemmodellierung
Universität Stuttgart

Pfaffenwaldring 61
70569 Stuttgart (Vaihingen)
Telefon (0711) 685 - 60156
Telefax (0711) 685 - 51073
E-Mail: iws@iws.uni-stuttgart.de
http://www.iws.uni-stuttgart.de

Direktoren
Prof. Dr. rer. nat. Dr.-Ing. András Bárdossy
Prof. Dr.-Ing. Rainer Helmig
Prof. Dr.-Ing. Wolfgang Nowak
Prof. Dr.-Ing. Silke Wieprecht

Vorstand *(Stand 1.5.2019)*
Prof. Dr. rer. nat. Dr.-Ing. A. Bárdossy
Prof. Dr.-Ing. R. Helmig
Prof. Dr.-Ing. W. Nowak
Prof. Dr.-Ing. S. Wieprecht
Prof. Dr. J.A. Sander Huisman
Jürgen Braun, PhD
apl. Prof. Dr.-Ing. H. Class
PD Dr.-Ing. Claus Haslauer
Stefan Haun, PhD
PD Dr.-Ing. habil. Sergey Oladyshkin
Dr. rer. nat. J. Seidel
Dr.-Ing. K. Terheiden

Emeriti
Prof. Dr.-Ing. habil. Dr.-Ing. E.h. Jürgen Giesecke
Prof. Dr.h.c. Dr.-Ing. E.h. Helmut Kobus, PhD

Lehrstuhl für Wasserbau und Wassermengenwirtschaft
Leiterin: Prof. Dr.-Ing. Silke Wieprecht
Stellv.: Dr.-Ing. Kristina Terheiden
Versuchsanstalt für Wasserbau
Leiter: Stefan Haun, PhD

Lehrstuhl für Hydromechanik und Hydrosystemmodellierung
Leiter: Prof. Dr.-Ing. Rainer Helmig
Stellv.: apl. Prof. Dr.-Ing. Holger Class

Lehrstuhl für Hydrologie und Geohydrologie
Leiter: Prof. Dr. rer. nat. Dr.-Ing. András Bárdossy
Stellv.: Dr. rer. nat. Jochen Seidel
Hydrogeophysik der Vadosen Zone
(mit Forschungszentrum Jülich)
Leiter: Prof. Dr. J.A. Sander Huisman

Lehrstuhl für Stochastische Simulation und Sicherheitsforschung für Hydrosysteme
Leiter: Prof. Dr.-Ing. Wolfgang Nowak
Stellv.: PD Dr.-Ing. habil. Sergey Oladyshkin

***VEGAS,* Versuchseinrichtung zur Grundwasser- und Altlastensanierung**
Leiter: Jürgen Braun, PhD
PD Dr.-Ing. Claus Haslauer

Verzeichnis der Mitteilungshefte

5 Plate, Erich: *Beitrag zur Bestimmung der Windgeschwindigkeitsverteilung in der durch eine Wand gestörten bodennahen Luftschicht*, und
Röhnisch, Arthur; Marotz, Günter: *Neue Baustoffe und Bauausführungen für den Schutz der Böschungen und der Sohle von Kanälen, Flüssen und Häfen; Gestehungskosten und jeweilige Vorteile*, sowie
Unny, T.E.: *Schwingungsuntersuchungen am Kegelstrahlschieber*, 1967

6 Seiler, Erich: *Die Ermittlung des Anlagenwertes der bundeseigenen Binnenschiffahrtsstraßen und Talsperren und des Anteils der Binnenschiffahrt an diesem Wert*, 1967

7 *Sonderheft anläßlich des 65. Geburtstages von Prof. Arthur Röhnisch mit Beiträgen von* Benk, Dieter; Breitling, J.; Gurr, Siegfried; Haberhauer, Robert; Honekamp, Hermann; Kuz, Klaus Dieter; Marotz, Günter; Mayer-Vorfelder, Hans-Jörg; Miller, Rudolf; Plate, Erich J.; Radomski, Helge; Schwarz, Helmut; Vollmer, Ernst; Wildenhahn, Eberhard; 1967

8 Jumikis, Alfred: *Beitrag zur experimentellen Untersuchung des Wassernachschubs in einem gefrierenden Boden und die Beurteilung der Ergebnisse*, 1968

9 Marotz, Günter: *Technische Grundlagen einer Wasserspeicherung im natürlichen Untergrund*, 1968

10 Radomski, Helge: *Untersuchungen über den Einfluß der Querschnittsform wellenförmiger Spundwände auf die statischen und rammtechnischen Eigenschaften*, 1968

11 Schwarz, Helmut: *Die Grenztragfähigkeit des Baugrundes bei Einwirkung vertikal gezogener Ankerplatten als zweidimensionales Bruchproblem*, 1969

12 Erbel, Klaus: *Ein Beitrag zur Untersuchung der Metamorphose von Mittelgebirgsschneedecken unter besonderer Berücksichtigung eines Verfahrens zur Bestimmung der thermischen Schneequalität*, 1969

13 Westhaus, Karl-Heinz: *Der Strukturwandel in der Binnenschiffahrt und sein Einfluß auf den Ausbau der Binnenschiffskanäle*, 1969

14 Mayer-Vorfelder, Hans-Jörg: *Ein Beitrag zur Berechnung des Erdwiderstandes unter Ansatz der logarithmischen Spirale als Gleitflächenfunktion*, 1970

15 Schulz, Manfred: *Berechnung des räumlichen Erddruckes auf die Wandung kreiszylindrischer Körper*, 1970

16 Mobasseri, Manoutschehr: *Die Rippenstützmauer. Konstruktion und Grenzen ihrer Standsicherheit*, 1970

17 Benk, Dieter: *Ein Beitrag zum Betrieb und zur Bemessung von Hochwasserrückhaltebecken*, 1970

18 Gàl, Attila: *Bestimmung der mitschwingenden Wassermasse bei überströmten Fischbauchklappen mit kreiszylindrischem Staublech*, 1971, vergriffen

19 Kuz, Klaus Dieter: *Ein Beitrag zur Frage des Einsetzens von Kavitationserscheinungen in einer Düsenströmung bei Berücksichtigung der im Wasser gelösten Gase*, 1971, vergriffen

20 Schaak, Hartmut: *Verteilleitungen von Wasserkraftanlagen*, 1971

21 *Sonderheft zur Eröffnung der neuen Versuchsanstalt des Instituts für Wasserbau der Universität Stuttgart mit Beiträgen von* Brombach, Hansjörg; Dirksen, Wolfram; Gàl, Attila; Gerlach, Reinhard; Giesecke, Jürgen; Holthoff, Franz-Josef; Kuz, Klaus Dieter; Marotz, Günter; Minor, Hans-Erwin; Petrikat, Kurt; Röhnisch, Arthur; Rueff, Helge; Schwarz, Helmut; Vollmer, Ernst; Wildenhahn, Eberhard; 1972

22 Wang, Chung-su: *Ein Beitrag zur Berechnung der Schwingungen an Kegelstrahlschiebern*, 1972

23 Mayer-Vorfelder, Hans-Jörg: *Erdwiderstandsbeiwerte nach dem Ohde-Variationsverfahren*, 1972

24 Minor, Hans-Erwin: *Beitrag zur Bestimmung der Schwingungsanfachungsfunktionen überströmter Stauklappen*, 1972, vergriffen

25 Brombach, Hansjörg: *Untersuchung strömungsmechanischer Elemente (Fluidik) und die Möglichkeit der Anwendung von Wirbelkammerelementen im Wasserbau*, 1972, vergriffen

26 Wildenhahn, Eberhard: *Beitrag zur Berechnung von Horizontalfilterbrunnen*, 1972

27 Steinlein, Helmut: *Die Eliminierung der Schwebstoffe aus Flußwasser zum Zweck der unterirdischen Wasserspeicherung, gezeigt am Beispiel der Iller*, 1972

28 Holthoff, Franz Josef: *Die Überwindung großer Hubhöhen in der Binnenschiffahrt durch Schwimmerhebewerke*, 1973

29 Röder, Karl: *Einwirkungen aus Baugrundbewegungen auf trog- und kastenförmige Konstruktionen des Wasser- und Tunnelbaues*, 1973

30 Kretschmer, Heinz: *Die Bemessung von Bogenstaumauern in Abhängigkeit von der Talform*, 1973

31 Honekamp, Hermann: *Beitrag zur Berechnung der Montage von Unterwasserpipelines*, 1973

32 Giesecke, Jürgen: *Die Wirbelkammertriode als neuartiges Steuerorgan im Wasserbau*, und Brombach, Hansjörg: *Entwicklung, Bauformen, Wirkungsweise und Steuereigenschaften von Wirbelkammerverstärkern*, 1974

33 Rueff, Helge: *Untersuchung der schwingungserregenden Kräfte an zwei hintereinander angeordneten Tiefschützen unter besonderer Berücksichtigung von Kavitation*, 1974

34 Röhnisch, Arthur: *Einpreßversuche mit Zementmörtel für Spannbeton - Vergleich der Ergebnisse von Modellversuchen mit Ausführungen in Hüllwellrohren*, 1975

35 *Sonderheft anläßlich des 65. Geburtstages von Prof. Dr.-Ing. Kurt Petrikat mit Beiträgen von*: Brombach, Hansjörg; Erbel, Klaus; Flinspach, Dieter; Fischer jr., Richard; Gàl, Attila; Gerlach, Reinhard; Giesecke, Jürgen; Haberhauer, Robert; Hafner Edzard; Hausenblas, Bernhard; Horlacher, Hans-Burkhard; Hutarew, Andreas; Knoll, Manfred; Krummet, Ralph; Marotz, Günter; Merkle, Theodor; Miller, Christoph; Minor, Hans-Erwin; Neumayer, Hans; Rao, Syamala; Rath, Paul; Rueff, Helge; Ruppert, Jürgen; Schwarz, Wolfgang; Topal-Gökceli, Mehmet; Vollmer, Ernst; Wang, Chung-su; Weber, Hans-Georg; 1975

36 Berger, Jochum: *Beitrag zur Berechnung des Spannungszustandes in rotationssymmetrisch belasteten Kugelschalen veränderlicher Wandstärke unter Gas- und Flüssigkeitsdruck durch Integration schwach singulärer Differentialgleichungen*, 1975

37 Dirksen, Wolfram: *Berechnung instationärer Abflußvorgänge in gestauten Gerinnen mittels Differenzenverfahren und die Anwendung auf Hochwasserrückhaltebecken*, 1976

38 Horlacher, Hans-Burkhard: *Berechnung instationärer Temperatur- und Wärmespannungsfelder in langen mehrschichtigen Hohlzylindern*, 1976

39 Hafner, Edzard: *Untersuchung der hydrodynamischen Kräfte auf Baukörper im Tiefwasserbereich des Meeres*, 1977, ISBN 3-921694-39-6

40 Ruppert, Jürgen: *Über den Axialwirbelkammerverstärker für den Einsatz im Wasserbau*, 1977, ISBN 3-921694-40-X

41 Hutarew, Andreas: *Beitrag zur Beeinflußbarkeit des Sauerstoffgehalts in Fließgewässern an Abstürzen und Wehren*, 1977, ISBN 3-921694-41-8, *vergriffen*

42 Miller, Christoph: *Ein Beitrag zur Bestimmung der schwingungserregenden Kräfte an überströmten Wehren*, 1977, ISBN 3-921694-42-6

43 Schwarz, Wolfgang: *Druckstoßberechnung unter Berücksichtigung der Radial- und Längsverschiebungen der Rohrwandung*, 1978, ISBN 3-921694-43-4

44 Kinzelbach, Wolfgang: *Numerische Untersuchungen über den optimalen Einsatz variabler Kühlsysteme einer Kraftwerkskette am Beispiel Oberrhein*, 1978, ISBN 3-921694-44-2

45 Barczewski, Baldur: *Neue Meßmethoden für Wasser-Luftgemische und deren Anwendung auf zweiphasige Auftriebsstrahlen*, 1979, ISBN 3-921694-45-0

46 Neumayer, Hans: *Untersuchung der Strömungsvorgänge in radialen Wirbelkammerverstärkern*, 1979, ISBN 3-921694-46-9

47 Elalfy, Youssef-Elhassan: *Untersuchung der Strömungsvorgänge in Wirbelkammerdioden und -drosseln*, 1979, ISBN 3-921694-47-7

48 Brombach, Hansjörg: *Automatisierung der Bewirtschaftung von Wasserspeichern*, 1981, ISBN 3-921694-48-5

49 Geldner, Peter: *Deterministische und stochastische Methoden zur Bestimmung der Selbstdichtung von Gewässern*, 1981, ISBN 3-921694-49-3, *vergriffen*

50 Mehlhorn, Hans: *Temperaturveränderungen im Grundwasser durch Brauchwassereinleitungen*, 1982, ISBN 3-921694-50-7, *vergriffen*

51 Hafner, Edzard: *Rohrleitungen und Behälter im Meer*, 1983, ISBN 3-921694-51-5

52 Rinnert, Bernd: *Hydrodynamische Dispersion in porösen Medien: Einfluß von Dichteunterschieden auf die Vertikalvermischung in horizontaler Strömung*, 1983, ISBN 3-921694-52-3, *vergriffen*

53 Lindner, Wulf: *Steuerung von Grundwasserentnahmen unter Einhaltung ökologischer Kriterien*, 1983, ISBN 3-921694-53-1, *vergriffen*

54 Herr, Michael; Herzer, Jörg; Kinzelbach, Wolfgang; Kobus, Helmut; Rinnert, Bernd: *Methoden zur rechnerischen Erfassung und hydraulischen Sanierung von Grundwasserkontaminationen*, 1983, ISBN 3-921694-54-X

55 Schmitt, Paul: *Wege zur Automatisierung der Niederschlagsermittlung*, 1984, ISBN 3-921694-55-8, *vergriffen*

56 Müller, Peter: *Transport und selektive Sedimentation von Schwebstoffen bei gestautem Abfluß*, 1985, ISBN 3-921694-56-6

57 El-Qawasmeh, Fuad: *Möglichkeiten und Grenzen der Tropfbewässerung unter besonderer Berücksichtigung der Verstopfungsanfälligkeit der Tropfelemente*, 1985, ISBN 3-921694-57-4, *vergriffen*

58 Kirchenbaur, Klaus: *Mikroprozessorgesteuerte Erfassung instationärer Druckfelder am Beispiel seegangsbelasteter Baukörper*, 1985, ISBN 3-921694-58-2

59 Kobus, Helmut (Hrsg.): *Modellierung des großräumigen Wärme- und Schadstofftransports im Grundwasser*, Tätigkeitsbericht 1984/85 (DFG-Forschergruppe an den Universitäten Hohenheim, Karlsruhe und Stuttgart), 1985, ISBN 3-921694-59-0, *vergriffen*

60 Spitz, Karlheinz: *Dispersion in porösen Medien: Einfluß von Inhomogenitäten und Dichteunterschieden*, 1985, ISBN 3-921694-60-4, *vergriffen*

61 Kobus, Helmut: *An Introduction to Air-Water Flows in Hydraulics*, 1985, ISBN 3-921694-61-2

62 Kaleris, Vassilios: *Erfassung des Austausches von Oberflächen- und Grundwasser in horizontalebenen Grundwassermodellen*, 1986, ISBN 3-921694-62-0

63 Herr, Michael: *Grundlagen der hydraulischen Sanierung verunreinigter Porengrundwasserleiter*, 1987, ISBN 3-921694-63-9

64 Marx, Walter: *Berechnung von Temperatur und Spannung in Massenbeton infolge Hydratation*, 1987, ISBN 3-921694-64-7

65 Koschitzky, Hans-Peter: *Dimensionierungskonzept für Sohlbelüfter in Schußrinnen zur Vermeidung von Kavitationsschäden*, 1987, ISBN 3-921694-65-5

66 Kobus, Helmut (Hrsg.): *Modellierung des großräumigen Wärme- und Schadstofftransports im Grundwasser*, Tätigkeitsbericht 1986/87 (DFG-Forschergruppe an den Universitäten Hohenheim, Karlsruhe und Stuttgart) 1987, ISBN 3-921694-66-3

67 Söll, Thomas: *Berechnungsverfahren zur Abschätzung anthropogener Temperaturanomalien im Grundwasser*, 1988, ISBN 3-921694-67-1

68 Dittrich, Andreas; Westrich, Bernd: *Bodenseeufererosion, Bestandsaufnahme und Bewertung*, 1988, ISBN 3-921694-68-X, *vergriffen*

69 Huwe, Bernd; van der Ploeg, Rienk R.: *Modelle zur Simulation des Stickstoffhaushaltes von Standorten mit unterschiedlicher landwirtschaftlicher Nutzung*, 1988, ISBN 3-921694-69-8, *vergriffen*

70 Stephan, Karl: *Integration elliptischer Funktionen*, 1988, ISBN 3-921694-70-1

71 Kobus, Helmut; Zilliox, Lothaire (Hrsg.): *Nitratbelastung des Grundwassers, Auswirkungen der Landwirtschaft auf die Grundwasser- und Rohwasserbeschaffenheit und Maßnahmen zum Schutz des Grundwassers*. Vorträge des deutsch-französischen Kolloquiums am 6. Oktober 1988, Universitäten Stuttgart und Louis Pasteur Strasbourg (Vorträge in deutsch oder französisch, Kurzfassungen zweisprachig), 1988, ISBN 3-921694-71-X

72 Soyeaux, Renald: *Unterströmung von Stauanlagen auf klüftigem Untergrund unter Berücksichtigung laminarer und turbulenter Fließzustände*,1991, ISBN 3-921694-72-8

73 Kohane, Roberto: *Berechnungsmethoden für Hochwasserabfluß in Fließgewässern mit überströmten Vorländern*, 1991, ISBN 3-921694-73-6

74 Hassinger, Reinhard: *Beitrag zur Hydraulik und Bemessung von Blocksteinrampen in flexibler Bauweise*, 1991, ISBN 3-921694-74-4, vergriffen

75 Schäfer, Gerhard: *Einfluß von Schichtenstrukturen und lokalen Einlagerungen auf die Längsdispersion in Porengrundwasserleitern*, 1991, ISBN 3-921694-75-2

76 Giesecke, Jürgen: *Vorträge, Wasserwirtschaft in stark besiedelten Regionen; Umweltforschung mit Schwerpunkt Wasserwirtschaft*, 1991, ISBN 3-921694-76-0

77 Huwe, Bernd: *Deterministische und stochastische Ansätze zur Modellierung des Stickstoffhaushalts landwirtschaftlich genutzter Flächen auf unterschiedlichem Skalenniveau*, 1992, ISBN 3-921694-77-9, vergriffen

78 Rommel, Michael: *Verwendung von Kluftdaten zur realitätsnahen Generierung von Kluftnetzen mit anschließender laminar-turbulenter Strömungsberechnung*, 1993, ISBN 3-92 1694-78-7

79 Marschall, Paul: *Die Ermittlung lokaler Stofffrachten im Grundwasser mit Hilfe von Einbohrloch-Meßverfahren*, 1993, ISBN 3-921694-79-5, vergriffen

80 Ptak, Thomas: *Stofftransport in heterogenen Porenaquiferen: Felduntersuchungen und stochastische Modellierung*, 1993, ISBN 3-921694-80-9, vergriffen

81 Haakh, Frieder: *Transientes Strömungsverhalten in Wirbelkammern,* 1993, ISBN 3-921694-81-7

82 Kobus, Helmut; Cirpka, Olaf; Barczewski, Baldur; Koschitzky, Hans-Peter: *Versuchseinrichtung zur Grundwasser- und Altlastensanierung VEGAS, Konzeption und Programmrahmen*, 1993, ISBN 3-921694-82-5

83 Zang, Weidong: *Optimaler Echtzeit-Betrieb eines Speichers mit aktueller Abflußregenerierung*, 1994, ISBN 3-921694-83-3, vergriffen

84 Franke, Hans-Jörg: *Stochastische Modellierung eines flächenhaften Stoffeintrages und Transports in Grundwasser am Beispiel der Pflanzenschutzmittelproblematik*, 1995, ISBN 3-921694-84-1

85 Lang, Ulrich: *Simulation regionaler Strömungs- und Transportvorgänge in Karstaquiferen mit Hilfe des Doppelkontinuum-Ansatzes: Methodenentwicklung und Parameteridentifikation*, 1995, ISBN 3-921694-85-X, vergriffen

86 Helmig, Rainer: *Einführung in die Numerischen Methoden der Hydromechanik*, 1996, ISBN 3-921694-86-8, vergriffen

87 Cirpka, Olaf: *CONTRACT: A Numerical Tool for Contaminant Transport and Chemical Transformations - Theory and Program Documentation -*, 1996, ISBN 3-921694-87-6

88 Haberlandt, Uwe: *Stochastische Synthese und Regionalisierung des Niederschlages für Schmutzfrachtberechnungen*, 1996, ISBN 3-921694-88-4

89 Croisé, Jean: *Extraktion von flüchtigen Chemikalien aus natürlichen Lockergesteinen mittels erzwungener Luftströmung*, 1996, ISBN 3-921694-89-2, vergriffen

90 Jorde, Klaus: *Ökologisch begründete, dynamische Mindestwasserregelungen bei Ausleitungskraftwerken*, 1997, ISBN 3-921694-90-6, vergriffen

91 Helmig, Rainer: *Gekoppelte Strömungs- und Transportprozesse im Untergrund - Ein Beitrag zur Hydrosystemmodellierung-*, 1998, ISBN 3-921694-91-4, vergriffen

92 Emmert, Martin: *Numerische Modellierung nichtisothermer Gas-Wasser Systeme in porösen Medien,* 1997, ISBN 3-921694-92-2

93 Kern, Ulrich: *Transport von Schweb- und Schadstoffen in staugeregelten Fließgewässern am Beispiel des Neckars*, 1997, ISBN 3-921694-93-0, vergriffen

94 Förster, Georg: *Druckstoßdämpfung durch große Luftblasen in Hochpunkten von Rohrleitungen 1997*, ISBN 3-921694-94-9

95 Cirpka, Olaf: *Numerische Methoden zur Simulation des reaktiven Mehrkomponententransports im Grundwasser*, 1997, ISBN 3-921694-95-7, vergriffen

96 Färber, Arne: *Wärmetransport in der ungesättigten Bodenzone: Entwicklung einer thermischen In-situ-Sanierungstechnologie*, 1997, ISBN 3-921694-96-5

97 Betz, Christoph: *Wasserdampfdestillation von Schadstoffen im porösen Medium: Entwicklung einer thermischen In-situ-Sanierungstechnologie*, 1998, SBN 3-921694-97-3

98 Xu, Yichun: *Numerical Modeling of Suspended Sediment Transport in Rivers*, 1998, ISBN 3-921694-98-1, vergriffen

99 Wüst, Wolfgang: *Geochemische Untersuchungen zur Sanierung CKW-kontaminierter Aquifere mit Fe(0)-Reaktionswänden,* 2000, ISBN 3-933761-02-2

100 Sheta, Hussam: *Simulation von Mehrphasenvorgängen in porösen Medien unter Einbeziehung von Hysterese-Effekten*, 2000, ISBN 3-933761-03-4

101 Ayros, Edwin: *Regionalisierung extremer Abflüsse auf der Grundlage statistischer Verfahren*, 2000, ISBN 3-933761-04-2, vergriffen

102 Huber, Ralf: *Compositional Multiphase Flow and Transport in Heterogeneous Porous Media*, 2000, ISBN 3-933761-05-0

103 Braun, Christopherus: *Ein Upscaling-Verfahren für Mehrphasenströmungen in porösen Medien*, 2000, ISBN 3-933761-06-9

104 Hofmann, Bernd: *Entwicklung eines rechnergestützten Managementsystems zur Beurteilung von Grundwasserschadensfällen*, 2000, ISBN 3-933761-07-7

105 Class, Holger: *Theorie und numerische Modellierung nichtisothermer Mehrphasenprozesse in NAPL-kontaminierten porösen Medien,* 2001, ISBN 3-933761-08-5

106 Schmidt, Reinhard: *Wasserdampf- und Heißluftinjektion zur thermischen Sanierung kontaminierter Standorte*, 2001, ISBN 3-933761-09-3

107 Josef, Reinhold: *Schadstoffextraktion mit hydraulischen Sanierungsverfahren unter Anwendung von grenzflächenaktiven Stoffen*, 2001, ISBN 3-933761-10-7

108 Schneider, Matthias: *Habitat- und Abflussmodellierung für Fließgewässer mit unscharfen Berechnungsansätzen*, 2001, ISBN 3-933761-11-5

109 Rathgeb, Andreas: *Hydrodynamische Bemessungsgrundlagen für Lockerdeckwerke an überströmbaren Erddämmen*, 2001, ISBN 3-933761-12-3

110 Lang, Stefan: *Parallele numerische Simulation instätionärer Probleme mit adaptiven Methoden auf unstrukturierten Gittern*, 2001, ISBN 3-933761-13-1

111 Appt, Jochen; Stumpp Simone: *Die Bodensee-Messkampagne 2001, IWS/CWR Lake Constance Measurement Program 2001*, 2002, ISBN 3-933761-14-X

112 Heimerl, Stephan: *Systematische Beurteilung von Wasserkraftprojekten,* 2002, ISBN 3-933761-15-8, vergriffen

113 Iqbal, Amin: *On the Management and Salinity Control of Drip Irrigation,* 2002, ISBN 3-933761-16-6

114 Silberhorn-Hemminger, Annette: *Modellierung von Kluftaquifersystemen: Geostatistische Analyse und deterministisch-stochastische Kluftgenerierung,* 2002, ISBN 3-933761-17-4

115 Winkler, Angela: *Prozesse des Wärme- und Stofftransports bei der In-situ-Sanierung mit festen Wärmequellen,* 2003, ISBN 3-933761-18-2

116 Marx, Walter: *Wasserkraft, Bewässerung, Umwelt - Planungs- und Bewertungsschwerpunkte der Wasserbewirtschaftung,* 2003, ISBN 3-933761-19-0

117 Hinkelmann, Reinhard: *Efficient Numerical Methods and Information-Processing Techniques in Environment Water,* 2003, ISBN 3-933761-20-4

118 Samaniego-Eguiguren, Luis Eduardo: *Hydrological Consequences of Land Use / Land Cover and Climatic Changes in Mesoscale Catchments*, 2003, ISBN 3-933761-21-2

119 Neunhäuserer, Lina: *Diskretisierungsansätze zur Modellierung von Strömungs- und Transportprozessen in geklüftet-porösen Medien*, 2003, ISBN 3-933761-22-0

120 Paul, Maren: *Simulation of Two-Phase Flow in Heterogeneous Poros Media with Adaptive Methods*, 2003, ISBN 3-933761-23-9

121 Ehret, Uwe: *Rainfall and Flood Nowcasting in Small Catchments using Weather Radar*, 2003, ISBN 3-933761-24-7

122 Haag, Ingo: *Der Sauerstoffhaushalt staugeregelter Flüsse am Beispiel des Neckars - Analysen, Experimente, Simulationen -,* 2003, ISBN 3-933761-25-5

123 Appt, Jochen: *Analysis of Basin-Scale Internal Waves in Upper Lake Constance,* 2003, ISBN 3-933761-26-3

124 Hrsg.: Schrenk, Volker; Batereau, Katrin; Barczewski, Baldur; Weber, Karolin und Koschitzky, Hans-Peter: *Symposium Ressource Fläche und VEGAS - Statuskolloquium 2003, 30. September und 1. Oktober 2003,* 2003, ISBN 3-933761-27-1

125 Omar Khalil Ouda: *Optimisation of Agricultural Water Use: A Decision Support System for the Gaza Strip,* 2003, ISBN 3-933761-28-0

126 Batereau, Katrin: *Sensorbasierte Bodenluftmessung zur Vor-Ort-Erkundung von Schadensherden im Untergrund*, 2004, ISBN 3-933761-29-8

127 Witt, Oliver: *Erosionsstabilität von Gewässersedimenten mit Auswirkung auf den Stofftransport bei Hochwasser am Beispiel ausgewählter Stauhaltungen des Oberrheins*, 2004, ISBN 3-933761-30-1

128 Jakobs, Hartmut: *Simulation nicht-isothermer Gas-Wasser-Prozesse in komplexen Kluft-Matrix-Systemen*, 2004, ISBN 3-933761-31-X

129 Li, Chen-Chien: *Deterministisch-stochastisches Berechnungskonzept zur Beurteilung der Auswirkungen erosiver Hochwasserereignisse in Flussstauhaltungen,* 2004, ISBN 3-933761-32-8

130 Reichenberger, Volker; Helmig, Rainer; Jakobs, Hartmut; Bastian, Peter; Niessner, Jennifer: *Complex Gas-Water Processes in Discrete Fracture-Matrix Systems: Up-scaling, Mass-Conservative Discretization and Efficient Multilevel Solution,* 2004, ISBN 3-933761-33-6

131 Hrsg.: Barczewski, Baldur; Koschitzky, Hans-Peter; Weber, Karolin; Wege, Ralf: *VEGAS - Statuskolloquium 2004,* Tagungsband zur Veranstaltung am 05. Oktober 2004 an der Universität Stuttgart, Campus Stuttgart-Vaihingen, 2004, ISBN 3-933761-34-4

132 Asie, Kemal Jabir: *Finite Volume Models for Multiphase Multicomponent Flow through Porous Media.* 2005, ISBN 3-933761-35-2

133 Jacoub, George: *Development of a 2-D Numerical Module for Particulate Contaminant Transport in Flood Retention Reservoirs and Impounded Rivers,* 2004, ISBN 3-933761-36-0

134 Nowak, Wolfgang: *Geostatistical Methods for the Identification of Flow and Transport Parameters in the Subsurface,* 2005, ISBN 3-933761-37-9

135 Süß, Mia: *Analysis of the influence of structures and boundaries on flow and transport processes in fractured porous media*, 2005, ISBN 3-933761-38-7

136 Jose, Surabhin Chackiath: *Experimental Investigations on Longitudinal Dispersive Mixing in Heterogeneous Aquifers,* 2005, ISBN: 3-933761-39-5

137 Filiz, Fulya: *Linking Large-Scale Meteorological Conditions to Floods in Mesoscale Catchments,* 2005, ISBN 3-933761-40-9

138 Qin, Minghao: *Wirklichkeitsnahe und recheneffiziente Ermittlung von Temperatur und Spannungen bei großen RCC-Staumauern*, 2005, ISBN 3-933761-41-7

139 Kobayashi, Kenichiro: *Optimization Methods for Multiphase Systems in the Subsurface - Application to Methane Migration in Coal Mining Areas*, 2005, ISBN 3-933761-42-5

140 Rahman, Md. Arifur: *Experimental Investigations on Transverse Dispersive Mixing in Heterogeneous Porous Media,* 2005, ISBN 3-933761-43-3

141 Schrenk, Volker: *Ökobilanzen zur Bewertung von Altlastensanierungsmaßnahmen,* 2005, ISBN 3-933761-44-1

142 Hundecha, Hirpa Yeshewatesfa: *Regionalization of Parameters of a Conceptual Rainfall-Runoff Model*, 2005, ISBN: 3-933761-45-X

143 Wege, Ralf: *Untersuchungs- und Überwachungsmethoden für die Beurteilung natürlicher Selbstreinigungsprozesse im Grundwasser,* 2005, ISBN 3-933761-46-8

144 Breiting, Thomas: *Techniken und Methoden der Hydroinformatik - Modellierung von komplexen Hydrosystemen im Untergrund*, 2006, ISBN 3-933761-47-6

145 Hrsg.: Braun, Jürgen; Koschitzky, Hans-Peter; Müller, Martin: *Ressource Untergrund: 10 Jahre VEGAS: Forschung und Technologieentwicklung zum Schutz von Grundwasser und Boden,* Tagungsband zur Veranstaltung am 28. und 29. September 2005 an der Universität Stuttgart, Campus Stuttgart-Vaihingen, 2005, ISBN 3-933761-48-4

146 Rojanschi, Vlad: *Abflusskonzentration in mesoskaligen Einzugsgebieten unter Berücksichtigung des Sickerraumes,* 2006, ISBN 3-933761-49-2

147 Winkler, Nina Simone: *Optimierung der Steuerung von Hochwasserrückhaltebeckensystemen,* 2006, ISBN 3-933761-50-6

148 Wolf, Jens: *Räumlich differenzierte Modellierung der Grundwasserströmung alluvialer Aquifere für mesoskalige Einzugsgebiete*, 2006, ISBN: 3-933761-51-4

149 Kohler, Beate: *Externe Effekte der Laufwasserkraftnutzung*, 2006, ISBN 3-933761-52-2

150 Hrsg.: Braun, Jürgen; Koschitzky, Hans-Peter; Stuhrmann, Matthias: *VEGAS-Statuskolloquium 2006,* Tagungsband zur Veranstaltung am 28. September 2006 an der Universität Stuttgart, Campus Stuttgart-Vaihingen, 2006, ISBN 3-933761-53-0

151 Niessner, Jennifer: *Multi-Scale Modeling of Multi-Phase - Multi-Component Processes in Heterogeneous Porous Media*, 2006, ISBN 3-933761-54-9

152 Fischer, Markus: *Beanspruchung eingeerdeter Rohrleitungen infolge Austrocknung bindiger Böden,* 2006, ISBN 3-933761-55-7

153 Schneck, Alexander: *Optimierung der Grundwasserbewirtschaftung unter Berücksichtigung der Belange der Wasserversorgung, der Landwirtschaft und des Naturschutzes*, 2006, ISBN 3-933761-56-5

154 Das, Tapash: *The Impact of Spatial Variability of Precipitation on the Predictive Uncertainty of Hydrological Models,* 2006, ISBN 3-33761-57-3

155 Bielinski, Andreas: *Numerical Simulation of CO_2 sequestration in geological formations*, 2007, ISBN 3-933761-58-1

156 Mödinger, Jens: *Entwicklung eines Bewertungs- und Entscheidungsunterstützungssystems für eine nachhaltige regionale Grundwasserbewirtschaftung*, 2006, ISBN 3-933761-60-3

157 Manthey, Sabine: *Two-phase flow processes with dynamic effects in porous media - parameter estimation and simulation,* 2007, ISBN 3-933761-61-1

158 Pozos Estrada, Oscar: *Investigation on the Effects of Entrained Air in Pipelines,* 2007, ISBN 3-933761-62-X

159 Ochs, Steffen Oliver: *Steam injection into saturated porous media – process analysis including experimental and numerical investigations*, 2007, ISBN 3-933761-63-8

160 Marx, Andreas: *Einsatz gekoppelter Modelle und Wetterradar zur Abschätzung von Niederschlagsintensitäten und zur Abflussvorhersage, 2007,* ISBN 3-933761-64-6

161 Hartmann, Gabriele Maria: *Investigation of Evapotranspiration Concepts in Hydrological Modelling for Climate Change Impact Assessment*, 2007, ISBN 3-933761-65-4

162 Kebede Gurmessa, Tesfaye: *Numerical Investigation on Flow and Transport Characteristics to Improve Long-Term Simulation of Reservoir Sedimentation*, 2007, ISBN 3-933761-66-2

163 Trifković, Aleksandar: *Multi-objective and Risk-based Modelling Methodology for Planning, Design and Operation of Water Supply Systems*, 2007, ISBN 3-933761-67-0

164 Götzinger, Jens: *Distributed Conceptual Hydrological Modelling - Simulation of Climate, Land Use Change Impact and Uncertainty Analysis*, 2007, ISBN 3-933761-68-9

165 Hrsg.: Braun, Jürgen; Koschitzky, Hans-Peter; Stuhrmann, Matthias: *VEGAS – Kolloquium 2007,* Tagungsband zur Veranstaltung am 26. September 2007 an der Universität Stuttgart, Campus Stuttgart-Vaihingen, 2007, ISBN 3-933761-69-7

166 Freeman, Beau: *Modernization Criteria Assessment for Water Resources Planning; Klamath Irrigation Project, U.S.*, 2008, ISBN 3-933761-70-0

167 Dreher, Thomas: *Selektive Sedimentation von Feinstschwebstoffen in Wechselwirkung mit wandnahen turbulenten Strömungsbedingungen*, 2008, ISBN 3-933761-71-9

168 Yang, Wei: *Discrete-Continuous Downscaling Model for Generating Daily Precipitation Time Series*, 2008, ISBN 3-933761-72-7

169 Kopecki, Ianina: *Calculational Approach to FST-Hemispheres for Multiparametrical Benthos Habitat Modelling,* 2008, ISBN 3-933761-73-5

170 Brommundt, Jürgen: *Stochastische Generierung räumlich zusammenhängender Niederschlagszeitreihen*, 2008, ISBN 3-933761-74-3

171 Papafotiou, *Alexandros: Numerical Investigations of the Role of Hysteresis in Heterogeneous Two-Phase Flow Systems*, 2008, ISBN 3-933761-75-1

172 He, Yi: *Application of a Non-Parametric Classification Scheme to Catchment Hydrology*, 2008, ISBN 978-3-933761-76-7

173 Wagner, Sven: *Water Balance in a Poorly Gauged Basin in West Africa Using Atmospheric Modelling and Remote Sensing Information*, 2008, ISBN 978-3-933761-77-4

174 Hrsg.: Braun, Jürgen; Koschitzky, Hans-Peter; Stuhrmann, Matthias; Schrenk, Volker: *VEGAS-Kolloquium 2008 Ressource Fläche III*, Tagungsband zur Veranstaltung am 01. Oktober 2008 an der Universität Stuttgart, Campus Stuttgart-Vaihingen, 2008, ISBN 978-3-933761-78-1

175 Patil, Sachin: *Regionalization of an Event Based Nash Cascade Model for Flood Predictions in Ungauged Basins*, 2008, ISBN 978-3-933761-79-8

176 Assteerawatt, Anongnart: *Flow and Transport Modelling of Fractured Aquifers based on a Geostatistical Approach,* 2008, ISBN 978-3-933761-80-4

177 Karnahl, Joachim Alexander: *2D numerische Modellierung von multifraktionalem Schwebstoff- und Schadstofftransport in Flüssen*, 2008, ISBN 978-3-933761-81-1

178 Hiester, Uwe: *Technologieentwicklung zur In-situ-Sanierung der ungesättigten Bodenzone mit festen Wärmequellen,* 2009, ISBN 978-3-933761-82-8

179 Laux, Patrick: *Statistical Modeling of Precipitation for Agricultural Planning in the Volta Basin of West Africa,* 2009, ISBN 978-3-933761-83-5

180 Ehsan, Saqib: *Evaluation of Life Safety Risks Related to Severe Flooding,* 2009, ISBN 978-3-933761-84-2

181 Prohaska, Sandra: *Development and Application of a 1D Multi-Strip Fine Sediment Transport Model for Regulated Rivers,* 2009, ISBN 978-3-933761-85-9

182 Kopp, Andreas: *Evaluation of CO_2 Injection Processes in Geological Formations for Site Screening,* 2009, ISBN 978-3-933761-86-6

183 Ebigbo, Anozie: *Modelling of biofilm growth and its influence on CO_2 and water (two-phase) flow in porous media,* 2009, ISBN 978-3-933761-87-3

184 Freiboth, Sandra: *A phenomenological model for the numerical simulation of multiphase multicomponent processes considering structural alterations of porous media*, 2009, ISBN 978-3-933761-88-0

185 Zöllner, Frank: *Implementierung und Anwendung netzfreier Methoden im Konstruktiven Wasserbau und in der Hydromechanik*, 2009, ISBN 978-3-933761-89-7

186 Vasin, Milos: *Influence of the soil structure and property contrast on flow and transport in the unsaturated zone*, 2010, ISBN 978-3-933761-90-3

187 Li, Jing: *Application of Copulas as a New Geostatistical Tool*, 2010, ISBN 978-3-933761-91-0

188 AghaKouchak, Amir: *Simulation of Remotely Sensed Rainfall Fields Using Copulas*, 2010, ISBN 978-3-933761-92-7

189 Thapa, Pawan Kumar: *Physically-based spatially distributed rainfall runoff modelling for soil erosion estimation*, 2010, ISBN 978-3-933761-93-4

190 Wurms, Sven: *Numerische Modellierung der Sedimentationsprozesse in Retentionsanlagen zur Steuerung von Stoffströmen bei extremen Hochwasserabflussereignissen*, 2011, ISBN 978-3-933761-94-1

191 Merkel, Uwe: *Unsicherheitsanalyse hydraulischer Einwirkungen auf Hochwasserschutzdeiche und Steigerung der Leistungsfähigkeit durch adaptive Strömungsmodellierung*, 2011, ISBN 978-3-933761-95-8

192 Fritz, Jochen: *A Decoupled Model for Compositional Non-Isothermal Multiphase Flow in Porous Media and Multiphysics Approaches for Two-Phase Flow*, 2010, ISBN 978-3-933761-96-5

193 Weber, Karolin (Hrsg.): *12. Treffen junger WissenschaftlerInnen an Wasserbauinstituten*, 2010, ISBN 978-3-933761-97-2

194 Bliefernicht, Jan-Geert: *Probability Forecasts of Daily Areal Precipitation for Small River Basins,* 2011, ISBN 978-3-933761-98-9

195 Hrsg.: Koschitzky, Hans-Peter; Braun, Jürgen: *VEGAS-Kolloquium 2010 In-situ-Sanierung - Stand und Entwicklung Nano und ISCO -,* Tagungsband zur Veranstaltung am 07. Oktober 2010 an der Universität Stuttgart, Campus Stuttgart-Vaihingen, 2010, ISBN 978-3-933761-99-6

196 Gafurov, Abror: *Water Balance Modeling Using Remote Sensing Information - Focus on Central Asia,* 2010, ISBN 978-3-942036-00-9

197 Mackenberg, Sylvia: *Die Quellstärke in der Sickerwasserprognose: Möglichkeiten und Grenzen von Labor- und Freilanduntersuchungen,* 2010, ISBN 978-3-942036-01-6

198 Singh, Shailesh Kumar: *Robust Parameter Estimation in Gauged and Ungauged Basins,* 2010, ISBN 978-3-942036-02-3

199 Doğan, Mehmet Onur: *Coupling of porous media flow with pipe flow,* 2011, ISBN 978-3-942036-03-0

200 Liu, Min: *Study of Topographic Effects on Hydrological Patterns and the Implication on Hydrological Modeling and Data Interpolation,* 2011, ISBN 978-3-942036-04-7

201 Geleta, Habtamu Itefa: *Watershed Sediment Yield Modeling for Data Scarce Areas,* 2011, ISBN 978-3-942036-05-4

202 Franke, Jörg: *Einfluss der Überwachung auf die Versagenswahrscheinlichkeit von Staustufen,* 2011, ISBN 978-3-942036-06-1

203 Bakimchandra, Oinam: *Integrated Fuzzy-GIS approach for assessing regional soil erosion risks,* 2011, ISBN 978-3-942036-07-8

204 Alam, Muhammad Mahboob: *Statistical Downscaling of Extremes of Precipitation in Mesoscale Catchments from Different RCMs and Their Effects on Local Hydrology,* 2011, ISBN 978-3-942036-08-5

205 Hrsg.: Koschitzky, Hans-Peter; Braun, Jürgen: *VEGAS-Kolloquium 2011 Flache Geothermie - Perspektiven und Risiken,* Tagungsband zur Veranstaltung am 06. Oktober 2011 an der Universität Stuttgart, Campus Stuttgart-Vaihingen, 2011, ISBN 978-3-933761-09-2

206 Haslauer, Claus: *Analysis of Real-World Spatial Dependence of Subsurface Hydraulic Properties Using Copulas with a Focus on Solute Transport Behaviour,* 2011, ISBN 978-3-942036-10-8

207 Dung, Nguyen Viet: *Multi-objective automatic calibration of hydrodynamic models – development of the concept and an application in the Mekong Delta,* 2011, ISBN 978-3-942036-11-5

208 Hung, Nguyen Nghia: *Sediment dynamics in the floodplain of the Mekong Delta, Vietnam,* 2011, ISBN 978-3-942036-12-2

209 Kuhlmann, Anna: *Influence of soil structure and root water uptake on flow in the unsaturated zone,* 2012, ISBN 978-3-942036-13-9

210 Tuhtan, Jeffrey Andrew: *Including the Second Law Inequality in Aquatic Ecodynamics: A Modeling Approach for Alpine Rivers Impacted by Hydropeaking,* 2012, ISBN 978-3-942036-14-6

211 Tolossa, Habtamu: *Sediment Transport Computation Using a Data-Driven Adaptive Neuro-Fuzzy Modelling Approach,* 2012, ISBN 978-3-942036-15-3

212 Tatomir, Alexandru-Bodgan: *From Discrete to Continuum Concepts of Flow in Fractured Porous Media,* 2012, ISBN 978-3-942036-16-0

213 Erbertseder, Karin: *A Multi-Scale Model for Describing Cancer-Therapeutic Transport in the Human Lung,* 2012, ISBN 978-3-942036-17-7

214 Noack, Markus: *Modelling Approach for Interstitial Sediment Dynamics and Reproduction of Gravel Spawning Fish,* 2012, ISBN 978-3-942036-18-4

215 De Boer, Cjestmir Volkert: *Transport of Nano Sized Zero Valent Iron Colloids during Injection into the Subsurface*, 2012, ISBN 978-3-942036-19-1

216 Pfaff, Thomas: *Processing and Analysis of Weather Radar Data for Use in Hydrology*, 2013, ISBN 978-3-942036-20-7

217 Lebrenz, Hans-Henning: *Addressing the Input Uncertainty for Hydrological Modeling by a New Geostatistical Method*, 2013, ISBN 978-3-942036-21-4

218 Darcis, Melanie Yvonne: *Coupling Models of Different Complexity for the Simulation of CO_2 Storage in Deep Saline Aquifers*, 2013, ISBN 978-3-942036-22-1

219 Beck, Ferdinand: *Generation of Spatially Correlated Synthetic Rainfall Time Series in High Temporal Resolution - A Data Driven Approach*, 2013, ISBN 978-3-942036-23-8

220 Guthke, Philipp: *Non-multi-Gaussian spatial structures: Process-driven natural genesis, manifestation, modeling approaches, and influences on dependent processes*, 2013, ISBN 978-3-942036-24-5

221 Walter, Lena: *Uncertainty studies and risk assessment for CO_2 storage in geological formations*, 2013, ISBN 978-3-942036-25-2

222 Wolff, Markus: *Multi-scale modeling of two-phase flow in porous media including capillary pressure effects,* 2013, ISBN 978-3-942036-26-9

223 Mosthaf, Klaus Roland: *Modeling and analysis of coupled porous-medium and free flow with application to evaporation processes,* 2014, ISBN 978-3-942036-27-6

224 Leube, Philipp Christoph: *Methods for Physically-Based Model Reduction in Time: Analysis, Comparison of Methods and Application*, 2013, ISBN 978-3-942036-28-3

225 Rodríguez Fernández, Jhan Ignacio: *High Order Interactions among environmental variables: Diagnostics and initial steps towards modeling*, 2013, ISBN 978-3-942036-29-0

226 Eder, Maria Magdalena: *Climate Sensitivity of a Large Lake*, 2013, ISBN 978-3-942036-30-6

227 Greiner, Philipp: *Alkoholinjektion zur In-situ-Sanierung von CKW Schadensherden in Grundwasserleitern: Charakterisierung der relevanten Prozesse auf unterschiedlichen Skalen*, 2014, ISBN 978-3-942036-31-3

228 Lauser, Andreas: *Theory and Numerical Applications of Compositional Multi-Phase Flow in Porous Media*, 2014, ISBN 978-3-942036-32-0

229 Enzenhöfer, Rainer: *Risk Quantification and Management in Water Production and Supply Systems*, 2014, ISBN 978-3-942036-33-7

230 Faigle, Benjamin: *Adaptive modelling of compositional multi-phase flow with capillary pressure*, 2014, ISBN 978-3-942036-34-4

231 Oladyshkin, Sergey: *Efficient modeling of environmental systems in the face of complexity and uncertainty*, 2014, ISBN 978-3-942036-35-1

232 Sugimoto, Takayuki: *Copula based Stochastic Analysis of Discharge Time Series*, 2014, ISBN 978-3-942036-36-8

233 Koch, Jonas: *Simulation, Identification and Characterization of Contaminant Source Architectures in the Subsurface*, 2014, ISBN 978-3-942036-37-5

234 Zhang, Jin: *Investigations on Urban River Regulation and Ecological Rehabilitation Measures, Case of Shenzhen in China*, 2014, ISBN 978-3-942036-38-2

235 Siebel, Rüdiger: *Experimentelle Untersuchungen zur hydrodynamischen Belastung und Standsicherheit von Deckwerken an überströmbaren Erddämmen,* 2014, ISBN 978-3-942036-39-9

236 Baber, Katherina: *Coupling free flow and flow in porous media in biological and technical applications: From a simple to a complex interface description,* 2014, ISBN 978-3-942036-40-5

237 Nuske, Klaus Philipp: *Beyond Local Equilibrium — Relaxing local equilibrium assumptions in multiphase flow in porous media,* 2014, ISBN 978-3-942036-41-2

238 Geiges, Andreas: *Efficient concepts for optimal experimental design in nonlinear environmental systems*, 2014, ISBN 978-3-942036-42-9

239 Schwenck, Nicolas: *An XFEM-Based Model for Fluid Flow in Fractured Porous Media*, 2014, ISBN 978-3-942036-43-6

240 Chamorro Chávez, Alejandro: *Stochastic and hydrological modelling for climate change prediction in the Lima region, Peru*, 2015, ISBN 978-3-942036-44-3

241 Yulizar: *Investigation of Changes in Hydro-Meteorological Time Series Using a Depth-Based Approach*, 2015, ISBN 978-3-942036-45-0

242 Kretschmer, Nicole: *Impacts of the existing water allocation scheme on the Limarí watershed – Chile, an integrative approach*, 2015, ISBN 978-3-942036-46-7

243 Kramer, Matthias: *Luftbedarf von Freistrahlturbinen im Gegendruckbetrieb*, 2015, ISBN 978-3-942036-47-4

244 Hommel, Johannes: *Modeling biogeochemical and mass transport processes in the subsurface: Investigation of microbially induced calcite precipitation*, 2016, ISBN 978-3-942036-48-1

245 Germer, Kai: *Wasserinfiltration in die ungesättigte Zone eines makroporösen Hanges und deren Einfluss auf die Hangstabilität*, 2016, ISBN 978-3-942036-49-8

246 Hörning, Sebastian: *Process-oriented modeling of spatial random fields using copulas*, 2016, ISBN 978-3-942036-50-4

247 Jambhekar, Vishal: *Numerical modeling and analysis of evaporative salinization in a coupled free-flow porous-media system,* 2016, ISBN 978-3-942036-51-1

248 Huang, Yingchun: *Study on the spatial and temporal transferability of conceptual hydrological models*, 2016, ISBN 978-3-942036-52-8

249 Kleinknecht, Simon Matthias: *Migration and retention of a heavy NAPL vapor and remediation of the unsaturated zone*, 2016, ISBN 978-3-942036-53-5

250 Kwakye, Stephen Oppong: *Study on the effects of climate change on the hydrology of the West African sub-region*, 2016, ISBN 978-3-942036-54-2

251 Kissinger, Alexander: *Basin-Scale Site Screening and Investigation of Possible Impacts of CO_2 Storage on Subsurface Hydrosystems*, 2016, ISBN 978-3-942036-55-9

252 Müller, Thomas: *Generation of a Realistic Temporal Structure of Synthetic Precipitation Time Series for Sewer Applications*, 2017, ISBN 978-3-942036-56-6

253 Grüninger, Christoph: *Numerical Coupling of Navier-Stokes and Darcy Flow for Soil-Water Evaporation*, 2017, ISBN 978-3-942036-57-3

254 Suroso: *Asymmetric Dependence Based Spatial Copula Models: Empirical Investigations and Consequences on Precipitation Fields*, 2017, ISBN 978-3-942036-58-0

255 Müller, Thomas; Mosthaf, Tobias; Gunzenhauser, Sarah; Seidel, Jochen; Bárdossy, András: *Grundlagenbericht Niederschlags-Simulator (NiedSim3)*, 2017, ISBN 978-3-942036-59-7

256 Mosthaf, Tobias: *New Concepts for Regionalizing Temporal Distributions of Precipitation and for its Application in Spatial Rainfall Simulation,* 2017, ISBN 978-3-942036-60-3

257 Fenrich, Eva Katrin: *Entwicklung eines ökologisch-ökonomischen Vernetzungsmodells für Wasserkraftanlagen und Mehrzweckspeicher,* 2018, ISBN 978-3-942036-61-0

258 Schmidt, Holger: *Microbial stabilization of lotic fine sediments*, 2018, ISBN 978-3-942036-62-7

259 Fetzer, Thomas: *Coupled Free and Porous-Medium Flow Processes Affected by Turbulence and Roughness – Models, Concepts and Analysis*, 2018, ISBN 978-3-942036-63-4

260 Schröder, Hans Christoph: *Large-scale High Head Pico Hydropower Potential Assessment*, 2018, ISBN 978-3-942036-64-1

261 Bode, Felix: *Early-Warning Monitoring Systems for Improved Drinking Water Resource Protection*, 2018, ISBN 978-3-942036-65-8

262 Gebler, Tobias: *Statistische Auswertung von simulierten Talsperrenüberwachungsdaten zur Identifikation von Schadensprozessen an Gewichtsstaumauern*, 2018, ISBN 978-3-942036-66-5

263 Harten, Matthias von: *Analyse des Zuppinger-Wasserrades – Hydraulische Optimierungen unter Berücksichtigung ökologischer Aspekte*, 2018, ISBN 978-3-942036-67-2

264 Yan, Jieru: *Nonlinear estimation of short time precipitation using weather radar and surface observations*, 2018, ISBN 978-3-942036-68-9

265 Beck, Martin: *Conceptual approaches for the analysis of coupled hydraulic and geomechanical processes*, 2019, ISBN 978-3-942036-69-6

266 Haas, Jannik: *Optimal planning of hydropower and energy storage technologies for fully renewable power systems*, 2019, ISBN 978-3-942036-70-2

267 Schneider, Martin: *Nonlinear Finite Volume Schemes for Complex Flow Processes and Challenging Grids*, 2019, ISBN 978-3-942036-71-9

268 Most, Sebastian Christopher: *Analysis and Simulation of Anomalous Transport in Porous Media*, 2019, ISBN 978-3-942036-72-6

Die Mitteilungshefte ab der Nr. 134 (Jg. 2005) stehen als pdf-Datei über die Homepage des Instituts: www.iws.uni-stuttgart.de zur Verfügung.